Fault systems of the eastern Indonesian triple junction: evaluation of Quaternary activity and implications for seismic hazards

IAN M. WATKINSON* & ROBERT HALL

SE Asia Research Group, Department of Earth Sciences, Royal Holloway University of London, Egham, Surrey TW20 0EX, UK

**Correspondence: ian.watkinson@rhul.ac.uk*

Abstract: Eastern Indonesia is the site of intense deformation related to convergence between Australia, Eurasia, the Pacific and the Philippine Sea Plate. Our analysis of the tectonic geomorphology, drainage patterns, exhumed faults and historical seismicity in this region has highlighted faults that have been active during the Quaternary (Pleistocene to present day), even if instrumental records suggest that some are presently inactive. Of the 27 largely onshore fault systems studied, 11 showed evidence of a maximal tectonic rate and a further five showed evidence of rapid tectonic activity. Three faults indicating a slow to minimal tectonic rate nonetheless showed indications of Quaternary activity and may simply have long interseismic periods. Although most studied fault systems are highly segmented, many are linked by narrow (<3 km) step-overs to form one or more long, quasi-continuous segment capable of producing M > 7.5 earthquakes. Sinistral shear across the soft-linked Yapen and Tarera–Aiduna faults and their continuation into the transpressive Seram fold–thrust belt represents perhaps the most active belt of deformation and hence the greatest seismic hazard in the region. However, the Palu–Koro Fault, which is long, straight and capable of generating super-shear ruptures, is considered to represent the greatest seismic risk of all the faults evaluated in this region in view of important strike-slip strands that appear to traverse the thick Quaternary basin-fill below Palu city.

During the last decade several devastating earthquakes occurred on faults around the world that were either poorly understood or not recognized at all. The M_w 6.6 Bam earthquake (Iran) of 26 December 2003 ruptured a section of the Bam Fault that had a poor surface expression and had not caused a destructive earthquake for 2000 years (Eshghi & Zare 2003; Fu *et al.* 2004). The M_w 8.0 Wenchuan earthquake (China) of 12 May 2008 resulted from complex rupture of part of the Lonmen Shan tectonic belt (Burchfiel *et al.* 2008), an area that was previously considered not to be at risk from large earthquakes (Chen & Hsu 2013). The M_w 7.1 Haiti earthquake of 12 January 2010 occurred on the well-known Enriquillo Fault, part of the fault system marking the northern boundary of the Caribbean plate, but which had previously been mapped as having low seismic hazard based on recent seismicity (Stein *et al.* 2012). The Canterbury earthquake sequence (New Zealand) ruptured the Greendale Fault, which was previously unrecognized because it was buried beneath alluvial sediments (Quigley *et al.* 2012). The Canterbury sequence culminated in the M_w 6.3 Christchurch earthquake of 22 February 2011. These events emphasize the need for the accurate identification of faults that have been active during the Quaternary and have the potential for modern tectonic activity.

Eastern Indonesia is a region of complex and rapid neotectonics. Convergence between Australia, Eurasia, the Pacific and the Philippine Sea plates (e.g. Hamilton 1979; DeMets *et al.* 1994; Hall 1996, 2012; Bock *et al.* 2003; Charlton 2010) results in both contraction and extension from subduction hinge rollback, lithospheric delamination and slab break-off (e.g. Harris 1992; Spakman & Hall 2010; Hall 2012).

Great uncertainty surrounds the position, tectonic role and modern activity of eastern Indonesia's many Quaternary faults (e.g. Hamilton 1979; Okal 1999; Bailly *et al.* 2009; Charlton 2010). New fault systems continue to be identified using both modern geophysical/remote sensing and conventional field techniques (e.g. Stevens *et al.* 2002; Spencer 2010, 2011; Watkinson *et al.* 2011; Pownall *et al.* 2013) and it is likely that many others remain unknown, with important implications for seismic hazard analysis.

Despite intense seismicity in eastern Indonesia, there have been few catastrophic earthquake disasters in the last 100 years compared with other rapidly deforming areas such as China, Iran, Japan and Pakistan (e.g. Holzer & Savage 2013; National Geophysical Data Center/World Data Service). Significant events include: the 25 June 1976 M_w 7.1 Papua earthquake, which killed 3000–6000

From: CUMMINS, P. R. & MEILANO, I. (eds) *Geohazards in Indonesia: Earth Science for Disaster Risk Reduction*. Geological Society, London, Special Publications, **441**, https://doi.org/10.1144/SP441.8, updated version

people; the 12 December 1992 M_w 7.8 Flores earthquake, which killed 2500 people and destroyed 31 800 houses; the 17 February 1996 M_w 8.2 Biak earthquake, which caused a 7 m tsunami and killed at least 100 people (Okal 1999); the 16 November 2008 M_w 7.4 Minahasa earthquake, which killed six people and displaced 10 000; and the 16 June 2010 M_w 7.0 Yapen earthquake, which killed 17 people and destroyed 2556 houses (National Geophysical Data Center/World Data Service; USGS Earthquake Hazards Program). With increasing urban development and the replacement of traditional wooden dwellings with concrete constructions, it is likely that damaging earthquakes will become more frequent in the future (e.g. Wyss 2005).

This paper catalogues Quaternary fault systems onshore eastern Indonesia from Sulawesi to Papua, providing evidence for Quaternary tectonic activity and a reconnaissance evaluation of the seismic hazard of the faults (Fig. 1).

Methods

Definitions and extent of study

This study was concerned with evaluating Quaternary (Pleistocene and Holocene, 2.59–0 Ma) fault activity. Quaternary activity lies within the realm of neotectonics, the study of broadly post-Miocene, 'young' and still-active tectonic events, the effects of which are compatible with modern seismotectonics (Pavlides 1989). Neotectonics is distinct from palaeoseismology – the study of deformation related to specific past earthquakes (e.g. Michetti *et al.* 2005). Thus faults that show evidence of Quaternary activity may or may not also show evidence of palaeoseismicity, depending on whether they have recently ruptured the surface, the rates of sedimentation and erosion, and whether they are truly 'active' in the sense that they have failed during the Holocene. Equally, Quaternary faults may or may not be present in records of instrumental or historical seismicity, depending on whether they have recently become inactive, have a long interseismic period, or have yielded historical earthquakes in locations where there was no written documentation. Quaternary fault activity is therefore distinct from, but influential in, the field of active tectonics, which includes future fault activity that may affect human society (Wallace 1986).

Quaternary fault activity was evaluated in this study by the following criteria: (1) instrumental/historical seismicity and geodetic observations; (2) deformation of Quaternary sediments, often indicated by topographic lineaments that could be linked to an underlying fault; (3) the systematic offset of modern streams across a topographic lineament; (4) evidence of structurally controlled drainage network modification where signs of an earlier arrangement were preserved; (5) geomorphic indices recording the relative youthfulness of fault-controlled mountain fronts; and (6) evidence of landslips localized to faults.

The study extent was a 2200 × 800 km swath of the Indonesian archipelago centred on the triple junction between Australia, Eurasia, the Pacific and the Philippine Sea plates. It includes much of eastern Indonesia from Sulawesi eastwards, except

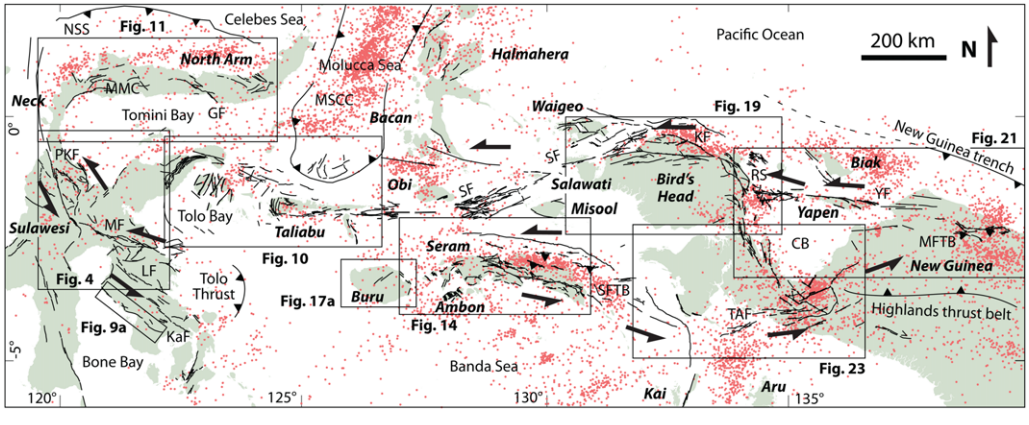

Fig. 1. Map of eastern Indonesia showing upper crustal structures with geomorphic evidence of Quaternary tectonic activity and seismicity (1973–2014, focal depths <35 km). CB, Cenderawasih Bay; GF, Gorontalo Fault; KaF, Kolaka Fault; KF, Koor Fault; LF, Lawanopo Fault; MF, Matano Fault; MFTB, Mamberamo fold–thrust belt; MMC, Molino Metamorphic Complex; MSCC, Molucca Sea Collision Complex; NSS, North Sulawesi Subduction; PKF, Palu–Koro Fault; RS, Ransiki Fault; SF, Sorong Fault; SFTB, Seram fold–thrust belt; TAF, Tarera–Aiduna Fault; YF, Yapen Fault. Locations of other figures as indicated.

the islands of the southern Banda Arc. Because of the focus on geomorphic expression, the study mainly dealt with onshore faults, except where multibeam bathymetry was available.

Datasets

Our interpretations of Quaternary fault activity are based on a variety of remote sensing data, field observations by both authors and their students over several years (e.g. Roques 1999; Watkinson 2011; Pownall *et al.* 2013; Hennig *et al.* 2014) and published geodetic/geophysical data. Digital elevation models (DEMs) based on Shuttle Radar Topography Mission (SRTM) 3 arc second/90 m resolution and ASTER 30 m resolution data were processed using ERMapper software. These data were also used to extract topographic contours and drainage networks using ArcGIS. Landsat TM and ETM+ scenes composed of the 30 m resolution bands 432, 451, 531 and 742 (red–green–blue combinations) were used and, where appropriate, sharpened with ETM+ band 8 panchromatic 15 m resolution data. Where available, high-resolution visible spectrum imagery from Google Earth and Bing Maps (compiled from a variety of sources) and the ESRI World Imagery compilation, which includes 2.5 m SPOT and <1 m DigitalGlobe imagery, was also interpreted. ESRI World Imagery is compiled from Esri, DigitalGlobe, GeoEye, Earthstar Geographics, CNES/Airbus DS, USDA, USGS, AEX, Getmapping, Aerogrid, IGN, IGP, swisstopo, and the GIS User Community.

Multibeam bathymetric data (kindly provided by TGS) from parts of the offshore Sorong Fault Zone and Cenderawasih Bay were interpreted in the same way as the DEMs. The multibeam data were acquired using a Kongsberg Simrad EM120 Multibeam Echo Sounder using 191 beams at equidistant spacing. Positioning control used a C-Nav Starfire DGPS. During processing, positioning, tidal and calibration corrections were applied, random noise and artefacts were removed, and a terrain model using a 25 m bin size was gridded and exported to ESRI format. The multibeam data were further processed in ERMapper to remove voids.

All data were integrated in ArcGIS together with previously published georeferenced maps. The CMT focal mechanisms were from the International Seismological Centre catalogue, plotted using Mirone software. We considered only earthquakes with a focal depth $\leq$35 km to avoid contamination from deeper structures that have little surface expression.

Geomorphic indices

Geomorphic indices are a valuable tool to rapidly evaluate the relative tectonic rate of surface faults on a reconnaissance scale (Keller 1986). We utilized mountain front sinuosity (S_{mf}) and the valley floor width to valley height index (V_f) following the method of Bull & McFadden (1977) and Bull (1978). The key parameters are summarized in Table 1. An excellent description of the method and its uncertainties is given in Bull (2007). Although conventionally applied to normal faults, geomorphic indices can been used in any setting where there is vertical motion, including regions of transpression and transtension. However, they are of little value in regions of pure strike-slip and were not applied to pure strike-slip segments in this study.

Mountain front sinuosity is the ratio $S_{mf} = L_{mf}/L_s$, where L_{mf} is the straight line length of the mountain front and L_s is the true, or sinuous, length along the mountain front following topographic contours at the contact between alluvial fans and the solid geology of the range front (Table 1). This method assumes that a fault-bounded range front will become more sinuous over time in the absence of tectonic activity (e.g. Bull & McFadden 1977; Rockwell *et al.* 1984). The method is well established for Quaternary fault evaluation in regions of extension (e.g. Ramírez-Herrera 1998), contraction and strike-slip (e.g. Dehbozorgi *et al.* 2010), transtension (e.g. Silva *et al.* 2003; Yıldırım 2014), combined extension and contraction (Wells *et al.* 1988) and differential uplift (e.g. Sohoni *et al.* 1999). Critical uncertainties include the interpreter's definition of the sinuous mountain front, which is partly dependent on the quality of the input satellite data, and the recognition of discrete mountain front segments. Climate also has an impact on S_{mf} independent of the tectonic rate. In a humid environment like eastern Indonesia it is expected that erosion and hence S_{mf} will be higher than in an arid region for a given tectonic rate.

The valley floor width to valley height index, V_f, measures the ratio between the valley floor width and the valley depth: $V_f = 2V_{fw}/(E_{ld} - E_{sc}) - (E_{rd} - E_{sc})$, where V_{fw} is the valley floor width, E_{ld} and E_{rd} are the topographic elevations of the left and right valley watersheds and E_{sc} is the elevation of the valley floor (Table 1). The method assumes that recently excavated river channels (i.e. those into which a river has incised as a result of recent uplift) are V-shaped and become more U-shaped over time (e.g. Bull & McFadden 1977; Rockwell *et al.* 1984). Like S_{mf}, V_f has been applied in a wide range of tectonic settings (e.g. Wells *et al.* 1988; Ramírez-Herrera 1998; Yıldırım 2014). V_f is sensitive to a number of variables apart from tectonic rate, so we standardized as much as possible by: measuring V_f in all cases 1 km upstream from the mountain front; measuring the valley width as the width of the river channel visible on the highest resolution satellite imagery available or the width

Table 1. *Summary of geomorphic indices used in mountain front analysis, modified after Wells* et al. *(1988)*

Parameter	Definition	Derivation*	Measurement†	Purpose	Potential difficulties
S_{mf}	Sinuosity of topographic mountain fronts	L_{mf}/L_s	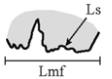	Defines the degree of topographic modification of mountain front from the position of possible controlling structures	Defining actual topographic junction Defining discrete mountain front segments
V_f	Valley floor width to valley height index	$2V_{fw}/[(E_{ld} - E_{sc}) - (E_{rd} - E_{sc})]$	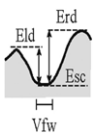	Defines the ratio of the valley floor width to the mean height of two adjacent divides, measured at given locations along a stream channel within the range block	Resolution of satellite imagery in defining V_{fw} and divide elevations Effects of changes in lithology Need to minimize variations in stream size (length and area)

*L_{mf}, straight line length of mountain front; L_s, sinuous length along mountain front; V_{fw}, valley floor width; E_{ld} and E_{rd}, topographic elevations of left and right valley watersheds; E_{sc}, elevation of valley floor.
†Schematic map view for S_{mf}, schematic cross-section view for V_f.
Both indices after Bull & McFadden (1977) and Bull (1978).

of the valley to the point where the floor rose 10 m above the minimum elevation in individual transects; measuring only streams that reached the mountain front without joining a higher order stream; and measuring only streams oriented $\geq 70^{\circ}$ from the mountain front. Noise in the V_f signal was reduced by averaging between three and ten separate V_f measurements along each fault segment.

High-quality topographic maps are not available for eastern Indonesia, so both S_{mf} and V_f were measured in ArcGIS software using a combination of 30 m ASTER GDEM satellite data and the ESRI World Imagery compilation. This allowed the finest possible resolution of L_s and V_{fw}, which are crucial, but potentially subjective, parameters. High-quality satellite imagery may be better for such measurements than conventional maps (Bull 2007).

Schemes for the classification of relative tectonic activity based on a combination of geomorphic indices have been proposed (e.g. Bull & McFadden 1977; Bull 1978, 2007). Here we applied a modified scheme from McCalpin (2009). This uses S_{mf} and V_f to classify relative tectonic activity as follows: $S_{mf} < 1.1$, mean $V_f < 0.15$, maximal activity; S_{mf} 1.1–1.3, mean V_f 0.15, rapid activity; S_{mf} 1.6–2.3, mean V_f 1.5, slow activity; $S_{mf} \geq 2.5$, V_f 1.7–2.5, minimal activity; and S_{mf} 2.6–4.0, mean V_f 7.4, inactive. This classification allows a comparison between faults with different relative tectonic rates and corresponding geomorphic expression. Because the indices record undated Quaternary fault activity expressed by geomorphology, the classes also correspond to a Quaternary tectonic rate and not necessarily to a modern tectonic rate comparable with geodetic measurements. It should also be remembered that the schemes were developed using faults in arid areas of the western USA where tectonic landforms are preserved for longer than in humid areas (e.g. Bull 1978), meaning faults in the tropics will generally be classified as tectonically 'slower' than equivalent faults at higher latitudes.

We analysed both S_{mf} and V_f for a total of 111 segments from 24 fault systems across the study area (Fig. 2a–r, Table 2) and found a good correlation between S_{mf} and V_f (Fig. 3), supporting the reliability of each method. A previous study of geomorphic indices along a segment of the Palu–Koro Fault (Vecchiotti 2008) obtained similar results to those presented here. However, we used these indices only as a simple quantitative means to support other evidence for Quaternary fault activity and did not classify faults on the basis of these data alone.

Sulawesi

Sulawesi lies at the triple junction between the Australian, Eurasian and Philippine Sea plates (e.g. Hamilton 1979; Silver *et al.* 1983*a*, *b*; Hall 1996). North of Sulawesi, the Celebes Sea is being subducted beneath Sulawesi (e.g. Hamilton 1979; Silver *et al.* 1983*a*). Convergence across the subduction margin increases from 20 ± 4 mm a^{-1} in the east to 54 ± 10 mm a^{-1} in the west, associated with a clockwise rotation of about 4° Ma^{-1} about a pole close to Manado (Walpersdorf *et al.* 1998; Rangin *et al.* 1999; Stevens *et al.* 1999; Beaudouin *et al.* 2003). Immediately east of Sulawesi's north 'arm', convergence between the Philippine Sea plate and Sundaland is partly accommodated by the Molucca Sea double subduction and the overlying Sangihe and Halmahera thrusts (e.g. Rangin *et al.* 1999; Hall 2002; Beaudouin *et al.* 2003).

Despite its setting within a collisional orogen, Sulawesi is subject to widespread and young extension. Tomini Bay encloses a deep, enigmatic basin containing up to 10 km of late Cenozoic sediments (Jablonski *et al.* 2007; Pholbud *et al.* 2012). Medium- to high-K Pliocene to modern volcanism in the Togian Islands within the bay results from Pliocene to Recent extension (Cottam *et al.* 2011) and onshore metamorphic core complexes are in the process of being exhumed by processes related to crustal thinning (Kavalieris *et al.* 1992; van Leeuwen *et al.* 2007; Spencer 2011).

Active strike-slip faults (e.g. Bellier *et al.* 2001), with left-lateral slip rates of up to 39 mm a^{-1} (Socquet *et al.* 2006), characterize much of Sulawesi's onshore Quaternary deformation. Often considered to result from NW-directed collision between the Sula platform and Sulawesi (e.g. Silver *et al.* 1983*b*; Simandjuntak 1986), modern reconstructions emphasize the process of subduction hinge rollback related to the substantial amounts of oceanic crust that have been, and continue to be, subducted around Sulawesi (e.g. Spakman & Hall 2010; Hall 2012). The occurrence of Late Miocene to apparently modern north–south-directed continental extension (e.g. Spencer 2011) in a broad region adjacent to the south-directed Celebes Sea subduction means that a rollback mechanism must be considered.

Palu–Koro Fault

The Palu–Koro Fault (Fig. 4) is the most prominent active fault of Sulawesi and is of particular importance because it is straddled by Palu city (population 340 000). The Palu–Koro Fault appears to pass from the SW corner of the Celebes Sea to a diffuse termination onshore at the northern end of Bone Bay, a distance of 500 km, of which 220 km is onshore.

The fault's tectonic role is disputed: sinistral shear along a joint Palu–Koro–Matano Fault system has been thought to accommodate clockwise rotation and the northwards movement of a rigid

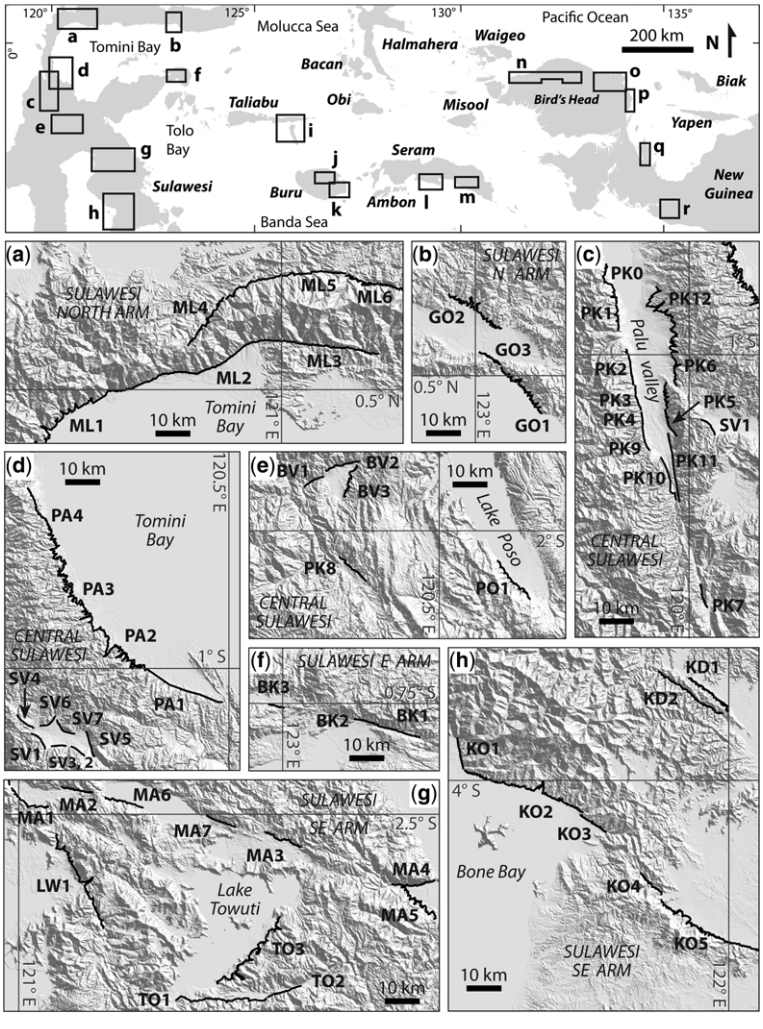

Fig. 2. Maps showing fault segments analysed for geomorphic indices. Index map at top. Bold lines are the sinuous mountain front trace (L_s) used in mountain front sinuosity calculations. Base map is a 90 m SRTM digital elevation model. All maps (a–r) drawn to the same scale. Fault segment codes correspond to the codes used in Table 2.

eastern Sulawesi block driven by collision of the Banggai–Sula block in the east (e.g. Hamilton 1979; Silver *et al.* 1983*b*; Beaudouin *et al.* 2003). However, it is significant that the Palu–Koro Fault and the North Sulawesi Trench form the western and northern limits, respectively, of a region of late Cenozoic extreme continental extension that includes deep sedimentary basins (e.g. Jablonski *et al.* 2007; Pholbud *et al.* 2012), exhumation of the mid- to lower crust in settings similar to metamorphic core complexes (e.g. van Leeuwen *et al.* 2007; Watkinson 2011), exhumed low-angle normal faults (Spencer 2011) and decompression-related mantle melts (Cottam *et al.* 2011). These features can be associated with the overriding plate above a retreating subduction hinge, particularly in the early stages of continent–continent collision (Royden 1993). The orientation and kinematics of the Palu–Koro Fault are compatible with an interpretation that it is passively bounding a region of lithospheric extension driven by northwards rollback in the Celebes Sea, although it is unclear whether there is a hard linkage between the fault and the trench.

It is not disputed that the fault is an active zone of high strain. Geodetic measurements suggest a 39 mm a^{-1} sinistral slip rate together with 11–14 mm a^{-1} of extension (Socquet *et al.* 2006),

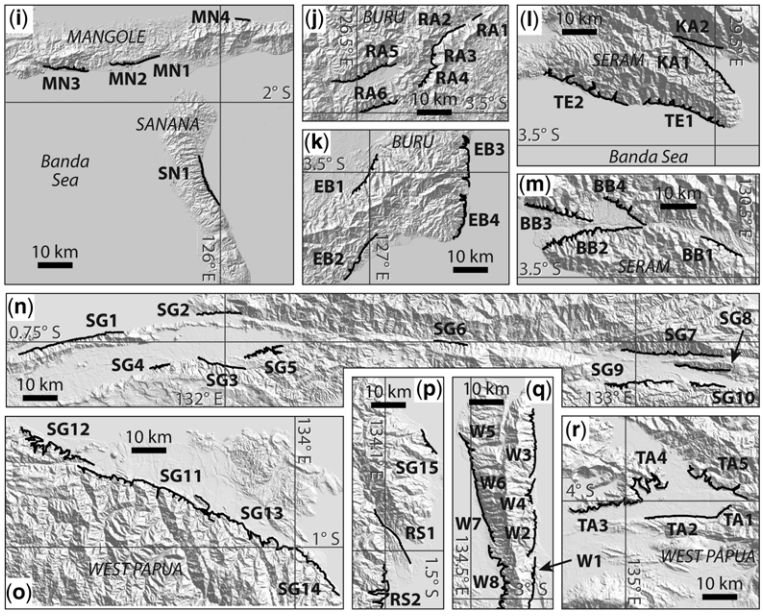

Fig. 2. *Continued.*

consistent with a 35 ± 8 mm a^{-1} strike-slip rate determined from displaced alluvial fans 11 000 $\pm$ 2300 years old (Bellier *et al.* 2001).

There is palaeoseismic evidence for three M_w 6.8–8.0 earthquakes during the last 2000 years, suggesting a recurrence interval of about 700 years (Beaudouin 1998; Bellier *et al.* 1998). However, even allowing for 10 m slip for each M_w 6.8–8.0 event, the resultant 30 m total displacement in 2000 years is less than the 54–86 m predicted from Holocene slip rates (Bellier *et al.* 2001). Although it has been proposed by these earlier researchers that the deficit is accommodated by aseismic creep, it is equally possible that large, undetected earthquakes occurred on unobserved fault strands and that the total recurrence interval for all the Palu–Koro Fault strands is much less than 700 years. Socquet *et al.* (2006) proposed four parallel strands across a zone *c.* 50 km wide, locked at depths between 0 and 5 km.

Records of historical seismicity in Sulawesi are poor. Damaging earthquakes occurred along the Palu–Koro Fault in 1905, 1907, 1909, 1927, 1934, 1968 (*c.* M_s 6.7), 1985 and 1993 (*c.* M_s 5.7) (Katili 1970; Hamilton 1979; Beaudouin 1998), but little detail is known. Large earthquakes close to the fault zone occurred in 1996 (M_w 7.7) and 1998 (M_w 6.6 and 6.0); the former caused a 2–4 m high tsunami in the Toli Toli region (Pelinovsky *et al.* 1997). However, these earthquakes originated offshore, did not clearly lie on the active Palu–Koro Fault and none had a focal mechanism indicating left-lateral slip along the Palu–Koro trend.

The Palu–Koro Fault has the clearest geomorphological expression of any eastern Indonesian fault. It occupies a steep-sided, narrow valley along much of its path through central Sulawesi, before branching into the Palu valley, which is up to 15 km wide (Fig. 5a). Two prominent scarps bound the valley and form the base of mountains that rise to >2.3 km elevation. The western scarp is highly linear, particularly the remarkable central segments *c.* 15 km south of Palu city. Mountain front sinuosity values are consistently low at 1.08–1.09, indicating maximal tectonic activity, increasing to 1.28–1.56 at the northern and southern ends of the valley, indicating rapid to moderate tectonic activity (Fig. 5a). The valley floor curvature is generally correspondingly tight, with an average V_f of 0.24 along the western scarp.

Features such as prominent triangular facets, hanging valleys and steep-sided, deeply incised streams are also focused along the central western basin-bounding segment (Fig. 5b). These landforms support dominantly rapid normal faulting along the basin margin faults. Wine glass canyons, in particular, indicate that the tectonic subsidence/uplift rate is faster than erosion. Lateral offset of the alluvial fans and rivers across the mountain front have been observed, notably in the northern and southern segments of the fault system (e.g. Hamilton 1979; Bellier *et al.* 2006).

Table 2. *Summary of measurements of mountain front sinuosity and average valley width to height ratio for analysed fault segments*

Fault	Segment	L_{mf}*	$L_s^{\dagger}$	$S_{mf}^{\ddagger}$	Ave. $V_f^{\S}$	Figure 2$^{\|\|}$	Fault	Segment	L_{mf}*	$L_s^{\dagger}$	$S_{mf}^{\ddagger}$	Ave. $V_f^{\S}$	Figure 2$^{\|\|}$
Malino boundary	ML1	45.16	27.17	1.66	1.01	a	Kolaka	KO1	8.79	8.38	1.05	1.25	h
Malino boundary	ML2	52.00	49.60	1.05	0.33	a	Kolaka	KO2	52.12	33.80	1.54	1.12	h
Malino boundary	ML3	28.79	27.53	1.05	0.64	a	Kolaka	KO3	10.07	8.24	1.22	1.68	h
Malino boundary	ML4	22.99	16.08	1.43	0.29	a	Kolaka	KO4	10.25	7.91	1.30	0.23	h
Malino boundary	ML5	38.22	33.86	1.13	0.22	a	Kolaka	KO5	49.44	30.21	1.64	1.19	h
Malino boundary	ML6	27.41	17.27	1.59	0.29	a		**Average**			**1.35**	**1.09**	
	Average			**1.32**	**0.46**		Mangole	MN1	7.07	6.33	1.12	0.49	i
Gorontalo	GO1	33.24	16.37	2.03	0.88	b	Mangole	MN2	9.64	6.60	1.46	0.49	i
Gorontalo	GO2	39.29	16.64	2.36	1.27	b	Mangole	MN3	18.96	12.08	1.57	0.55	i
Gorontalo	GO3	12.03	6.58	1.83	1.69	b	Mangole	MN4	4.56	3.86	1.18	N/A	i
	Average			**2.07**	**1.28**		Sanana	SN1	2.45	1.93	1.27	0.44	i
Palu–Koro	PK0	16.94	10.99	1.54	0.31	c		**Average**			**1.32**	**0.49**	
Palu–Koro	PK1	8.94	6.60	1.35	0.22	c	Rana	RA1	2.86	2.83	1.01	0.35	j
Palu–Koro	PK2	10.48	9.64	1.09	0.29	c	Rana	RA2	3.68	3.12	1.18	0.23	j
Palu–Koro	PK3	7.24	6.69	1.08	0.21	c	Rana	RA3	8.19	7.73	1.06	0.18	j
Palu–Koro	PK4	4.33	3.99	1.09	0.19	c	Rana	RA4	20.19	10.31	1.96	1.53	j
Palu–Koro	PK5	9.43	7.90	1.19	0.99	c	Rana	RA5	24.35	18.31	1.33	0.28	j
Palu–Koro	PK6	11.02	6.91	1.59	0.35	c	Rana	RA6	15.49	10.40	1.49	0.68	j
Palu–Koro	PK7	7.15	6.44	1.11	0.56	c	East Buru	EB1	18.09	12.56	1.44	0.47	k
Palu–Koro	PK8	10.78	9.61	1.12	0.89	e	East Buru	EB2	18.61	15.08	1.23	0.50	k
Palu–Koro	PK9	9.72	6.22	1.56	0.20	c	East Buru	EB3	26.93	12.53	2.15	1.13	k
Palu–Koro	PK10	16.34	12.80	1.28	1.10	c	East Buru	EB4	25.16	12.62	1.99	0.75	k
Palu–Koro	PK11	27.15	19.02	1.43	0.32	c		**Average**			**1.48**	**0.61**	
Palu–Koro	PK12	64.23	27.88	2.30	0.80	c	Southern Seram	TE1	42.32	23.05	1.84	1.88	l
	Average			**1.36**	**0.47**		Southern Seram	TE2	49.68	23.89	2.08	1.36	l
Parigi boundary	PA1	69.67	21.44	3.25	0.90	d		**Average**			**1.96**	**1.62**	
Parigi boundary	PA2	72.43	26.17	2.77	0.78	d	Kawa	KA1	27.55	20.75	1.33	0.28	l
Parigi boundary	PA3	62.33	19.92	3.13	1.45	d	Kawa	KA2	15.16	13.76	1.10	0.26	l
Parigi boundary	PA4	17.86	13.48	1.32	0.50	d		**Average**			**1.21**	**0.27**	
	Average			**2.62**	**0.91**		Bobol	BB1	14.59	11.61	1.26	1.57	m
Sapu valley	SV1	6.17	5.67	1.09	0.40	d	Bobol	BB2	51.83	26.37	1.97	2.60	m
Sapu valley	SV2	3.64	3.38	1.08	N/A	d	Bobol	BB3	35.56	17.84	1.99	1.44	m
Sapu valley	SV3	4.99	3.90	1.28	N/A	d	Bobol	BB4	23.05	12.73	1.81	1.04	m
Sapu valley	SV4	6.30	5.60	1.13	N/A	d		**Average**			**1.76**	**1.66**	
Sapu valley	SV5	6.89	4.74	1.45	N/A	d	Sorong	SG1	33.89	28.77	1.18	1.15	n
Sapu valley	SV6	4.67	3.78	1.24	N/A	d	Sorong	SG2	13.90	11.94	1.16	1.54	n
Sapu valley	SV7	5.27	3.84	1.37	N/A	d	Sorong	SG3	15.11	13.16	1.15	0.48	n
	Average			**1.23**	**0.40**		Sorong	SG4	8.54	5.35	1.60	0.59	n

Bada valley	BV1	5.97	5.73	1.04	0.57	e	Sorong	SG5	29.39	10.53	2.79	4.90	n
Bada valley	BV2	10.09	9.47	1.07	0.36	e	Sorong	SG6	10.19	8.94	1.14	0.27	n
Bada valley	BV3	13.27	9.30	1.43	0.73	e	Sorong	SG7	36.50	27.47	1.33	0.45	n
	Average			**1.18**	**0.55**		Sorong	SG8	17.73	14.83	1.20	0.44	n
Poso area	PO1	18.15	13.74	1.32	0.29	e	Sorong	SG9	31.90	18.34	1.74	1.33	n
	Average			**1.32**	**0.29**		Sorong	SG10	15.44	9.57	1.61	0.40	n
Balantak	BK1	13.02	11.80	1.10	0.25	f	Sorong	SG11	65.53	40.33	1.62	0.42	o
Balantak	BK2	6.85	6.59	1.04	0.47	f	Sorong	SG12	62.92	22.04	2.85	5.10	o
Balantak	BK3	5.16	4.24	1.22	N/A	f	Sorong	SG13	54.48	30.12	1.81	8.68	o
	Average			**1.12**	**0.36**		Sorong	SG14	22.17	17.39	1.27	0.32	o
Matano	MA1	15.06	11.78	1.28	1.12	g	Sorong	SG15	11.44	7.61	1.50	0.49	p
Matano	MA2	9.21	8.66	1.06	0.25	g		**Average**			**1.60**	**1.77**	
Matano	MA3	12.54	10.57	1.19	0.45	g	Ransiki	RS1	18.83	17.71	1.06	N/A	p
Matano	MA4	12.56	11.63	1.08	0.23	g	Ransiki	RS2	31.31	11.87	2.64	N/A	p
Matano	MA5	23.51	12.35	1.90	0.79	g		**Average**			**1.85**	**N/A**	
Matano	MA6	12.34	10.52	1.17	0.72	g	Wandaman boundary	WM1	17.22	13.76	1.25	N/A	q
Matano	MA7	8.46	8.31	1.02	0.84	g	Wandaman boundary	WM2	15.55	12.08	1.29	N/A	q
	Average			**1.24**	**0.63**		Wandaman boundary	WM3	23.73	18.57	1.28	N/A	q
Kendari	KD1	24.61	14.03	1.75	0.52	h	Wandaman boundary	WM4	11.58	6.74	1.72	N/A	q
Kendari	KD2	24.62	20.42	1.21	0.58	h	Wandaman boundary	WM5	19.75	13.83	1.43	N/A	q
	Average			**1.48**	**0.55**		Wandaman boundary	WM6	9.84	9.33	1.05	N/A	q
Lawanopo	LW1	43.13	28.29	1.52	0.83	g	Wandaman boundary	WM7	9.99	7.80	1.28	N/A	q
	Average			**1.52**	**0.83**		Wandaman boundary	WM8	45.67	19.61	2.33	N/A	q
Towuti bounding	TO1	27.98	24.39	1.15	0.41	g		**Average**			**1.45**	N/A	
Towuti bounding	TO2	9.58	9.30	1.03	0.56	g	Tarera–Aiduna	TA1	6.11	5.05	1.21	N/A	r
Towuti bounding	TO3	51.16	25.10	2.04	1.22	g	Tarera–Aiduna	TA2	20.74	19.19	1.08	N/A	r
	Average			**1.41**	**0.73**		Tarera–Aiduna	TA3	32.26	19.75	1.63	N/A	r
							Tarera–Aiduna	TA4	38.83	8.48	4.58	N/A	r
							Tarera–Aiduna	TA5	35.31	18.46	1.91	N/A	r
								Average			**2.08**	**N/A**	

*Straight line length of mountain front.
†Sinuous length of mountain front.
‡Mountain front sinuosity ($S_{mf} = L_{mf}/L_s$).
§Average valley floor width to valley depth ratio ($V_f = 2V_{fw}/(E_{ld} - E_{sc}) - (E_{rd} - E_{sc})$, where V_{fw} is the valley floor width, E_{ld} and E_{rd} are the topographic elevations of the left and right valley watersheds and E_{sc} is the elevation of the valley floor).
||Location of sinuosity segment on Figure 2.

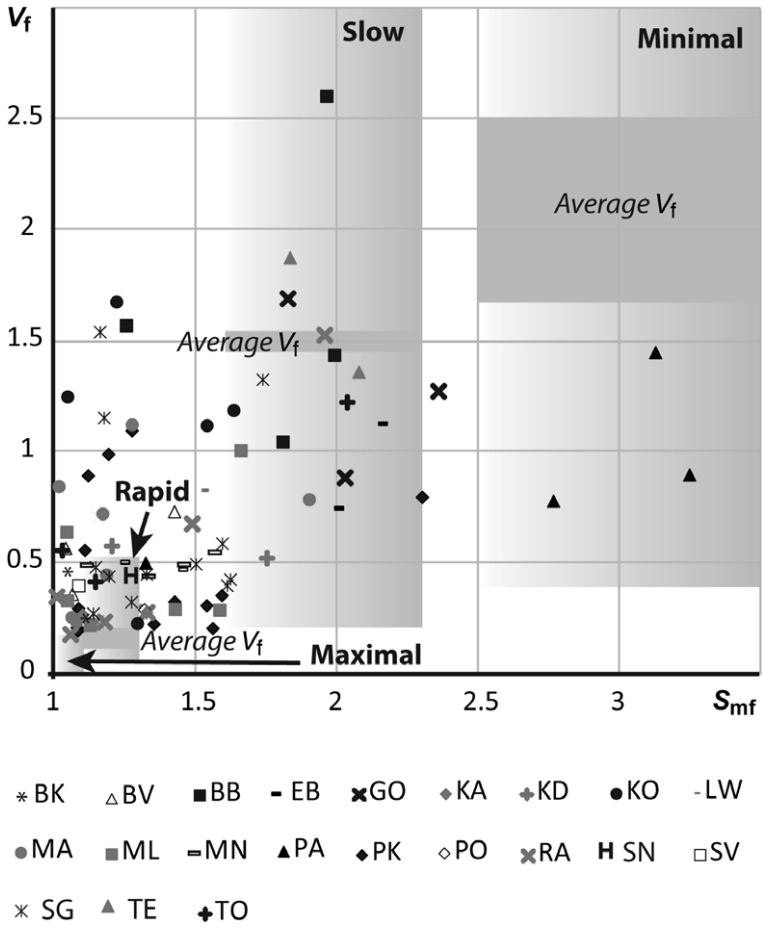

Fig. 3. Graph of mountain front sinuosity (S_{mf}) v. valley floor width to valley height index (V_f) for studied faults. Grey boxes indicate tectonic activity rates, after McCalpin (2009), with average V_f marked by the darker grey bar. BB, Bobol Fault; BK, Balantak Fault; BV, Bada valley faults; EB, East Buru faults; GO, Gorontalo Fault; KA, Kawa Fault; KD, Kendari faults; KO, Kolaka Fault; LW, Lawanopo Fault; MA, Matano Fault; ML, Malino boundary faults; MN, Mangole faults; PA, Parigi faults; PK, Palu–Koro Fault; PO, Poso faults; RA, Rana Fault; SG, Sorong Fault; SN, Sanana faults; SV, Sapu valley faults; TE, Southern Seram faults; TO, Towuti faults.

A 5° releasing bend/step-over is required to link the southern segments of the Palu–Koro Fault, where it emerges from its narrow valley at Pakuli, with the northern segments NW of Palu city. In analogue models and other non-linear strike-slip faults, such releasing geometries are often associated with well-defined oblique-normal sidewall faults and a cross-basin fault system with a more subtle surface expression that accommodates most of the strike-slip strain (e.g. Mann *et al.* 1995; Mann 2007; Wu *et al.* 2009) (Fig. 6a inset).

Analysis of Palu River channels since 2003 from satellite imagery and the pattern of older filled oxbow lakes on the valley floor indicates that long reaches of the river rarely deviate from a linear path directly along-strike from the strike-slip fault where it enters the Palu valley in the south (Fig. 6a, b). Many meanders have a square aspect with linear longitudinal segments parallel to the projected fault (Fig. 6c). In the south of the valley a linear braided reach is similarly parallel to the projected fault; individual braid channels are anomalously linear (Fig. 6d). Strands of the Palu–Koro Fault cutting an alluvial fan and offsetting its incised drainage directly along-strike to the south confirm that the river is structurally controlled. It is more reasonable to project this southern fault strand directly north across the basin than it is to consider strike-slip strain transferring immediately to the western sidewall fault between Pakuli and Bolongga, particularly as

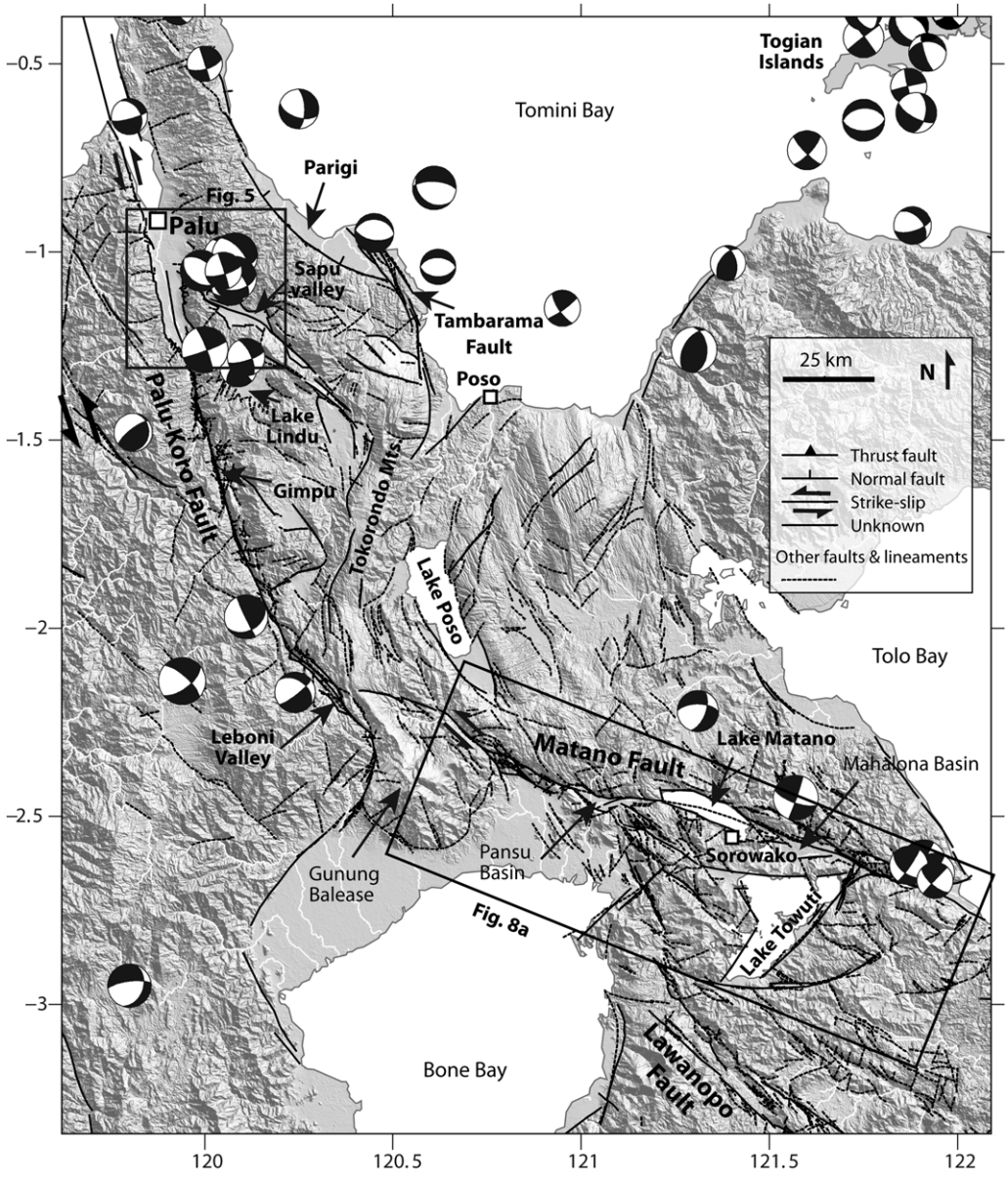

Fig. 4. Central Sulawesi overview digital elevation model (SRTM), CMT catalogue earthquakes <35 km depth and structures that show geomorphic evidence of Quaternary tectonic activity. Rivers marked in white. Illumination from NE. Location shown in Figure 1.

geomorphic indices in that region indicate a relatively low tectonic rate (Fig. 5a).

Thus we propose that much of the Palu–Koro Fault strike-slip strain through the Palu valley is not accommodated on the prominent sidewall faults, but on a cross-basin fault system that is obscured by fluvial deposits during interseismic periods (as it is now) (Figs 5a & 6a). The sidewall faults are largely an extensional partition, explaining the lateral slip deficit across them, noted by Bellier *et al.* (2001). Confinement of the Palu River meander belts within the strike-slip cross-basin fault system may be due to the development of a subtle graben, or to changes in permeability, cementation or compaction in the

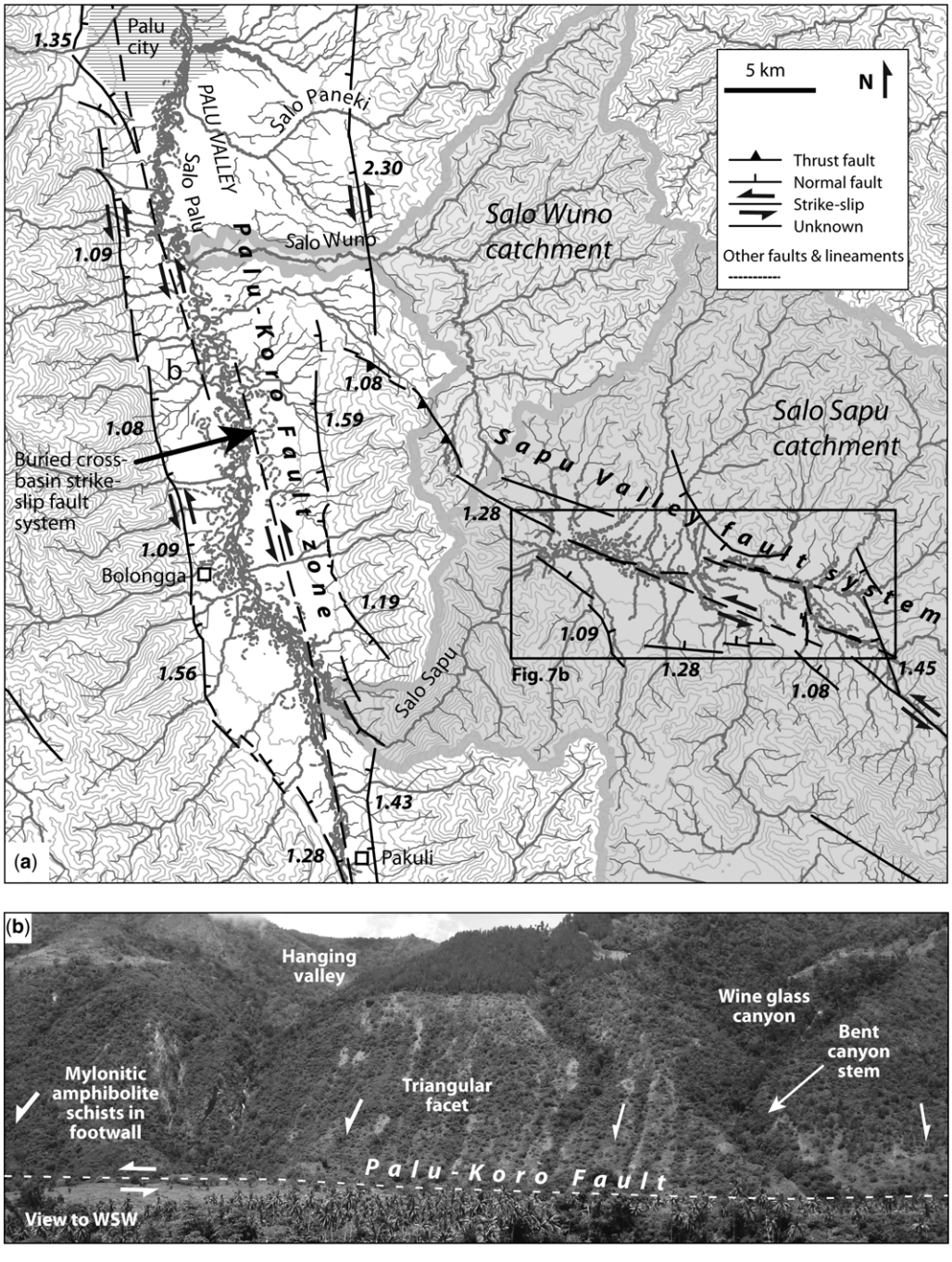

Fig. 5. (**a**) The Palu and Sapu valleys showing structures that with geomorphic evidence of Quaternary tectonic activity, plus topography and drainage. Mountain front sinuosity values in bold italic text. For location, see Figure 4. Major drainage basins for Salo Sapu and Salo Wuno are marked, separated by uplift at the western end of the Sapu valley fault system. (**b**) View of the Palu–Koro Fault scarp from the Palu valley, showing geomorphic evidence of Quaternary tectonic activity.

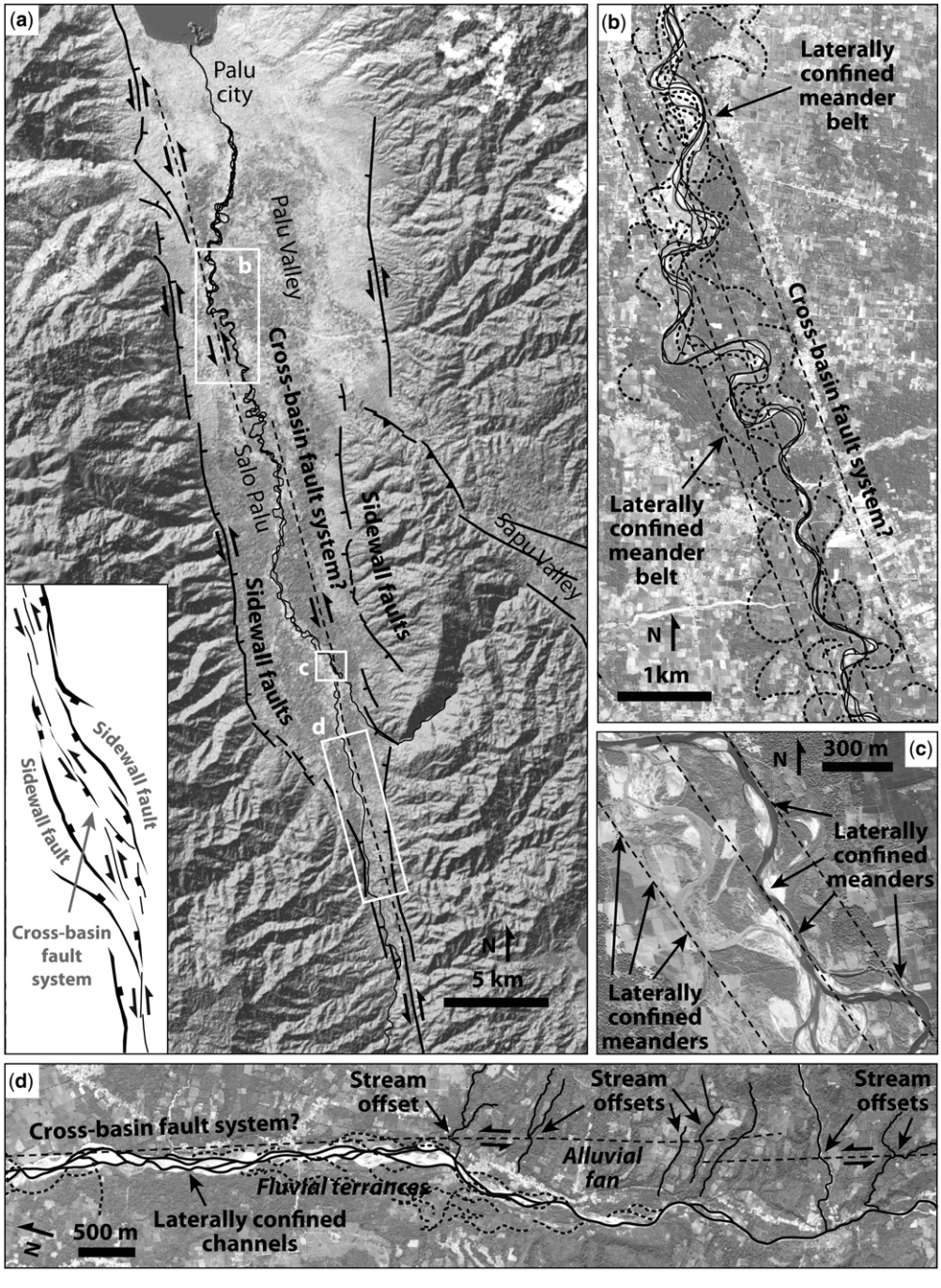

Fig. 6. Evidence of a cross-basin fault system within the Palu valley Quaternary fill. (**a**) Overview ASTER digital elevation model draped with ESRI imagery layer. Illumination from NW. Palu River channels traced from six separate images from 2003 to 2015. Inset shows fault pattern developed in an analogue model of a releasing bend, modified after Wu *et al.* (2009), reflected and rotated to mimic the Palu valley. Sidewall faults and cross-basin fault system are highlighted in the model and on the satellite imagery. (**b**, **c**) Laterally confined meander belts, interpreted as representing minor subsidence within the cross-basin fault system. (**d**) Laterally confined river channels directly along-strike from a Palu–Koro Fault strand seen to offset alluvial fans in the south of the valley. (**c**, **d**, **e**) show ESRI imagery.

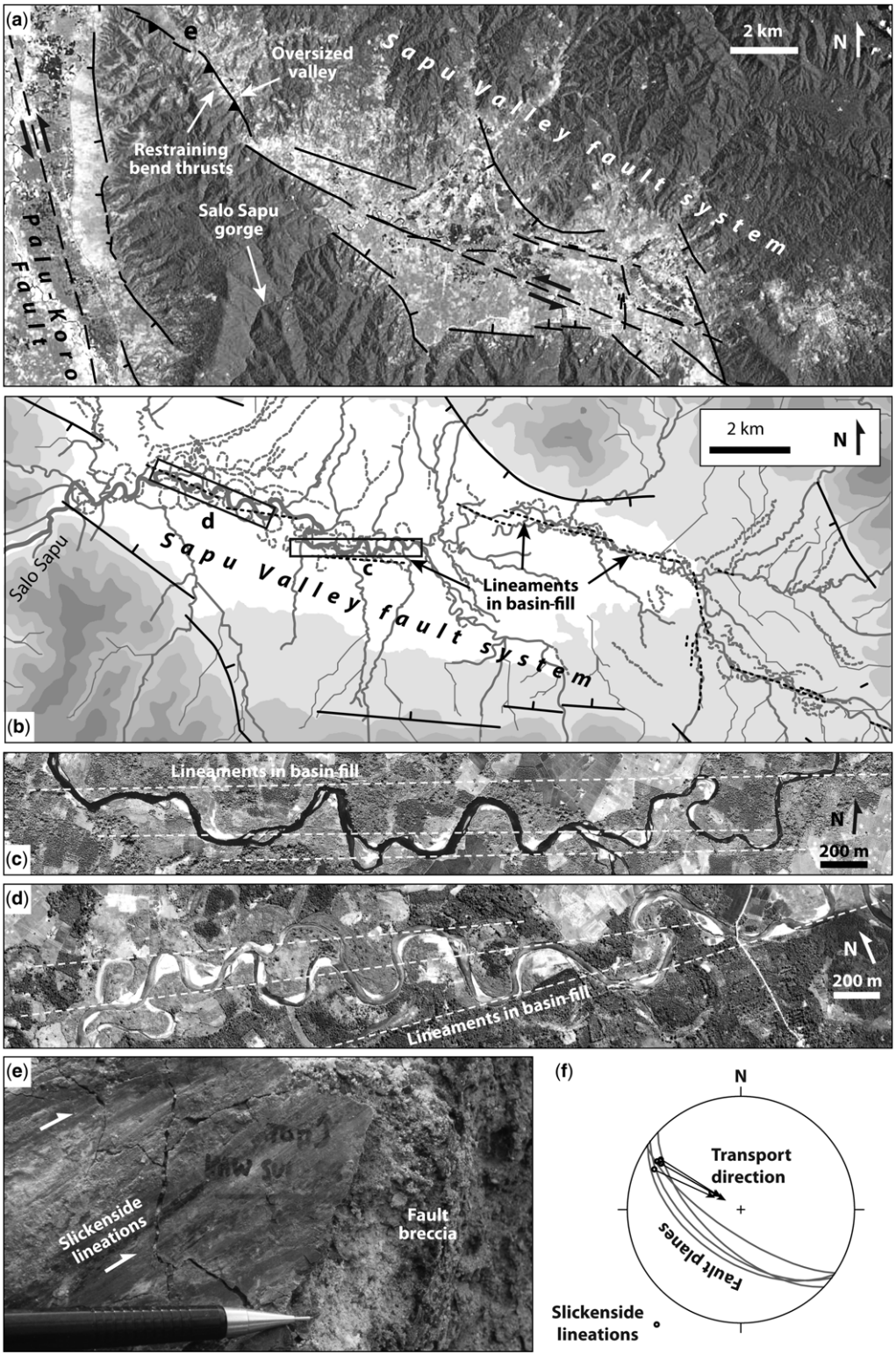

Quaternary valley-fill resulting from penetration by strike-slip strands.

The valley's eastern sidewall fault is generally much more segmented and strongly eroded than in the west, with gentle slopes and irregular mountain fronts (Fig. 6a). South of the intersection with the Sapu valley fault system, S_{mf} values are 1.19–1.59 and V_f averages of 0.55 indicate rapid to moderate tectonic activity. North of the Sapu valley intersection, S_{mf} is 2.30 and the average V_f is 0.80, indicating slow tectonic activity.

Further south along the Palu–Koro Fault, the Gimpu basin exists at a small releasing step-over and the Leboni basin occupies a releasing bend near the southern termination of the fault (Fig. 4). The Palu–Koro Fault bounding these flat-topped Quaternary basins has S_{mf} values of 1.11 and 1.12, respectively, and similarly low V_f values of 0.56 and 0.89, indicating rapid to moderate tectonic activity.

Sapu valley fault system

A complex NW–SE-trending, 75 km long fault system cuts across crystalline basement between Palu valley and the Tokorondo Mountains in the east (Fig. 4). The fault system is dominated by a double bend: a releasing bend forming the intermontane Sapu valley (*c.* 600 m elevation) and a restraining bend associated with uplift at the head of the valley (Fig. 5a). Both bends are consistent with an overall left-lateral shear sense for the fault system. Anecdotal reports from residents of the valley (various, pers. comm. 2009) suggest that earthquakes are frequent and well known, although there is little instrumental seismicity and no record of historical earthquakes.

Sapu valley is an irregular rhomboidal basin bounded by normal faults trending NNE–SSE and east–west (Fig. 7a). Many of the faults are arcuate, convex into the basin. Their range front slopes are generally gentle, but S_{mf} values of 1.09–1.45 and an average V_f of 0.40 suggest rapid to moderate tectonic activity (Fig. 7b). A conspicuous feature of the basin floor is the strong confinement of river channels to narrow linear meander belts (Fig. 7b), as discussed earlier for the Palu River. Both modern and abandoned channels have linear meander belt margins and square longitudinal sections parallel to the projected trace of the fault system through the valley, implying fault penetration through the Quaternary basin-fill (Fig. 7c, d). In the same way as for the Palu valley, this evidence supports a cross-basin fault system that accommodates most of the strike-slip strain, whereas the prominent sidewall faults are dominantly extensional structures. The cross-basin fault system is buried by fluvial sediments, but co-seismic subsidence, or changes in permeability, cementation or compaction caused by periodic surface rupture through the Quaternary basin-fill continue to influence the meander patterns.

At the head of the valley the entire fault system curves to a more NNW–SSE trend – a restraining geometry under sinistral shear. A broad, oversized valley in the west is presently at 700 m elevation (Fig. 7a), i.e. 100 m above the modern Sapu valley floor. Exhumed brittle SW-dipping reverse-sinistral faults in mica schists along the uplifted valley support long-lived uplift at this restraining bend (Fig. 7e, f). At the foot of the westernmost oblique-reverse fault, S_{mf} is 1.08, suggesting maximal tectonic activity (Fig. 5a).

Drainage networks extracted from SRTM data show that there is presently a drainage divide separating the Salo Wuno and Salo Sapu catchment basins at the position of the thrust-related uplift and oversized valley (Fig. 5a). Water presently exits Sapu valley via a narrow, steep-sided gorge (Fig. 7a). The extreme steepness and geomorphic immaturity of that gorge suggests that it has recently captured the Sapu valley drainage, perhaps in response to tectonic uplift of its former well-established route to the NW via Salo Wuno. It is likely that the Sapu valley was internally drained for some time after uplift in the NW and may have contained an intermontane lake similar to Lake Lindu to the south (Fig. 4), explaining the flat base of the Sapu valley.

Four lines of evidence suggest the Sapu valley fault system has been active during the Quaternary: (1) control of the modern river meander belts by a cross-basin fault system that traverses the Quaternary basin-fill; (2) youthful geomorphic expression of the Salo Sapu gorge where it has recently captured the Salo Sapu drainage in response to tectonic uplift in the NW; (3) rapid to moderate tectonic activity along the transtensional segment sidewall faults, indicated by geomorphic indices; and (4) maximal tectonic activity along the transpressional

Fig. 7. Details of the Sapu valley fault system. (**a**) ESRI imagery of the Sapu and central Palu valleys showing major structural and geomorphic features, particularly the releasing–restraining double bend and re-routing of axial drainage from the NW valley to the Salo Sapu gorge. (**b**) Detail of the Sapu valley showing drainage and highlighting fault control of the axial river. Location shown on Figure 5a. (**c**, **d**) Laterally confined meander belts and lineaments, interpreted as representing minor subsidence within the cross-basin fault system. (**e**) Lineated slickenside surface from an exhumed fault core within the Sapu restraining bend. Location shown in Figure 7a. (**f**) Lower hemisphere stereographic projection of fault planes (great circles) and slickenside lineations (points) from the fault shown in Figure 7e. ESRI imagery.

segment's reverse faults implicated in uplifting the oversized palaeovalley in the east, indicated by geomorphic indices.

Matano Fault

The Matano Fault passes from southern central Sulawesi through the island's SE arm to Tolo Bay (Fig. 4). It is typically shown to mark the southern edge of the Sula Block, linking to the Palu–Koro Fault to the west and the North Sulawesi Trench to the north (e.g. Hamilton 1979; Rangin *et al.* 1999). A hard linkage between either the Lawanopo or Matano and Palu–Koro faults is a requirement of many rigid-block models for Sulawesi (e.g. Bellier *et al.* 2006; Socquet *et al.* 2006). However, Silver *et al.* (1983*b*) noted that the nature of the connection was not known. Modern satellite imagery shows a highly segmented and discontinuous westernmost Matano Fault curving towards the Palu–Koro Fault, but the two structures remain largely isolated either side of the Gunung Balease massif (Fig. 4).

In the east, the Matano Fault passes into the northern Banda Sea. Some workers link it to the Tolo Thrust (sometimes referred to as the Hamilton Thrust or the East Sulawesi Trench) (Fig. 1), an ESE-verging thrust zone NE of Buton. Silver *et al.* (1983*b*) suggest that the Matano and Palu–Koro faults act as a trench–trench transform between the north Sulawesi subduction and the Tolo Thrust. This thrust has been considered to accommodate convergence between the Makassar block and the Banda Sea block (e.g. Socquet *et al.* 2006). However, recent work suggests that the Tolo Thrust is a gravity-driven feature at the foot of a series of slumps (Rudyawan 2011), rather than a structure bounding a tectonic block (e.g. Silver *et al.* 1983*b*; Rangin *et al.* 1999).

Geological offsets (e.g. Ahmad 1978) and stream offsets (e.g. Hamilton 1979) across the Matano Fault confirm that it is a left-lateral structure and that it has been active during the Quaternary (Bellier *et al.* 2006). Laterally offset streams are routinely used to assess the shear sense and Quaternary activity of strike-slip faults, usually in arid environments (e.g. Sieh & Jahns 1984), but also in humid, forested environments (e.g. Lacassin *et al.* 1998; Wang *et al.* 2014). Nonetheless, such observations must be interpreted cautiously, as stream offset may result from stream diversion along a fault and capture by another downstream reach, as well as by the genuine tectonic displacement of a single stream (Wallace 1990). No study has used such offsets to evaluate Quaternary slip rates along the Matano Fault.

The Matano Fault is highly segmented and lacks a single through-going strand (Fig. 8a). Several linear basins (e.g. Pansu, Matano and Mahalona) lie within or adjacent to the fault zone, often at stepovers between strands. Each basin is 4–6 km wide and 20–30 km long. The Matano basin hosts Lake Matano, which, at 590 m deep (Haffner *et al.* 2001), is the deepest lake in Indonesia and the tenth deepest lake in the world. A fault passing from the northern margin of the Pansu Basin is very prominent as it cuts through ultramafic rocks in the SW corner of Lake Matano, just south of Desa Matano (Fig. 8a). The fault then steps to the left to another very prominent fault in the NW of the lake, from where it passes across the northern margin of the Mahalona Basin. Rapid subsidence in the lake and earthquake focal mechanisms recording east–west extension close to the lake probably result from this releasing geometry (McCaffrey & Sutardjo 1982). Two major pop-ups associated with the uplift, thrusting and exhumation of metamorphic rocks and serpentinite at restraining bends occur east of the Mahalona Basin and west of the Pansu Basin (Fig. 8a).

A number of consistent left-lateral stream offsets, evidence of stream capture across two fault strands west of Pansu Basin (Fig. 8b) and steep-sided, narrow fault valleys (Fig. 8c) suggest youthful fault activity. Geomorphic indices of oblique basin-bounding faults range from S_{mf} 1.06–1.28, average V_f 0.69 (Pansu Basin), S_{mf} 1.02–1.17, average V_f 0.78 (Matano Basin), S_{mf} 1.19, V_f 0.45 (Mahalona Basin) to S_{mf} 1.08–1.9, average V_f 0.51 (eastern termination splay) and indicate mostly rapid to moderate tectonic activity.

On 15 February 2011, a shallow focus M_w 6.1 earthquake near the western end of Lake Matano (NEIC) had a focal mechanism consistent with left-lateral slip along the Matano Fault. The earthquake caused damage to concrete walls and buildings, including a newly built hospital in the Mahalona valley (Fig. 8d). The earthquake's location suggested that the prominent fault segment that links the NE corner of Lake Matano with the Mahalona Basin failed (Fig. 8e). 'Surface cracks' were reported by local people at the eastern end of the basin but, although we visited the area in October 2011, a surface rupture could not be located. Close to the lake, very high resolution satellite imagery recently made available (Bing Maps) shows three clear lineaments cutting across boggy ground and low-lying forest (Fig. 8f) along-strike from a Matano Fault strand that offsets drainage to the left. Although it is not possible to confirm that they represent the 2011 surface rupture, these lineaments appear to be tectonic in origin and are clearly very young. Linking these lineaments with the reported surface cracks in the east, along a topographically clearly defined fault strand, yields a postulated surface rupture length of >39 km, which is longer than expected for a M_w 6.1 earthquake from empirical relationships (Wells & Coppersmith 1994).

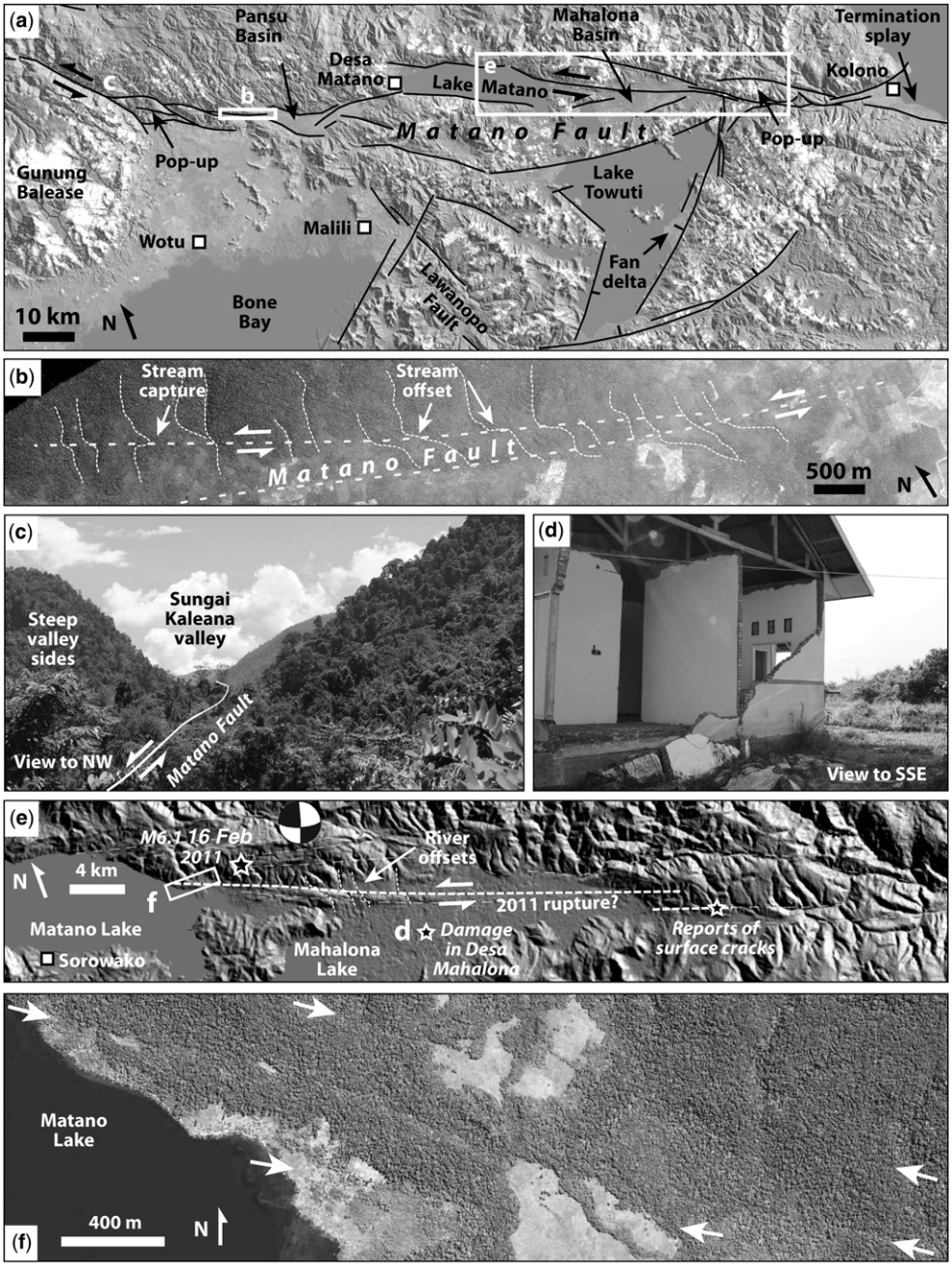

Fig. 8. Details of the Matano Fault. (**a**) Map of the Matano Fault, Lake Towuti and the northern part of the Lawanopo Fault. Base map is ASTER digital elevation model draped with ESRI imagery. Location shown in Figure 4. (**b**) Systematic stream offsets along strands of the Matano Fault west of the Pansu Basin. (**c**) Deep, steep-sided valley marking the westernmost Matano Fault NE of Gunung Balease. (**d**) Hospital in the Mahalona valley damaged during the 15 February 2011 M_w 6.1 earthquake. Location shown in Figure 8e. (**e**) Detail of the eastern Matano and Mahalona valleys, showing features related to the 2011 earthquake and inferred surface rupture extent. ASTER base map. (**f**) Imagery from Bing Maps showing strong topographic lineaments in low ground in the NE corner of Lake Matano, inferred to represent recent (2011?) surface ruptures. Location shown in Figure 8e. (**b**) and (**f**) images © 2016 DigitalGlobe.

Lawanopo Fault and Lake Towuti

The Lawanopo Fault (Fig. 4) consists of several straight NW-trending fault segments that cross Sulawesi's SE arm south of the Matano Fault. The Lawanopo Fault is used in preference to the Matano Fault by Socquet *et al.* (2006) as the southern margin of the 'East Sula Block'. However, discontinuous and eroded fault traces along strands of the Lawanopo Fault system suggest that it has been mostly inactive during the Quaternary (Bellier *et al.* 2006; Natawidjaja & Daryono 2014). Nonetheless, recent earthquakes close to Kendari may indicate that at least some strands of the Lawanopo Fault system remain active. An M_w 7.5 earthquake in the Banda Sea 170 km SE of Kendari on 19 October 2001 had a strike-slip focal mechanism and may have originated on the projected offshore trace of the Lawanopo Fault (Yeats 2010).

Like the Matano Fault, the Lawanopo Fault is highly segmented and there is no through-going strand at the surface (Fig. 4). Mountain front sinuosity values on the few segments associated with adjacent basins range from 1.21 to 1.75 and valley depth to width ratios average 0.55–0.83, indicating moderate to slow tectonic activity.

Lake Towuti, the largest of the Malili lakes, occupies an intermontane basin at 318 m elevation and has a maximum water depth of 203 m (Haffner *et al.* 2001). The basin lies in the wedge between the Matano and Lawanopo faults and is itself cut by linear fault strands that internally deform the wedge (Fig. 4). Two prominent curvilinear faults lie along the south and east of the lake (Fig. 8a). The closest, trending NE–SW and downthrown to the NW, forms the linear eastern lake boundary and is marked by a number of fans prograding into the lake. Its high mountain front sinuosity (2.04) and valley depth to width ratio (1.22) suggest slow tectonic activity. However, a large earthquake along this >25 km long structure could cause a substantial tsunami or seiche in the lake. The second fault, to the east, is longer still (>55 km) and highly continuous. It intersects the Lawanopo Fault at a small angle and may directly transfer slip away from that structure. Mountain front sinuosity ranges from 1.03 to 1.15, suggesting maximal to rapid tectonic activity, although the valley floors are rather rounded (average V_f 0.49). Lake Towuti would rapidly fill with sediment if it were not actively subsiding, therefore the bounding normal faults must be considered to be active during the Quaternary.

Kolaka Fault

The Kolaka Fault (Simandjuntak *et al.* 1984, 1994; Surono 1994) (Fig. 9a) lies along the southern margin of the Mengkoka mountains and is sub-parallel to the Lawanopo Fault to its north. It is equivalent to the Mendoke Fault of Bellier *et al.* (2006). Hamilton (1979) interpreted the fault as a SW-dipping thrust and Bellier *et al.* (2006) considered the fault as a pre-Early Pleistocene strike-slip continuation of the Palu–Koro Fault, but there is little evidence to support either hypothesis. One strand of the Kolaka Fault is sealed by 4.4 ± 0.2 Ma dacites, potentially placing a limit on the timing of faulting (White *et al.* 2014).

The fault is composed of several NE–SW-trending, gently arcuate segments up to 45 km long in map view. Along the Bone Bay coast and at Kolaka town the downthrown side is to the south and the easternmost segment is downthrown to the north (Fig. 9a). The polarity shift occurs across a 10 km wide relay straddling the Anggowala mountains. The orientation of these two apparently normal fault systems is kinematically consistent with sinistral slip along the overall Kolaka trend.

Geomorphic indices are highest closest to Kolaka town, where S_{mf} values of 1.22–1.30 and V_f values of 0.23–1.68 suggest that there is rapid to slow active dip-slip across the fault, which has a clear surface expression and is marked by triangular facets (Fig. 9c). Along-strike to the NW a series of linear valleys and low ridges near Lasusua may be a continuation of the Kolaka Fault (Fig. 9b). An absence of fault scarps or clearly displaced features makes fault activity hard to evaluate, but meander confinement within a linear graben across the Lasusua alluvial plain and asymmetrical subsidence highlighted by the river's proximity to the bounding fault suggests recent fault activity (Fig. 9d).

Faults downthrown to the WSW at the western end of the Kolaka Fault have very low S_{mf} and V_f values (1.05 and 1.25, respectively), deeply incised streams and well-developed triangular facets, suggesting Quaternary dip-slip. These faults face into Bone Bay and may be related to basin-bounding extensional structures accommodating subsidence in the bay (Camplin & Hall 2014).

Balantak Fault

A prominent ENE-trending linear structure, the Balantak Fault, lies at the eastern end of Sulawesi's east arm and separates the Batui thrust system in the south from mountainous highlands in the north (Fig. 10a). It has been considered to be part of the Batui thrust system (Silver *et al.* 1983*b*), but its remarkably straight outcrop, field observations (Simandjuntak 1986) and along-strike alternation between local uplift and subsidence suggest that it is a steep, possibly strike-slip, fault.

Onshore, where the fault bends gently to the right, small, apparently Quaternary basins are developed (Fig. 10b). There is uplift where the fault bends

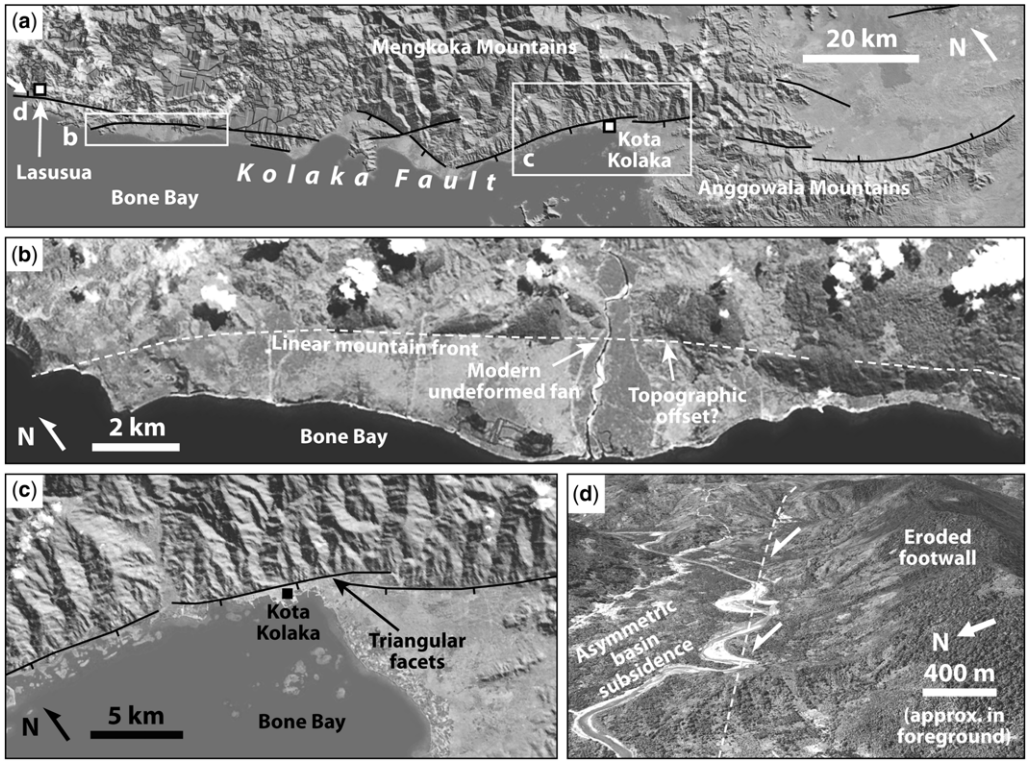

Fig. 9. Details of the Kolaka Fault. (**a**) Overview map of the main Kolaka Fault segments. Base map is ASTER digital elevation model draped with ESRI imagery. Location shown in Figure 1. (**b**) Straight segment of the Kolaka Fault associated with linear ridges and valleys. ESRI imagery. (**c**) Linear fault-bounded mountain front and triangular facets indicating Quaternary fault activity at Kolaka town. (**d**) Asymmetrical axial drainage at a splaying fault segment near the western fault termination, indicating Quaternary subsidence along the bounding fault system.

gently to the left. Both observations are kinematically compatible with a dextral shear sense. One of the zones of Quaternary subsidence is shown in Figure 10c. A basin-bounding fault at a small clockwise angle from the regional Balantak Fault trend is crossed by streams that show no systematic offset, suggesting dominant dip-slip. To the north, a prominent lineament crosses the basin, expressed by lines of vegetation and slightly darker (moister?) soil. This lineament's parallelism with the Balantak Fault to the east and its negligible topographic relief suggests it is the through-going strike-slip fault strand. Although stream avulsion across the flat-topped basin is too dynamic to preserve meaningful offsets, the clear expression of the fault in the young sediments suggests the Balantak Fault has been active during the Quaternary.

The Balantak Fault's termination system offshore to the east of Poh Head is composed of left-stepping segments separated by folds and thrusts (Fig. 10d). Contraction between left-stepping main segments, an apparently antithetic sinistral fault and the orientation of folds and thrusts are all kinematically compatible with dextral shear along the Balantak Fault (Watkinson *et al.* 2011). Earthquakes located onshore and west of Poh Head also suggest right-lateral and reverse slip parallel to the Balantak Fault (Fig. 10a). However, a swarm of offshore earthquakes between Peleng and Taliabu to the east have focal mechanisms that support sinistral slip along the Balantak trend. This apparent contradiction is discussed in Watkinson *et al.* (2011). Here we conclude that the geological and geomorphic evidence supports long-term Quaternary dextral slip. Further work is required to understand the significance of a small number of contradictory seismological signals in the area.

The Balantak Fault is almost continuous for 54 km from Balantak town in the east to Poh Bay in the west, where it probably continues just offshore for another >30 km. Extending to include the dextral fault system offshore to the SE makes the

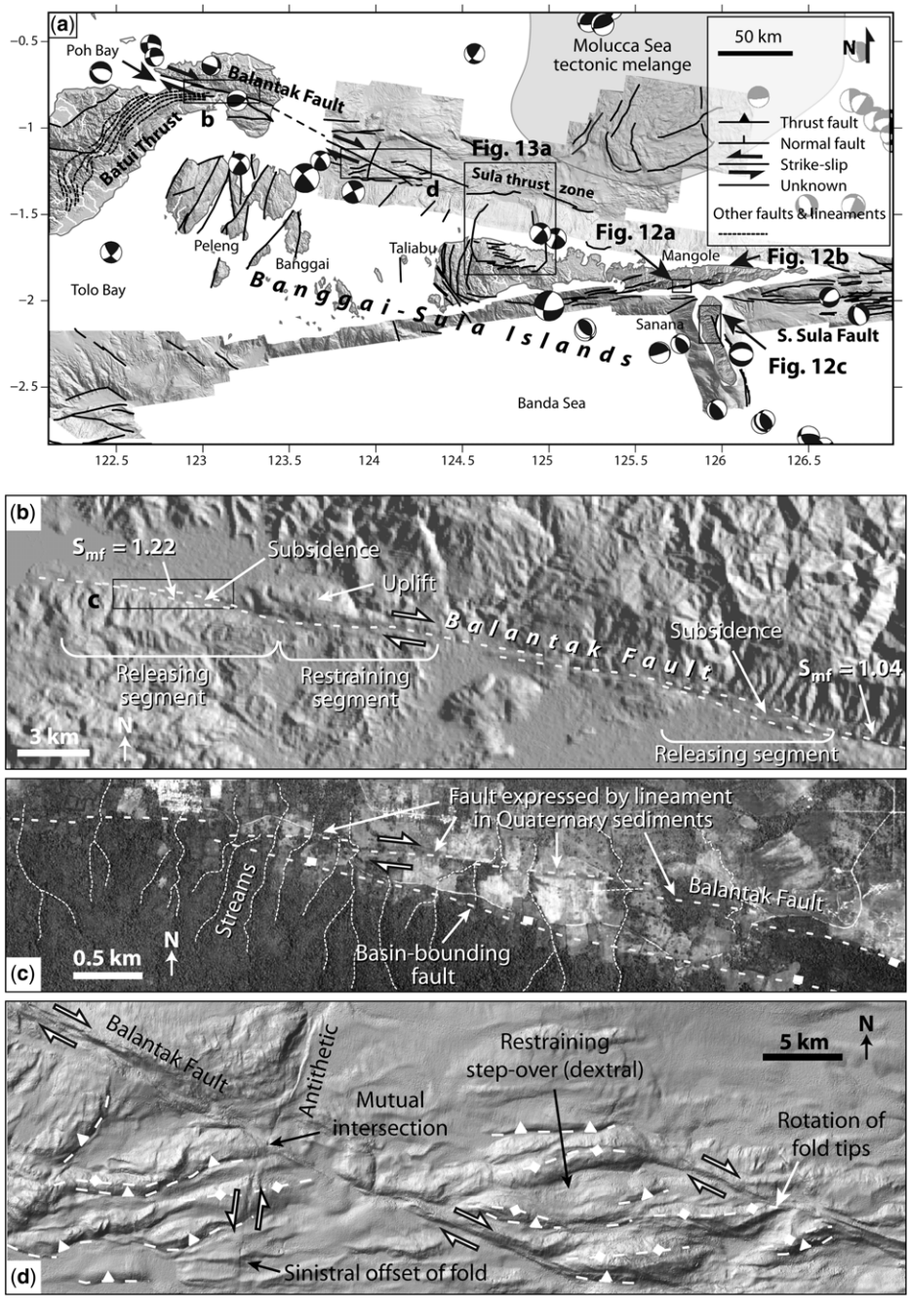

Fig. 10. (**a**) East arm of Sulawesi and Banggai–Sula Islands digital elevation model (SRTM), multibeam bathymetry, CMT catalogue earthquakes <35 km depth and structures showing geomorphic evidence of Quaternary tectonic activity. After Watkinson *et al.* (2011). Location shown in Figure 1. (**b**) Subsidence and uplift associated with releasing and restraining segments of the onshore Balantak Fault. ASTER digital elevation model base map. (**c**) Detail of bounding fault system of a Balantak Fault releasing segment, showing a north-dipping normal fault and sub-parallel lineament in agricultural land, inferred to represent a through-going strike-slip strand. ESRI imagery base map. (**d**) Detail of the offshore Balantak Fault expressed in multibeam imagery (illumination from NW) showing evidence of dextral shear.

fault up to 250 km long. The onshore fault scarp has exceptionally low S_{mf} values, from 1.04 to 1.22 (Fig. 10b), with correspondingly low average V_f values of 0.36, suggesting maximal to moderate tectonic activity.

Gorontalo Fault

The Gorontalo Fault (Katili 1973) (Fig. 11a) has been considered to be one of the major block-bounding structures of Sulawesi (e.g. Socquet *et al.* 2006; Molnar & Dayem 2010). Geodetic modelling suggests a 11 mm a^{-1} dextral slip rate and 10 km locking depth; however, because the observation points are widely spaced, it remains possible that global positioning system (GPS) data record rotation of the entire north arm of the island rather than discrete slip across a fault (Socquet *et al.* 2006). There is little modern shallow seismicity in the Gorontalo area, suggesting that the fault is inactive or remains locked (Fig. 11a).

The fault is composed of several branching segments, including major *c.* 30 km long segments south and north of Gorontalo city (Fig. 11b). Limboto Lake lies in the 7 km wide step-over between these two segments, indicating local transtension. The fault is expressed by highly eroded scarps passing along the Tomini Bay coast and bounding the Gorontalo/Limboto depression. Geomorphic indices suggest that the segments experience slow to minimal tectonic activity, with S_{mf} values ranging from 1.83 to 2.36 and an average V_f of 1.28. Although there is considerable human development within the Gorontalo/Limboto depression, which may obscure neotectonic activity, there appears to be little evidence of deformation within the Quaternary sediment-fill, except for the presence of Limboto Lake subsidence at the releasing step-over.

Western Tomini Bay bounding faults

A series of faults along the margin of Tomini Bay shows evidence of recent activity. The faults are arcuate and generally mark the boundary between mountainous ground along Sulawesi's narrow 'neck' and Tomini Bay, which is up to 2 km deep and contains a sedimentary succession up to 10 km thick (Jablonski *et al.* 2007; Pholbud *et al.* 2012). Extension and mantle decompression across the bay are associated with Plio-Pleistocene volcanism in the Togian Islands and possibly with modern volcanism at Una Una volcano (Cottam *et al.* 2011), supporting recent extensional faulting and lithospheric thinning both onshore and offshore (Pholbud *et al.* 2012).

The northernmost bounding fault bounds the 2.5 km high Molino Metamorphic Complex (Fig. 11c), a suite of quartzo-feldspathic mica schists and gneisses that may be an exhumed metamorphic core complex (van Leeuwen & Muhardjo 2005). The faults dip north and south on the north and south sides of the complex, respectively, and have crystalline basement in their footwalls. The southern segment has a curvilinear trace >75 km long with extremely low S_{mf} values (1.05) and well-developed triangular facets at the end of V-shaped valleys with V_f values of 0.33–0.64 within an uplifted footwall block. On this basis, combined with no evidence of strike-slip, it is interpreted as a normal fault.

Further SW, the Tomini Bay bounding faults are crossed by a number of fan deltas prograding into the bay. These are surprisingly short (<3 km), given the potential upstream sediment source, suggesting rapid and recent hanging wall subsidence (Fig. 11d, e). Segments further south along the 'neck' have higher S_{mf} values (1.66) and the fan delta lobe length increases to >10 km, suggesting less significant recent subsidence (Fig. 11f).

At the southern end of the neck, a NE-dipping fault system, including the Tambarama Fault (Pholbud *et al.* 2012), forms an apparently continuous arcuate trace at Parigi (Fig. 4), marking the boundary between the Palu Metamorphic Complex onshore (van Leeuwen & Muhardjo 2005) and Tomini Bay subsidence offshore. S_{mf} values are generally high (2.77–3.25), although a short northern segment is less sinuous at 1.32. A well-developed apron of fan deltas extends 6 km from the mountain front.

Maluku and North Maluku

Maluku and North Maluku are composed of numerous islands affected by disparate neotectonic processes. In the north, Halmahera (Fig. 1) and the Sangihe Arc are involved in the active collision of two accretionary complexes above the subducted Molucca Sea slab, where the Sangihe forearc is being thrust eastwards over the Halmahera forearc (e.g. Silver & Moore 1978; Hamilton 1979; Hall 1987; Hall *et al.* 1995). The entire system accommodates 80 mm a^{-1} of the 105 mm a^{-1} Philippine Sea plate–Sundaland convergence (Rangin *et al.* 1999). Splays of the left-lateral Sorong Fault pass through and to the south of Halmahera and Bacan, where there is abundant modern seismicity (e.g. Ali & Hall 1995; Hall *et al.* 1995) (Fig. 1).

South of Bacan, islands with Australian continental basement, such as the Banggai–Sula Islands and Obi, are bounded by strands of the Sorong Fault and were for a long time considered to have been translated from New Guinea along a 1900 km long Sorong Fault passing from northern Papua New Guinea towards Sulawesi (e.g. Visser & Hermes 1962; Audley-Charles *et al.* 1972; Hamilton 1979; Pigram *et al.* 1985; Garrard *et al.* 1988; Hutchison

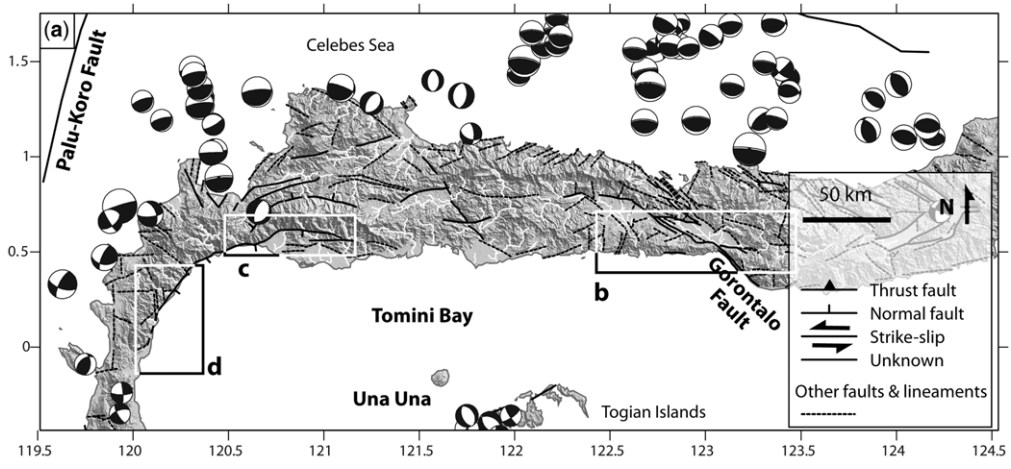

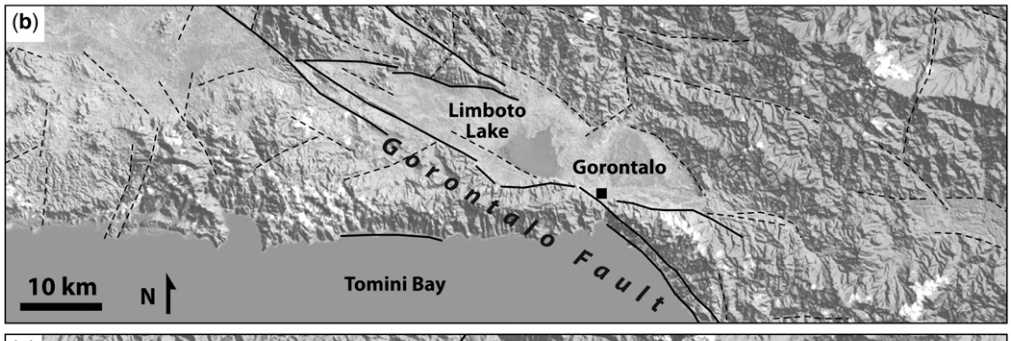

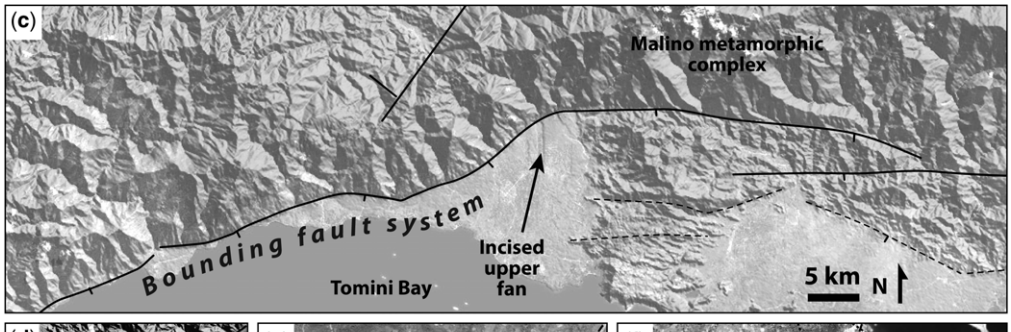

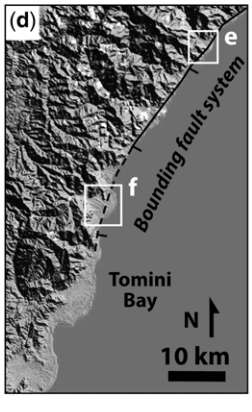

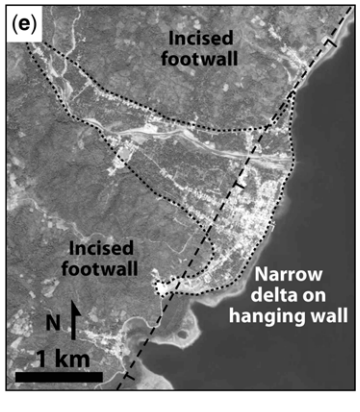

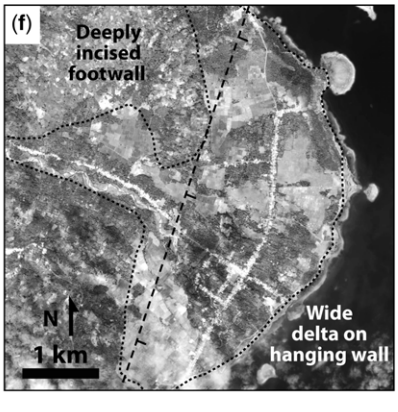

1989). New interpretations based on evidence of extreme crustal extension and mantle exhumation, mantle tomography and geodynamic models (e.g. Spakman & Hall 2010; Hall 2011; Spencer 2010, 2011; Pownall *et al.* 2014) suggest that those islands, together with others along the northern Banda Arc such as Buru and Seram, were part of a continental spur that was fragmented during Miocene–Pliocene times by lower crustal delamination driven by Banda Sea rollback.

Quaternary extension in Maluku appears to be as important as it is in Sulawesi, despite an overall collisional tectonic setting. Young metamorphic core complexes exhumed in Seram (Pownall *et al.* 2013) and possibly Buru (Roques 1999) are associated with low-angle and steep normal faults. A significant component of the seismic moment release in Maluku is by normal and strike-slip earthquakes, alongside important thrusting in the Molucca Sea and north Seram (e.g. Rangin *et al.* 1999). Sinistral transpression through Seram accommodates Australia–Pacific convergence and links into the Tarera–Aiduna Fault of West Papua (e.g. Rangin *et al.* 1999; Stevens *et al.* 2002; Teas *et al.* 2009).

Banggai–Sula Islands

The Banggai–Sula Islands (Fig. 10a) occupy a fragment of continental crust of Australian affinity that has collided with the east arm of Sulawesi (e.g. Audley-Charles *et al.* 1972; Hamilton 1979; Pigram *et al.* 1985; Garrard *et al.* 1988). The South Sula–Sorong Fault was interpreted by Hamilton (1979) to follow the break in slope south of Taliabu and pass between Mangole and Sanana. North of the Banggai–Sula Islands the North Sula–Sorong Fault (e.g. Hamilton 1979; Norvick 1979; Silver *et al.* 1983*b*; Sukamto & Simandjuntak 1983), previously considered to pass from the Bird's Head, past Obi and along the north margin of the Banggai–Sula Islands towards Sulawesi's east arm, cannot be detected in new geophysical data and must lie below the Molucca Sea collision complex to the north (Ferdian *et al.* 2010; Watkinson *et al.* 2011).

Despite the density of deformation in the area, there is very little shallow seismicity immediately north of the Banggai–Sula margin (Engdahl *et al.* 1998; Rangin *et al.* 1999; Beaudouin *et al.* 2003), indicating that there are few active structures, that deformation is largely aseismic or that the main faults have interseismic periods that exceed instrumental records. This is a marked contrast with the abundant shallow seismicity associated with the Molucca Sea collisional zone further north. However, a number of focal mechanisms north and south of the islands indicate that there is some residual left-lateral slip on east–west- to NW–SE-trending faults (Fig. 10a).

Mangole Island appears to be bordered along its north and south sides by several linear east–west-trending normal faults, indicated by straight traces and well-developed triangular facets (Fig. 12a, b). Mountain front sinuosity values range from 1.11 to 1.57 and V_f is from 0.44 to 0.55, suggesting that some of the structures have been active during the Quaternary. Sanana Island, topographically orthogonal to Mangole, is bounded by NNW–SSE-trending faults that can be traced offshore in multibeam bathymetry. The most prominent fault, on the east coast, forms a well-defined scarp >20 km long, dipping and downthrown to the east, making it likely to be a normal fault (Fig. 12c). Triangular facets, hanging valleys, deeply incised streams (Fig. 12d) and an absence of subaerial prograding fan delta tops wider than *c.* 400 m suggest rapid recent eastwards subsidence along the fault, supported by S_{mf} values of 1.27–1.34.

Taliabu Island (Fig. 10a) is cut by a number of east–west- and north–south-trending Quaternary faults. The north–south-trending faults in the west have a particularly fresh geomorphic expression. A north coast bedding-parallel dip slope dips 6° into the Molucca Sea (Fig. 13a). Offshore to the north a planar detachment surface 34 km wide exactly corresponds to the Taliabu dip slope onshore and represents a submarine slope failure (Watkinson *et al.* 2011). Both onshore and offshore slopes appear to be part of a single large glide surface of a mega-debris slide that translated much of north Taliabu at least 37 km north into the Molucca Sea, probably causing a significant tsunami.

Fig. 11. (**a**) North arm of Sulawesi digital elevation model (SRTM), CMT catalogue earthquakes <35 km depth and structures showing geomorphic evidence of Quaternary tectonic activity. Rivers marked in white. Location shown in Figure 1. (**b**) Detail of the onshore Gorontalo Fault and associated basins. ASTER digital elevation model draped with ESRI imagery layer. (**c**) Fault system bounding the Malino metamorphic complex showing remarkably straight and steep mountain front and well-developed triangular facets. (**d**) Overview of fan deltas prograding into western Tomini Bay across the bounding fault system. (**e**) Narrow fan delta clearly cut by the basin-bounding fault, indicating rapid subsidence. Google Earth imagery. Image © 2016 DigitalGlobe. Data SIO, NOAA, U.S. Navy, NGA, GEBCO. Image (2016) Terrametrics. Image Landsat. (**f**) Wide fan delta further south indicating a slower rate of hanging wall subsidence. Google Earth imagery. Image © 2016 DigitalGlobe. Data SIO, NOAA, U.S. Navy, NGA, GEBCO. Image (2016) Terrametrics. Image Landsat.

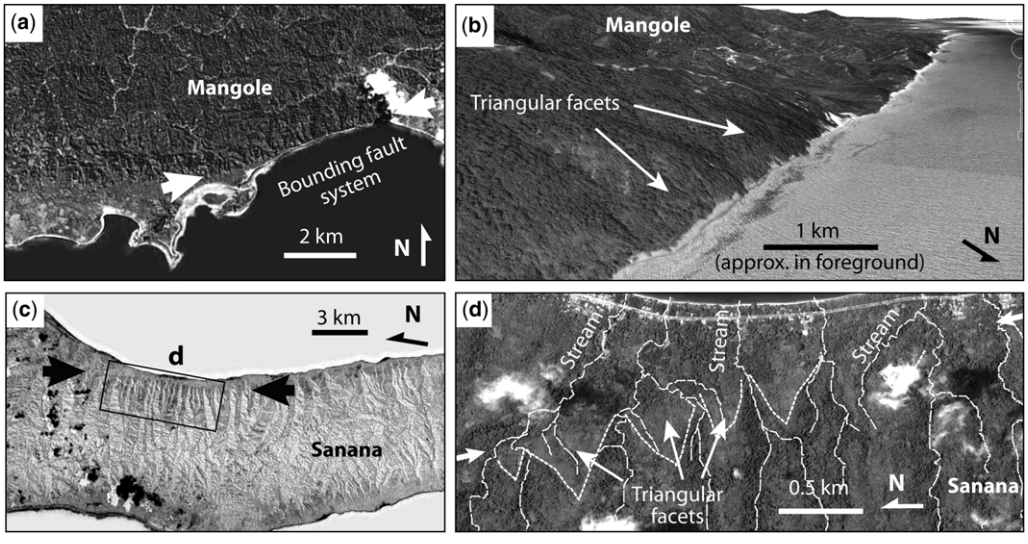

Fig. 12. Details of Quaternary faults in the Banggai–Sula Islands. For locations, see Figure 10a. (**a**) Part of the linear normal fault system bounding the southern margin of Mangole Island. Google Earth image. Data SIO, NOAA, U.S. Navy, NGA, GEBCO, Image Landsat. Image © 2016 TerraMetrics. (**b**) Triangular facets along the north coast of Mangole Island. Oblique view in Google Earth. Data SIO, NOAA, U.S. Navy, NGA, GEBCO. Image © DigitalGlobe. Image © 2016 TerraMetrics. Image Landsat. (**c**) Fault control along the eastern coast of Sanana Island. Image from Google Earth (greyscale inverted for clarity). Image Landsat. Image © DigitalGlobe. Image © 2016 TerraMetrics. Data SIO, NOAA, U.S. Navy, NGA, GEBCO. (**d**) Detail of the Sanana fault, showing the extremely linear mountain front, narrow V-shaped valleys and triangular facets. Image © DigitalGlobe.

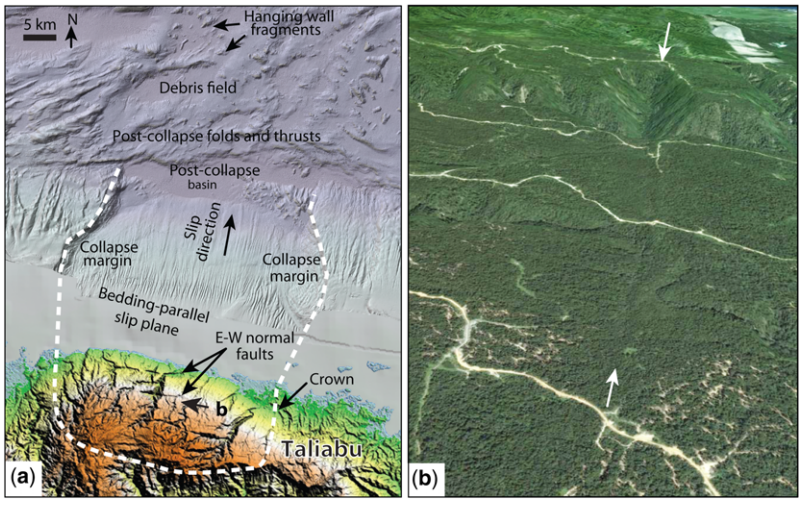

Fig. 13. (**a**) Mega-debris slide and post-collapse normal faults, north coast of Taliabu. Base map is SRTM topography onshore and multibeam bathymetry offshore. Location shown in Figure 10a. (**b**) Oblique perspective view from Google Earth of one of the normal faults on the north slope of Taliabu. White arrows mark fault tips. View to the west. Field of view is *c.* 1 km in foreground. View location and direction indicated by arrow in Figure 13a. Image Landsat. Image © DigitalGlobe. Data SIO, NOAA, U.S. Navy, NGA, GEBCO.

The north Taliabu dip slope is truncated by several prominent east–west-trending faults that dip steeply north. The geomorphic expression is very fresh (Fig. 13b). The footwall crests are only slightly eroded and, in most cases, the drainage runs parallel to fault scarps and has not cut across them, except for a few prominent high-order streams. The faults displace the dip slope and must therefore post-date the mega-debris slide. Although we have no absolute constraint on the timing of the slide, reef build-ups are conspicuously poorly developed along the section of coast at the foot of the dip slope, but are extensive along the coast and small islands on either side. The slide must have happened recently enough that corals have been unable to fully recolonize the new coastline, suggesting that the post-slide normal faults are late Quaternary and probably still active.

Sorong Fault from Obi to Waigeo

Westward splaying segments of the Sorong Fault emanate from the western Bird's Head and pass close to the islands of Salawati, Misool, Obi, Bacan, south Halmahera and Waigeo (e.g. Katili 1975; Hamilton 1979; Ali & Hall 1995) (Fig. 1). Although there is debate about whether the Sorong Fault onshore West Papua is tectonically active (discussed later in this paper), at the latitude of Obi there is 19 ± 8 mm a^{-1} left-lateral displacement between Ternate and the Bird's Head that may be accommodated by one or more strands of the Sorong Fault (Bock *et al.* 2003). Seismicity is limited in the islands immediately west of the Bird's Head, but intense seismicity occurs around Obi, Bacan and south Halmahera (Rangin *et al.* 1999), which may be where sinistral strain is transferred from Seram into the Molucca Sea.

Seram fold–thrust belt

Between northern Seram and the Bird's Head is a broad zone of transpression linked to convergence between Australia and the Pacific plate (Fig. 1). A deep bathymetric trough, the Seram Trough, lies 150 km north of Seram Island and curves around the Banda Sea, linking to the Timor Trough and ultimately the Java Trench. The Seram Trough has been interpreted as a subduction trench (e.g. Hamilton 1979), a foredeep ahead of a fold–thrust belt (e.g. Audley-Charles 1986) and a hinge zone marking the northern limit of delaminated and subducted lower continental crust (Spakman & Hall 2010).

Convergence across the Seram Trough is presently 20 mm a^{-1} (Rangin *et al.* 1999; Stevens *et al.* 2002) and is associated with intense seismicity generated by shallow thrust faulting (McCaffrey 1989; Engdahl *et al.* 1998) mainly concentrated along the northern edge of Seram (Fig. 14a) and entirely in the western part of the fold belt (Teas *et al.* 2009).

Seram is centred on a belt of high mountains (>3 km elevation), which include tracts of continental metamorphic rocks, ultramafic rocks and the Earth's youngest exposed ultra-high-temperature granulites, exhumed since 16 Ma (Pownall *et al.* 2014). The Plio-Pleistocene Wahai and Fufa formations onlap the elevated pre-Pliocene succession, forming low plains along the northern coast (Pairault *et al.* 2003), and are themselves overlain by modern alluvial and reef deposits. There is evidence of active contraction within these plains.

On the north coast of Seram, onshore fold growth affects the modern drainage, suggesting that the folds have been active during the Quaternary (Fig. 15a). Three large rivers draining the northern slopes of the Kobipoto Mountains are deflected from a linear route to the coast by two sets of segmented east–west- to NW–SE-trending hills. Progressive migration of the rivers away from the hilltops is recorded by a trail of abandoned and filled river channels left behind by the deflected river, expressed by oxbow-shaped fields and areas of vegetation (Fig. 15b, c). Larger hills, like that in the centre of Figure 15a, cause more deflection than smaller folds, like that in the east which only deflects Wai (stream) Kobi slightly. In all cases the abandoned channels are located upslope of the modern river, suggesting that progressive uplift is forcing river avulsion. This tendency for the hills to grow symmetrically from a central axis, their elongate morphology and their asymmetry (steep northern slopes, shallow southern slopes) support the interpretation that they are the surface expression of shallow, north-vergent fault propagation folds above south-dipping thrusts (Fig. 15d).

Abandoned meander channels and point bars on the coastal plain in the central part of Figure 15d are not associated with any obvious modern river, but seem to originate at the foot of the central frontal thrust. Abandoned remnants of a comparably large river can also be observed in an uplifted valley immediately to the south, and directly north of a fourth major north-flowing river, which presently abruptly curves around the eastern tip of the fault before joining Wai Musi. It is interpreted that the abandoned channels here represent a river that flowed directly north before the fold developed. An uplifted valley across the mid-point of the fold shows that the river attempted to downcut as the fold grew, but was ultimately thwarted by a high uplift rate and swung east to be captured by Wai Musi. Deep lateral incision by the captured river into the back limb of the fold (Fig. 15b) suggests that the fold growth, and presumably underlying thrust activity, is ongoing.

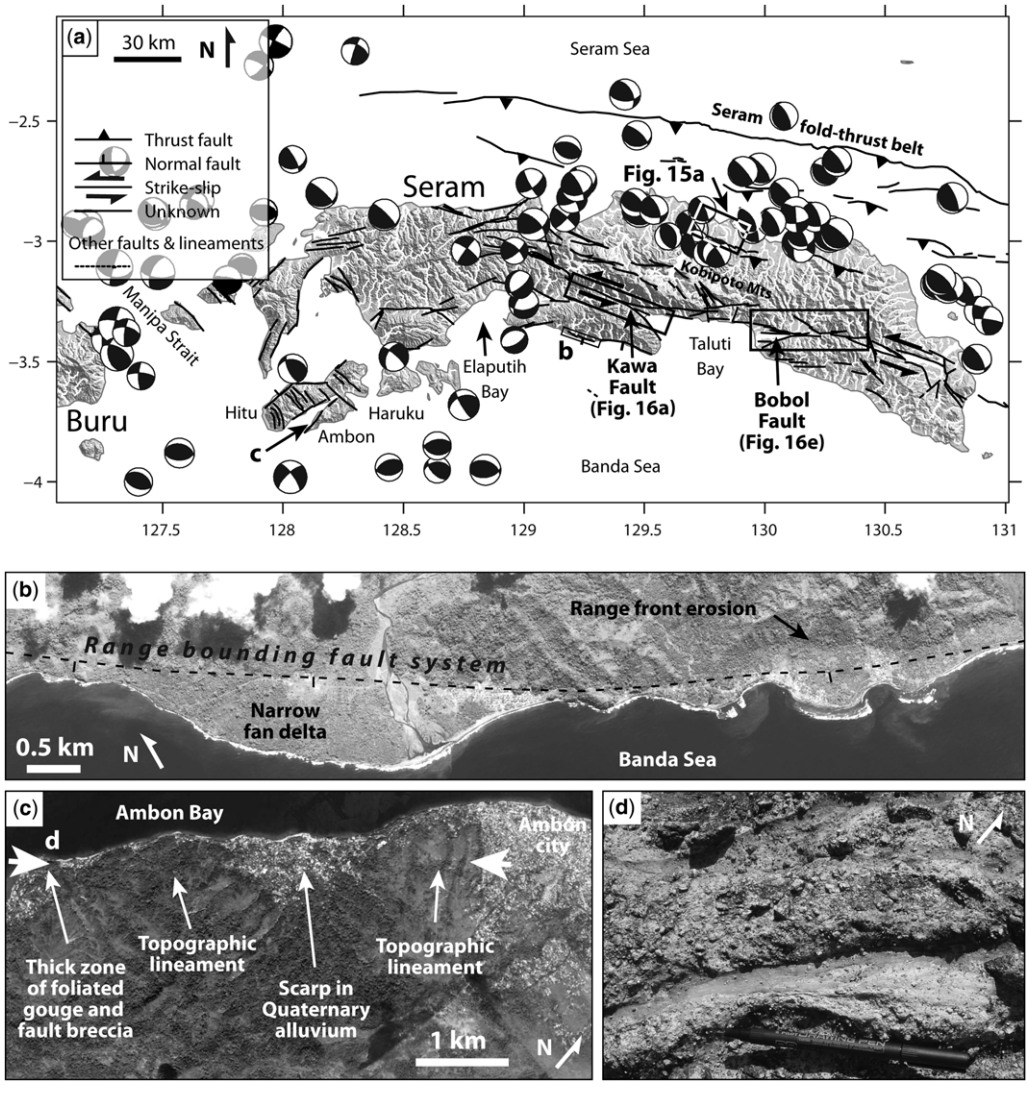

Fig. 14. (**a**) Seram digital elevation model (SRTM), CMT catalogue earthquakes <35 km depth and structures showing geomorphic evidence of Quaternary tectonic activity. Rivers marked in white. Offshore structures from Teas *et al.* (2009). Location shown in Figure 1. (**b**) Normal faults along the south coast of Seram, marked by a linear mountain front and a prominent lineament crossing a narrow fan delta. Google Earth imagery. Data SIO, NOAA, U.S. Navy, NGA, GEBCO. Image © 2016 DigitalGlobe. Image © 2016 TerraMetrics. (**c**) Possible Quaternary fault SW of Ambon, marked by a lineament that crosses volcanic hills and Quaternary drift. Google Earth imagery. Image © 2016 DigitalGlobe. (**d**) Example of foliated gouge from a thick fault zone located where the lineament illustrated in Figure 14c reaches the coast. Pen is 14 cm long.

A series of abandoned channels east of Wai Musi, the easternmost of which link to Wai Kobi, indicates that river itself may previously have been a tributary to Wai Kobi, before being deflected to the west and ultimately cut off from the trunk stream, presumably by uplift above the eastern frontal thrust.

Such evidence of recent hanging wall uplift and tectonic folding, together with the low relief of the range front, leads to the conclusion that the faults are youthful, low-angle, south- to SW-dipping thrusts supported by focal mechanisms along the north coast (Fig. 14a). Uplifted coastal terraces in the foreland of the onshore thrusts and a

conspicuously wide coastal plain (Fig. 15d) suggest additional young uplift north of the onshore thrusts, perhaps in response to a third set of active faults just offshore. This is consistent with modern thrust activity within the broad fold–thrust belt offshore (e.g. Engdahl *et al.* 1998; Teas *et al.* 2009) and a 1629 mega-thrust earthquake probably originating in the Seram Trough (Liu & Harris 2013).

Kawa Fault

The Kawa Fault (Pownall *et al.* 2013) lies in the prominent ESE-WNW-trending deep linear valley that passes through central Seram (Fig. 14a) and is occupied by the Kawa River. The fault broadly separates upper greenschist to mid-amphibolite facies Tehoru Formation rocks in the south from generally higher grade metamorphic rocks of the Saku and Taunusa complexes in the north (Germeraad 1946; Tjokrosapoetro *et al.* 1993; Pownall *et al.* 2013). The Kawa Fault coincides with the position of strongly mylonitic garnet-bearing Tehoru Formation schists with a steeply dipping foliation considered by Linthout *et al.* (1991) to record dextral shear, but now recognized to have been intensely folded and possibly originating in a low-angle normal fault, resulting in complexly re-oriented kinematic indicators (Pownall *et al.* 2013).

A brittle fault zone up to 2 km wide (Pownall *et al.* 2013) overprints the mylonitic rocks and controls the modern topography (Fig. 16a, b). Fault strands are generally parallel to the mylonitic foliation and contain abundant serpentinite slivers and smears. Mid-way along the fault is a prominent right step associated with uplift and a major drainage divide, pointing to local transpression due to left-lateral slip. Stream offsets measured from Landsat and Google Earth imagery along the fault (Fig. 16a) range from 66–605 m of left-lateral offset (22 measurements) to 62–334 m of right-lateral offset (five measurements). Most measurements have a high uncertainty, increased by Seram's extremely humid climate and thick forest cover. Nonetheless, some measurements – for example, the 268 and 253 m left-lateral offsets (e.g. Fig. 16c) – are considered to be robust because: (1) they lie on fault segments that are well defined (narrow linear valleys with other independent evidence of a fault origin such as triangular facets and steps/bends with the corresponding uplift/subsidence appropriate to the sense of river offset); (2) there is no evidence of stream capture; and (3) upstream and downstream valleys have a similar geomorphic character. A left-lateral shutter ridge displacement and a NW–SE-trending fold within the Kawa River delta (Fig. 16a) support recent sinistral shear. A few earthquakes close to the western end of the fault yield CMT solutions suggesting dextral slip along NW–SE-trending planes, whereas one close to the westernmost splay indicates sinistral slip (Fig. 14a).

The fault zone splays as it enters Taluti Bay in the east (Fig. 16a). The splay strands are associated with well-developed triangular facets that record Quaternary normal faulting (Fig. 16d). The two major splays have low S_{mf} values of 1.10 in the north and 1.33 in the south and an average V_f of 0.27, indicating rapid to moderate tectonic activity. The Kawa River flows hard against the southern splay, suggesting active subsidence along that segment, despite its higher S_{mf} indicating slower tectonic activity than in the north. However, the river's position may also be influenced by landslips, debris flows and anticline growth in the northern part of its valley. In the west, the fault splays north of Elaputih Bay, attaining a total onshore length of 90 km, or 120 km including a possible splay fault along the north coast of Taluti Bay (Fig. 14a).

Although the fault zone is thickly forested, numerous landslip scars can be recognized along the fault, indicating recent seismicity (Fig. 16a). In addition, the eastern termination is characterized by a series of discontinuous tilted blocks suggestive of slope failure along the southern margin of the Manusela Mountains (Fig. 16a). An M 7.8 earthquake in 1899 triggered landslides that caused a 12 m high local tsunami at Tehoru (http://www.ngdc.noaa.gov; Brune *et al.* 2010), although it is unclear whether the source was the Kawa Fault or a more distant earthquake. However, all evidence points to the Kawa Fault being active during the Quaternary and capable of generating large earthquakes.

Other active faults of Seram

Along-strike from the Kawa Fault on the east side of Taluti Bay, a fault zone occupies the valleys of Wai Masumang and Wai Bobol and is here termed the Bobol Fault (Fig. 14a). It is highly segmented, although with a total onshore length of 100 km and possible along-strike continuity with the Kawa Fault, it is a significant structure. Four large basins are developed along its length, each bounded by ESE–WNW- to SE–NW-trending normal faults. The mountain front sinuosity along these structures ranges from 1.26 in the central section to 1.99 in the west and the average V_f is 1.66, indicating moderate to slow tectonic activity. There are a number of stream offsets both across the basin-bounding faults and across parallel faults in adjacent mountains (Fig. 16e). Convincing displacements are all left-lateral and range from 310 m to 2.06 km (Fig. 16f). Most strike-slip fault segments within the fault zone are parallel to the Kawa Fault and the two fault systems appear to be tectonically related and part of a broader zone of active left-lateral shear linking to the Tarera–Aiduna Fault in West Papua.

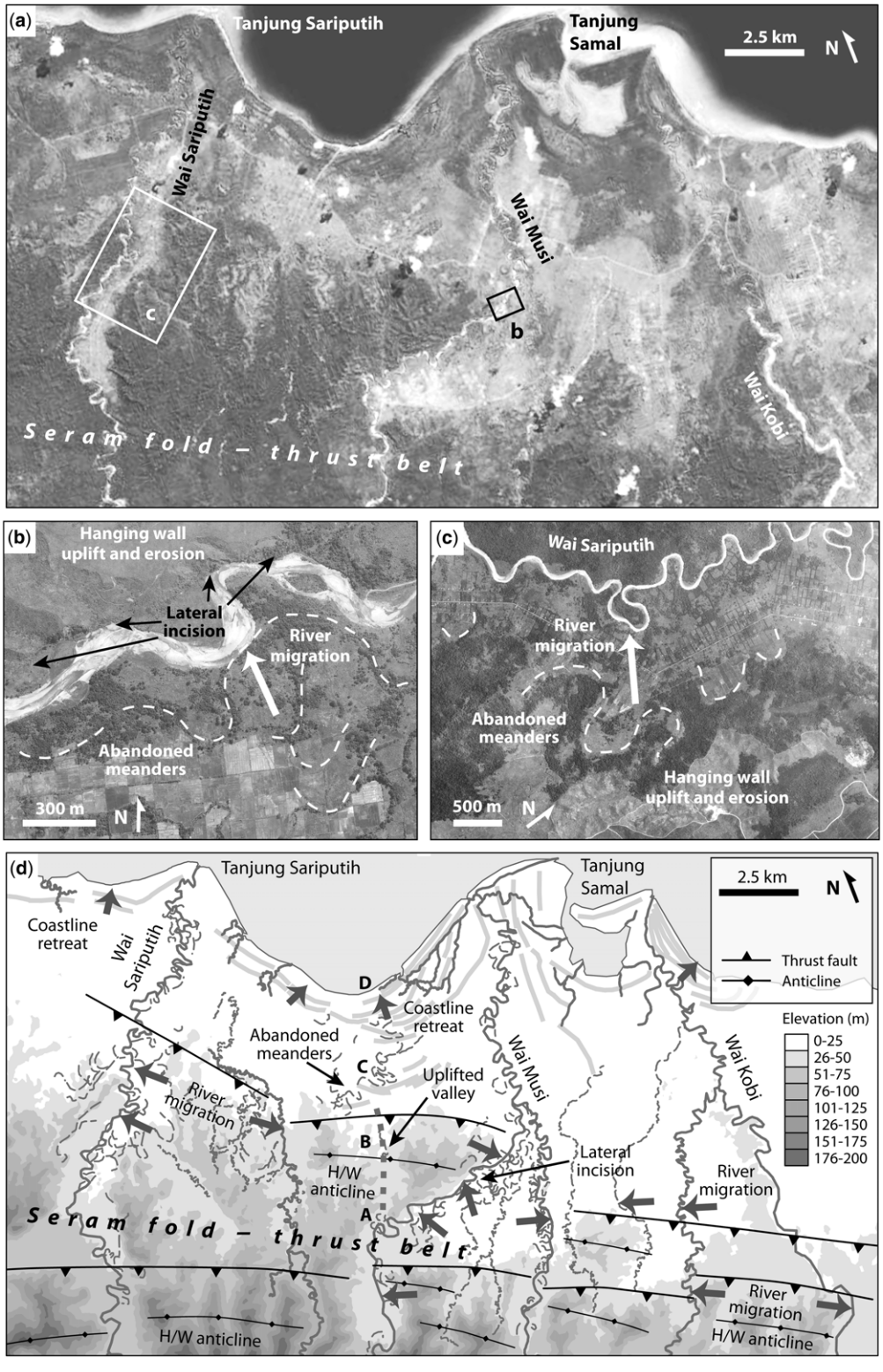

The southern margin of Seram is locally formed by linear mountain fronts flanked by narrow fan deltas not more than 1 km wide. The steep, linear aspect and high topographic relief of the mountain fronts and the topographic lineaments that cross the fans parallel to the mountain front (Fig. 14b) suggest that the mountain front is defined by Quaternary normal faults. However, the coastal range is deeply eroded, with S_{mf} values of 1.84–2.08 and an average V_f of 1.62, indicating slow tectonic activity. Earthquake focal mechanisms towards the west of the coastal fault system in the region of Elaputih Bay support shallow focus, broadly south-directed, steep normal faulting (Fig. 14a).

A number of other small suspected normal fault systems occur around the SW coast of Seram, including those bounding the Ambon Islands. One fault along the northern coast of Hitu (Fig. 14a) is particularly steep and straight, with an S_{mf} of 1.16 and well-developed triangular facets along its 16 km long trace. A NE–SW-trending lineament that passes through Ambon city marks the southern coast of Ambon Bay (Fig. 14c) and is associated with a zone of fault breccia and foliated gouge several metres thick (Fig. 14d). An M 7.6 earthquake occurred on 8 October 1950 close to the south coast of Ambon (Bath & Duda 1979), although it is unlikely that such an event could have been caused by the relatively short, dominantly normal faults visible onshore.

Buru

Buru consists of a presumed Palaeozoic continental metamorphic basement flanked by a Mesozoic sedimentary succession (Tjokrosapoetro *et al.* 1993), both of which are probably continuous with similar units in Seram (e.g. Pigram & Panggabean 1984; Linthout *et al.* 1989). Young K–Ar ages of 4–5 Ma (Linthout *et al.* 1989) and an apatite fission track central age of 2.5 ± 0.5 Ma suggest late Neogene exhumation, possibly accommodated by low-angle normal faults (Roques 1999) as similarly postulated for western Seram (Pownall *et al.* 2013).

Intense shallow seismicity associated with Seram terminates abruptly in Manipa Strait, east of Buru (Fig. 17a). A broad belt of earthquakes in Manipa Strait have CMT solutions indicating either NNE–SSW dextral events or WNW–ESE sinistral events, including a 14 March 2006 M_w 6.7 earthquake 25 km offshore. Most earthquakes have a component of reverse slip; others are pure thrust earthquakes with a NW–SE trend.

Most of Buru's sparse population lives in the NE of the island, including the major town, Namlea. A 5–10 km wide system of NW–SE-trending faults cuts through the town, across Kayeli Bay, and defines the coastline (Fig. 17b). The faults are expressed in remote sensing data by linear hills and sag ponds at releasing right step-overs, notably at Jikumerasa (Fig. 17c). Fault strands that cut through basement metamorphic rocks and alluvial fans show consistent stream offsets and pass directly into Quaternary alluvium and control modern river channels (Fig. 17d). Stream offsets of up to 85 m across individual strands are mostly right-lateral; where they are left-lateral there is clear evidence for stream capture. Variations in offset sense and amount are to be expected – streams are dynamic and are not passively offset like pre-kinematic geological markers. The process of offset, beheading and capture, leading to stream offsets of zero or opposite to the fault's shear sense, is well documented and widely observable in active faults worldwide (e.g. Wallace 1968; Sieh & Jahns 1984; Huang 1993; Walker & Allen 2012). All these features imply Quaternary NW–SE-trending dextral fault activity in NE Buru, despite the apparent discordance with the few earthquake focal mechanisms recorded.

A broad fault zone 65 km long almost bisects Buru from the NE to SW (Figs 17a & 18a). Identified as left-lateral on early geological maps (e.g. Tjokrosapoetro *et al.* 1981), little else is known about the fault zone, here termed the Rana Fault. Danau (lake) Rana, in the centre of Buru, occupies an intermontane basin within a right step-over between two segments of the Rana Fault, suggesting that the fault is dextral. West of Wadule, Wa (river) Geren is abruptly diverted 90° from a broad oversized valley, which would have taken it to the coast in the NE of the island, into a narrow and steep-sided canyon (Fig. 18a) that links with Wa Apu and empties into Kayeli Bay further south

Fig. 15. Evidence of Quaternary thrusting along the north coast of Seram. (**a**) ESRI image showing a number of NE-flowing rivers flowing around linear elevated and forested regions. Location shown in Figure 14a. (**b**, **c**) Migrating rivers marked by filled channels and oxbow lakes and incision into uplifting regions. Google Earth imagery. Image © 2016 DigitalGlobe. (**d**) Interpretation of Figure 15a. Thick arrows indicate progressive migration of river channels; short arrows show coastline regression. Abandoned channels at points A, B and C are interpreted to represent the previous route of a river that entered the sea at D north of a meander plain at C, but was cut off by thrust hanging wall (HW) uplift at B and was forced to divert east from point A to join Wai Musi, leaving previous channels abandoned. Other rivers show lateral migration away from the growing tips of thrusts in response to hanging wall fold growth. See text for further details.

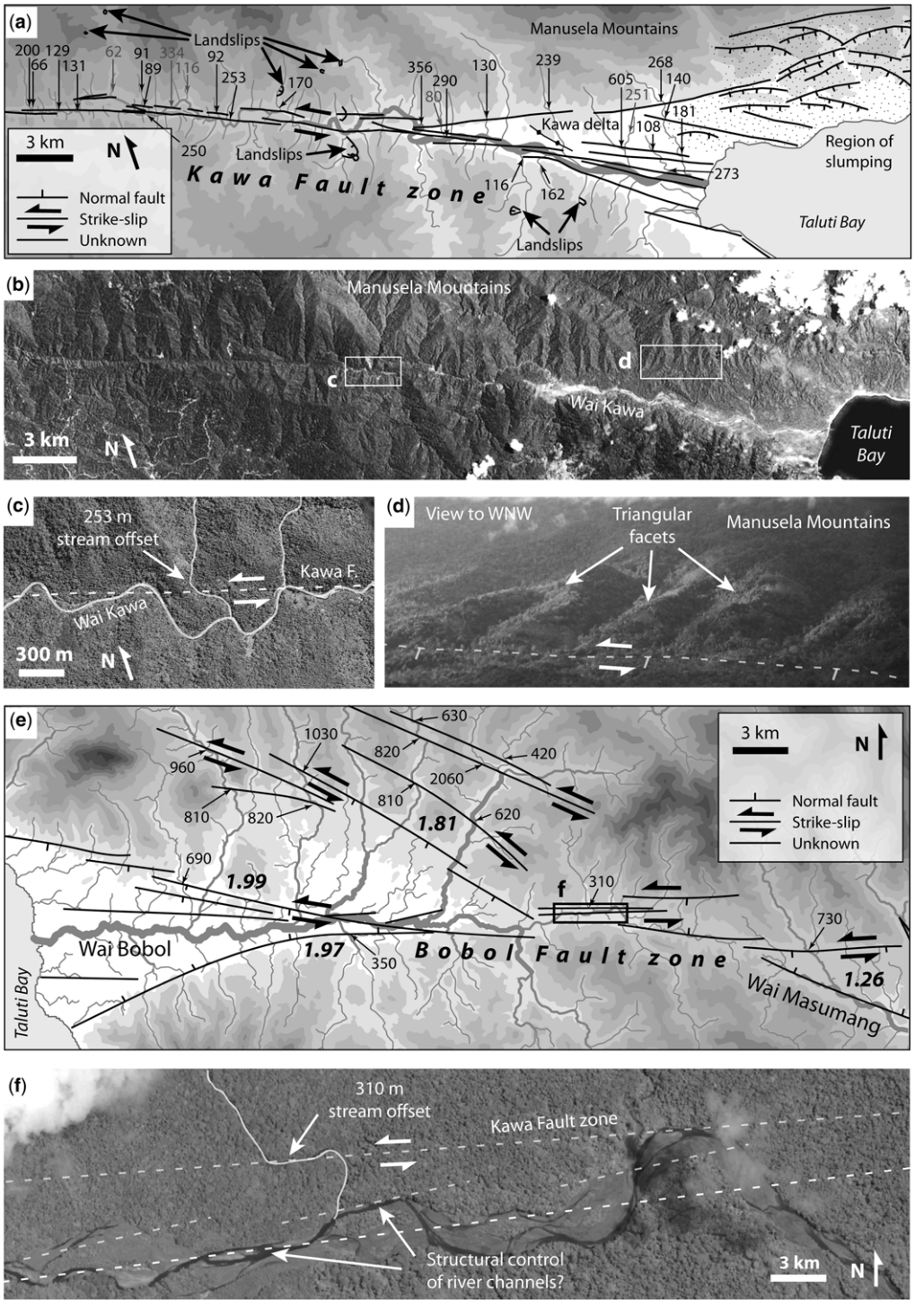

Fig. 16. Strike-slip faults of southern Seram. (**a**) Overview map of the Kawa fault zone showing Quaternary fault strands, rivers, river offsets (in metres) and landslips. Left-lateral offsets in black, right-lateral offsets in grey. See Figure 14a for location. (**b**) ESRI image of the Kawa fault zone highlighting its clear geomorphic expression and

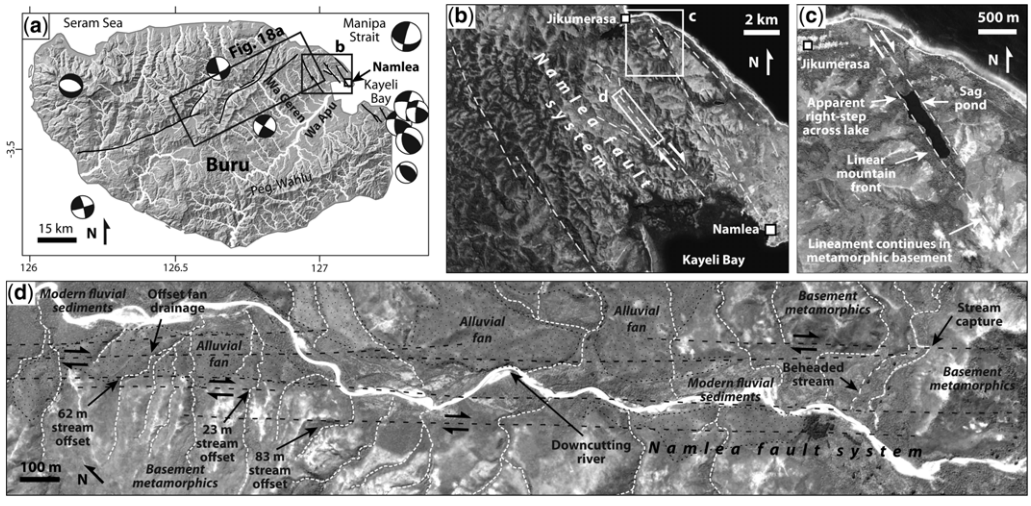

Fig. 17. Quaternary fault features in Buru. (**a**) Digital elevation model (SRTM), CMT catalogue earthquakes <35 km depth and structures that show geomorphic evidence of Quaternary tectonic activity. Rivers marked in white. Location shown in Figure 1. (**b**) Overview of topographic lineaments passing through Namlea and NE Buru. ESRI imagery. (**c**) Detail showing possible sag pond developed at the releasing step-over between right-stepping fault segments. (**d**) Evidence of strike-slip faulting along the Namlea lineament trend. Lineaments pass from basement rock through Quaternary drift and are associated with systematic right-lateral stream offsets. Image © 2016 DigitalGlobe.

(Fig. 17a). This pronounced capture of a northern drainage basin by a relatively minor tributary of Wa Apu appears to have been triggered by uplift at a left bend in the Rana Fault immediately east of the capture point (Fig. 18a), again suggesting Quaternary dextral shear.

Upstream of the Wa Geren stream capture, the Rana Fault has exceptionally fresh geomorphic expression (Fig. 18b, c), with pronounced triangular facets and very low S_{mf} values from 1.01 to 1.18 along the southern valley slope and a correspondingly low average V_f of 0.25, all suggesting a maximal to rapid tectonic rate. There are a number of beheaded and offset streams along the southern valley slope, although there is no consistent tectonic lateral offset. The axial river has migrated systematically eastwards in two places, leaving behind abandoned channels uplifted up to 10 m above the modern river channel (Fig. 18c). The uplift defines a pair of low-amplitude right-stepping en echelon periclines, consistent with Quaternary right-lateral shear. There is abundant evidence of revegetated landslip scars in the surrounding hills close to the fault.

A *c.* 10 m high scarp along the base of alluvial fans in the valley, visible in high-resolution DigitalGlobe satellite imagery from Google Earth, has the appearance of a normal fault surface rupture (Fig. 18d, e). The valley is relatively thinly vegetated and the scarp, discontinuous over *c.* 7.5 km, is well preserved. Although in places it is parallel to the modern river valley, the linear scarp also crosses higher ground, proving that it is not simply an erosional feature. By analogy with proved historical earthquake surface ruptures with a similar topographic expression – for example, the 1857 Lone Pine earthquake (Beanland & Clark 1994) and the 1609 Hongyazi earthquake (Xu *et al.* 2010) – the Buru scarp may have formed during the last few hundred years. The entire 10 m throw could have developed during a single M 7.5 earthquake, according to empirical relationships (Wells & Coppersmith 1994), or during a number of smaller events, similar to the Star Valley Fault at Afton, Wyoming,

Fig. 16. (*Continued*) thick forest cover. (**c**) Representative stream offset across the main Kawa Fault strand, image from Google Earth. (**d**) View into the Kawa Fault from the Wai Kawa delta showing the linear mountain front and triangular facets developed along the northern strand of the Taluti Bay splay. Image © 2016 DigitalGlobe. (**e**) Overview map of the Bobol fault zone showing Quaternary fault strands, rivers and left-lateral river offsets (in metres). Bold italic numbers are S_{mf} values. See Figure 14a for location. (**f**) Representative stream offset across the main Kawa Fault strand, also showing fault control of river channels. ESRI imagery.

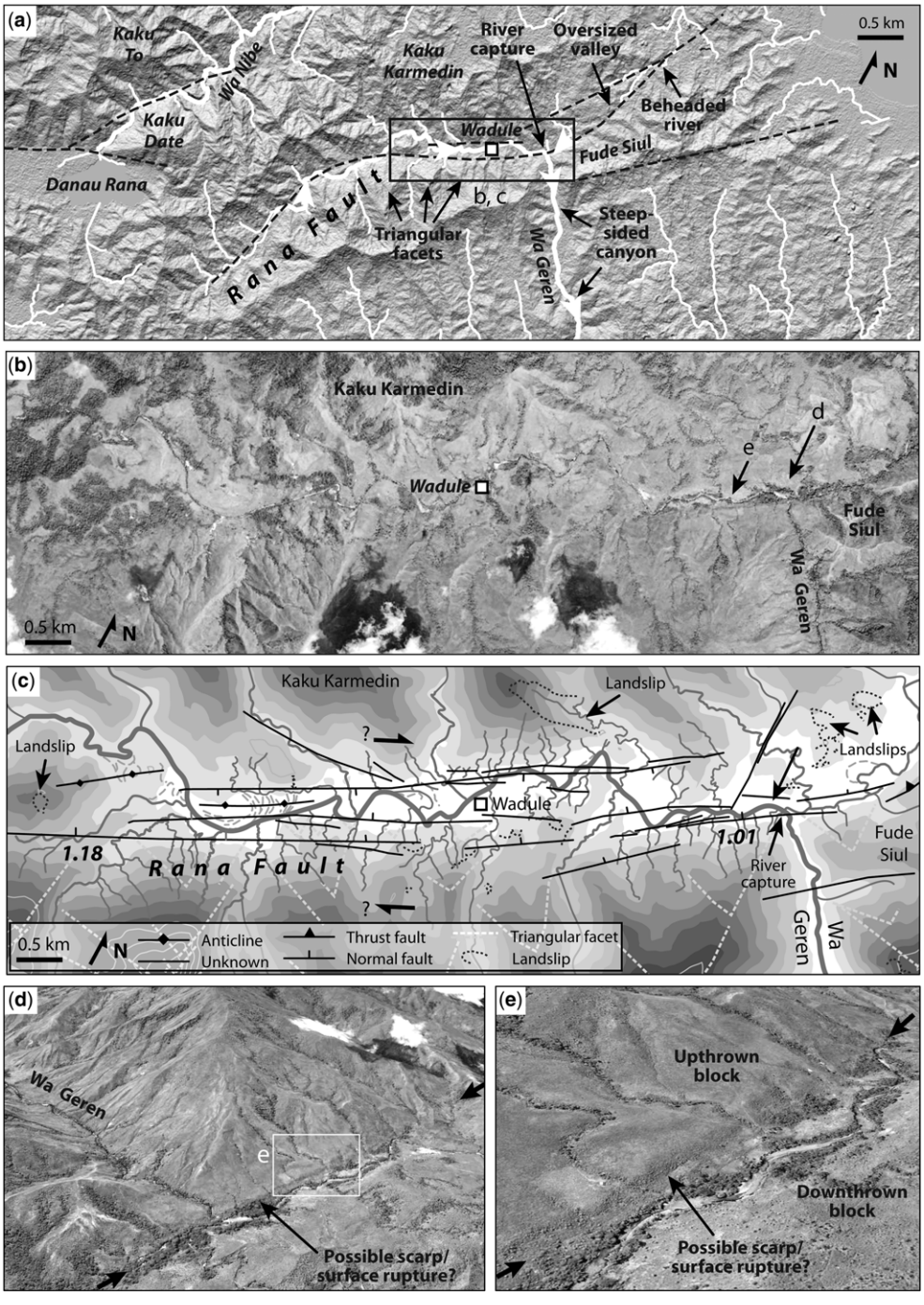

Fig. 18. Rana Fault, central Buru. (**a**) Overview of the Rana Fault, ASTER GDEM base map. Rivers marked in white, with white arrows showing the flow direction of major rivers discussed in the text. Location shown in Figure 17a. (**b**) ESRI image of the central part of the Rana Fault. (**c**) Interpretation of the image in (b), showing evidence of Quaternary fault activity. (**d**) Possible fault scarp along the foot of triangular facets marking the Rana Fault. (**e**) Detail of the possible fault scarp, showing steep dip, fresh geomorphic expression and straight trace. (d) and (e) are oblique views from Google Earth. Image © 2016 DigitalGlobe.

where an 11 m high scarp formed during three late Quaternary earthquakes (Piety *et al.* 1992). This is perhaps a more likely scenario given the relatively short length of the Rana Fault.

Elsewhere in Buru the geomorphic expression of other steep normal faults suggests rapid to moderate tectonic activity. Faults associated with the Rana Lake basin have S_{mf} values of 1.33–1.49 (Fig. 2j). Short fault segments in the SE of the island have S_{mf} values of 1.23 and 1.44, whereas those on the extreme east coast are more eroded, with S_{mf} values of 1.99 and 2.14 (Fig. 2k), indicating that they have been less active during the Quaternary.

Papua and West Papua

Oblique convergence at an angle of *c.* 60° between Australia and the Pacific is accommodated across Papua and West Papua in a complex zone of strain partitioning between shortening and left-lateral shear (e.g. Abers & McCaffrey 1988; McCaffrey 1996). West of about 138° E shortening is largely accommodated on a variety of structures in the New Guinea Trench and Manokwari Trough, in the Mamberamo fold–thrust belt and in the central Highlands to the south (e.g. Milsom *et al.* 1992; Puntodewo *et al.* 1994; Stevens *et al.* 2002). The largest earthquake to occur in eastern Indonesia since 1938 was the tsunamigenic 17 February 1996 M_w 8.2 Biak earthquake, which was also the largest thrust event worldwide since 1977 (Henry & Das 2002) and may have been associated with the 1979 M 7.9 Yapen earthquake (Okal 1999).

Left-lateral strain of up to 80 mm a^{-1} resulting from oblique Australia–Pacific convergence is accommodated across a 300 km wide zone of sinistral shear (Stevens *et al.* 2002) focused on the Yapen Fault system in the north and stepping across Cenderawasih Bay to the Tarera–Aiduna Fault system in the south, largely bypassing the antecedent Sorong Fault in West Papua (e.g. Puntodewo *et al.* 1994; McCaffrey 1996; Stevens *et al.* 2002; Bock *et al.* 2003). Left-lateral shear is passed from the Tarera–Aiduna Fault westwards into Maluku via the highly transpressive Seram fold–thrust belt (Teas *et al.* 2009).

As in Sulawesi, Maluku and North Maluku, extension is important within the overall convergent orogen. Cenderawasih Bay and the adjacent Waipoga Basin contain thick sediment piles (e.g. Dow & Sukamto 1984; Pubellier *et al.* 1999; Charlton 2010) and metamorphic core complex exhumation at the Wandamen Peninsula (e.g. Bailly *et al.* 2009) indicates extreme lithospheric stretching. Although extension may be related to processes within the wide left-lateral shear zone (Stevens *et al.* 2002), lessons from Sulawesi suggest that

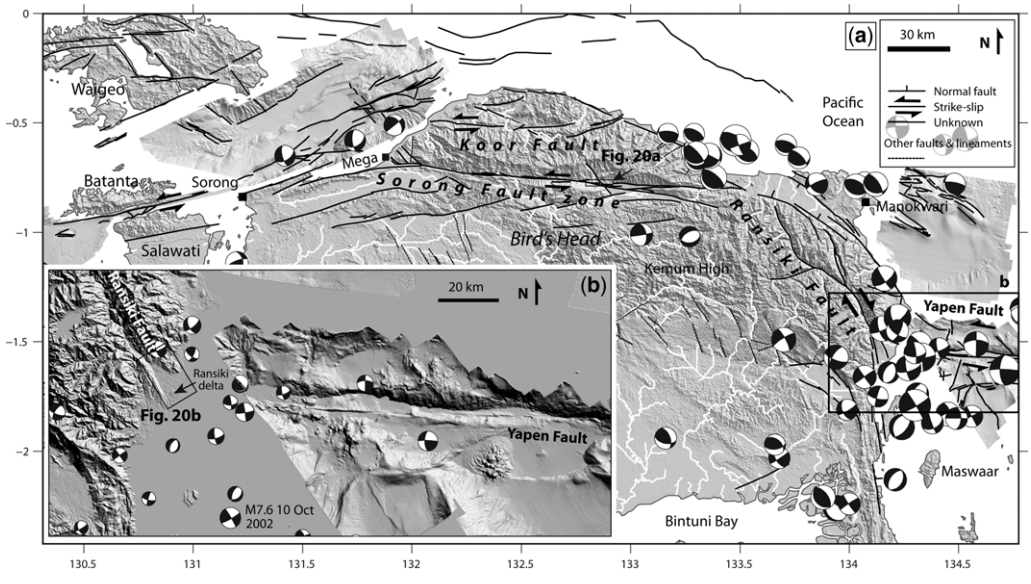

Fig. 19. (**a**) Bird's Head (West Papua) digital elevation model (SRTM), multibeam bathymetry, CMT catalogue earthquakes <35 km depth and structures showing evidence of Quaternary tectonic activity. Rivers marked in white. Location shown in Figure 1. Offshore structures north of the Koor Fault from Milsom *et al.* (1992). (**b**) Detail of the intersection between the Ransiki and Yapen faults, south of Manokwari. Eastern limit of image is to the east of the main map. SRTM onshore, multibeam bathymetry offshore.

far-field subduction-related mechanisms may also be significant.

Sorong Fault in West Papua

The Sorong Fault in West Papua is marked by a 15 km wide zone of pronounced linear ridges and valleys trending ENE from northern Salawati through Sorong city and into the deep valley cutting across the northernmost mainland towards Manokwari in the east (Fig. 19a). Hamilton (1979) questioned whether this structure was significant in post-Miocene tectonics, pointing out that parts of it were covered by post-Miocene strata, and it is now generally considered to be inactive (e.g. Puntodewo *et al.* 1994; Decker *et al.* 2009; Charlton 2010).

There is little significant seismicity along much of the fault and geodetic measurements suggest that both sides of the fault are broadly moving together and with the Pacific (e.g. Puntodewo *et al.* 1994; Stevens *et al.* 2002), with slight residual left-lateral motion between the Sorong and Fakfak GPS stations possibly accommodated on the Sorong Fault or the Koor Fault to the north (Bock *et al.* 2003). However, the Sorong GPS station is south of important strands of the Sorong Fault, which lie offshore to the north and come onshore at Mega, and the station is certainly south of the Koor Fault, leaving substantial uncertainty in the amount of present day left-lateral strain accommodated across this zone. The April 1937 M 6.9 and April 1944 M 7.2 and 7.4 earthquakes relocated by Okal (1999) were located on the onshore Sorong Fault 50–100 km west of Manokwari and had focal mechanisms indicating left-lateral shear. Apparent right-lateral motion between the Sorong and Biak GPS stations, taken to lie on opposite sides of the Sorong Fault (Puntodewo *et al.* 1994), is complicated by other structures such as the Ransiki and Yapen faults, which also lie between the stations.

Numerous convincing left-lateral stream offsets of up to 300 m are documented in the central part of the fault valley (Dow & Sukamto 1984) (Fig. 20a). Similar sized displacements of Wallace Creek crossing the San Andreas Fault have been dated to 13 259 years (Sieh & Jahns 1984). It is unclear how long such offsets can be preserved in the landscape of an environment like West Papua, but it is unlikely they are pre-Quaternary. Given that few such offsets are preserved in the more obviously active faults of eastern Indonesia, such as the Palu–Koro and Matano faults, the Sorong Fault examples must reflect relatively recent and significant strike-slip. Mountain front sinuosity along those segments of the fault associated with vertical motions is also conspicuously low, ranging from 1.16 to 1.17 along segments NNE of Sorong city to 1.14 along the central section, where Dow &

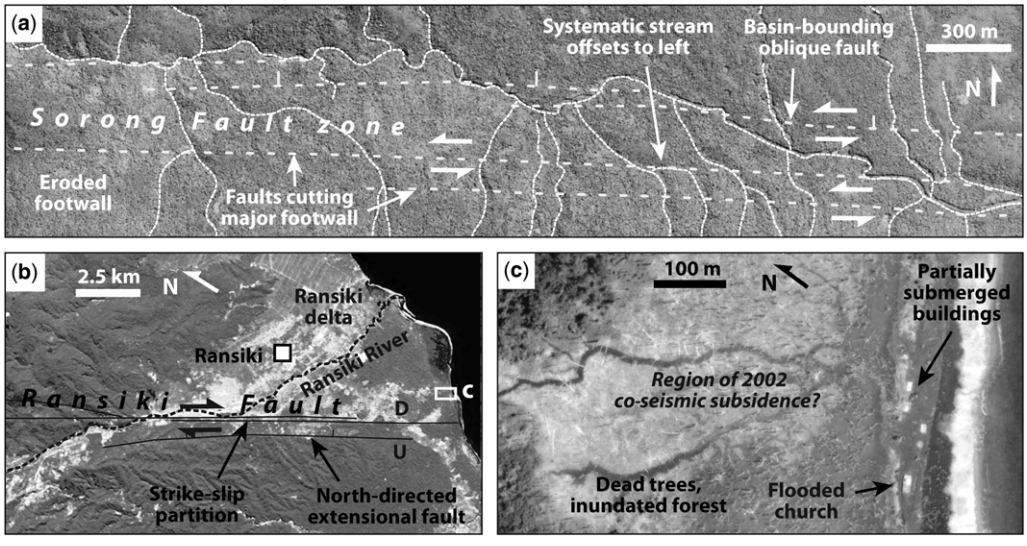

Fig. 20. Evidence of Quaternary fault activity in the Bird's Head. (**a**) Section of the onshore Sorong Fault showing a basin-bounding normal fault in the north and two strike-slip fault strands offsetting streams to the left in the south. Location shown in Figure 19a. ESRI imagery. (**b**) Ransiki delta at the southern end of the Ransiki Fault showing prominent western normal fault. Location shown in Figure 19b. (**c**) Region of co-seismic subsidence showing flooded forest and buildings adjacent to the western normal fault. Google Earth Imagery. Image © 2016 DigitalGlobe.

Sukamto (1984) measured displaced streams and where triangular facets and shutter ridges are well developed. In the east, S_{mf} values of 1.20 and 1.33 also suggest active tectonics. Faults adjacent to flat-topped Quaternary basins associated with Sorong Fault releasing geometries are interpreted to be dominantly normal faults (Fig. 20a) and these structures have generally higher S_{mf} values, including 1.60, 1.61, 1.74 and 2.79. The average V_f value for all these fault segments is 1.15, consistent with moderate to slow tectonic activity.

Koor Fault and Ransiki Fault

The Koor Fault is an east–west-trending structure 20–30 km north of the Sorong Fault (Fig. 19a), which lies within a boundary zone between the oceanic Pacific plate and continental crust in the south (Dow & Sukamto 1984). The NNW-trending Ransiki Fault (Fig. 19a) has been viewed as a dextral shear zone linking the easternmost Sorong Fault and the Yapen Fault (e.g. Robinson & Ratman 1978; Milsom *et al.* 1992; Charlton 2010).

Like the Sorong Fault in West Papua, both the Koor and Ransiki faults have been considered to be inactive (e.g. Hamilton 1979; Puntodewo *et al.* 1994). However, a shallow M 7.6 earthquake on 10 October 2002 at the southern end of the Ransiki Fault (Fig. 19b) had a focal mechanism and aftershock distribution consistent with dextral slip along the Ransiki Fault (NEIC), although the possibility of sinistral slip along a NE–SW-trending splay of the Yapen Fault cannot be excluded. Topographic and bathymetric data from the intersection (Fig. 19b) could be interpreted to show the two structures curving gently into each other, leading to the possibility of contraction in the Ransiki area.

Mountain front sinuosity measured along two splays of the southern Ransiki Fault yields values of 2.64 for a clearly inactive, *c.* north–south-trending southwestern strand, and 1.06 for the linear fault bounding the southern margin of Ransiki delta (Figs 2p & 19b). The very low S_{mf} and the asymmetrical position of the Ransiki River close to the fault scarp (Fig. 20b) support recent extensional activity along the fault. A 2 m high co-seismic surface rupture formed close to the fault scarp during the 2002 earthquake and was associated with subsidence of the delta that flooded a low-lying church (D. Gold, pers. comm. 2013), visible in satellite imagery to be coincident with a large region of flooded forest (Fig. 20c).

Yapen Fault

The Yapen Fault (Fig. 21a) is a highly linear east–west-trending structure that crosses the 320 km wide northern Cenderawasih Bay and is similar in character to the Sorong Fault in West Papua (e.g. Hamilton 1979; Dow & Sukamto 1984). In the east, the Yapen Fault vanishes into the Mamberamo delta (Fig. 21a), where it forms a subtle linear valley delineated by active mud volcanoes (Dow & Sukamto 1984) and may dissipate into the Mamberamo fold–thrust belt (Puntodewo *et al.* 1994). In the west, the Yapen Fault has an unclear termination, variously interpreted as being dextrally offset from the Sorong Fault along the Ransiki Fault (Puntodewo *et al.* 1994; Charlton 2010), linking/terminating against the Ransiki Fault (Milsom *et al.* 1992) and unconnected to inactive Ransiki/onshore Sorong faults, but transferring strain south to the Wandamen fault system (Bailly *et al.* 2009).

Geodetic measurements indicate a fast left-lateral slip rate of 46 ± 12 mm a^{-1} across the Yapen Fault (Bock *et al.* 2003), expressed by intense seismicity and focal mechanisms indicating left-lateral slip along east–west-trending subvertical planes (e.g. Okal 1999; Stevens *et al.* 2002). The 12 September 1979 M 7.9 tsunamigenic earthquake on the south coast of Yapen island (Fig. 21a) was associated with sinistral slip along a ESE–WNW-trending plane focused at a depth of 5 km and probably caused 2 m of displacement (Okal 1999).

The Randaway Fault Zone (Dow & Hartono 1982) is a set of NW–SE-trending faults onshore Yapen that link to strands of the Yapen Fault in the north (Fig. 21b). Interpreted as post-Plio-Pleistocene normal faults, they have previously been used to support a period of right-lateral shear along the Yapen Fault zone (Charlton 2010). However, we saw no geomorphic evidence of significant normal faulting along the Randaway trend – instead we saw a small linear basin and lake near the northern tip of the Randaway Fault at a left step-over and a deeply incised stream offset to the left by almost 1 km – both evidence of Quaternary sinistral shear (Fig. 21b).

Although the north coast of Yapen is remarkably straight and clearly fault-controlled, the main fault mostly lies just offshore to the north, meaning that geomorphic indices could not be usefully measured along the Yapen Fault. Multibeam bathymetry east of the island shows the Yapen Fault expressed by a straight, narrow lineament marked by pressure ridges and parallel to a prominent set of curvilinear normal faults (Fig. 21c). Splays of the fault curving to the WSW delimit at least two rhomboidal pull-apart basins. At the western limit of the multibeam data a splay appears to enter a third pull-apart basin, which is associated with a prominent north–south-trending sidewall fault. It is significant that this structure is parallel to, and 60 km north, of the Wandamen Peninsula – perhaps support for the southwards transfer of sinistral shear from the Yapen

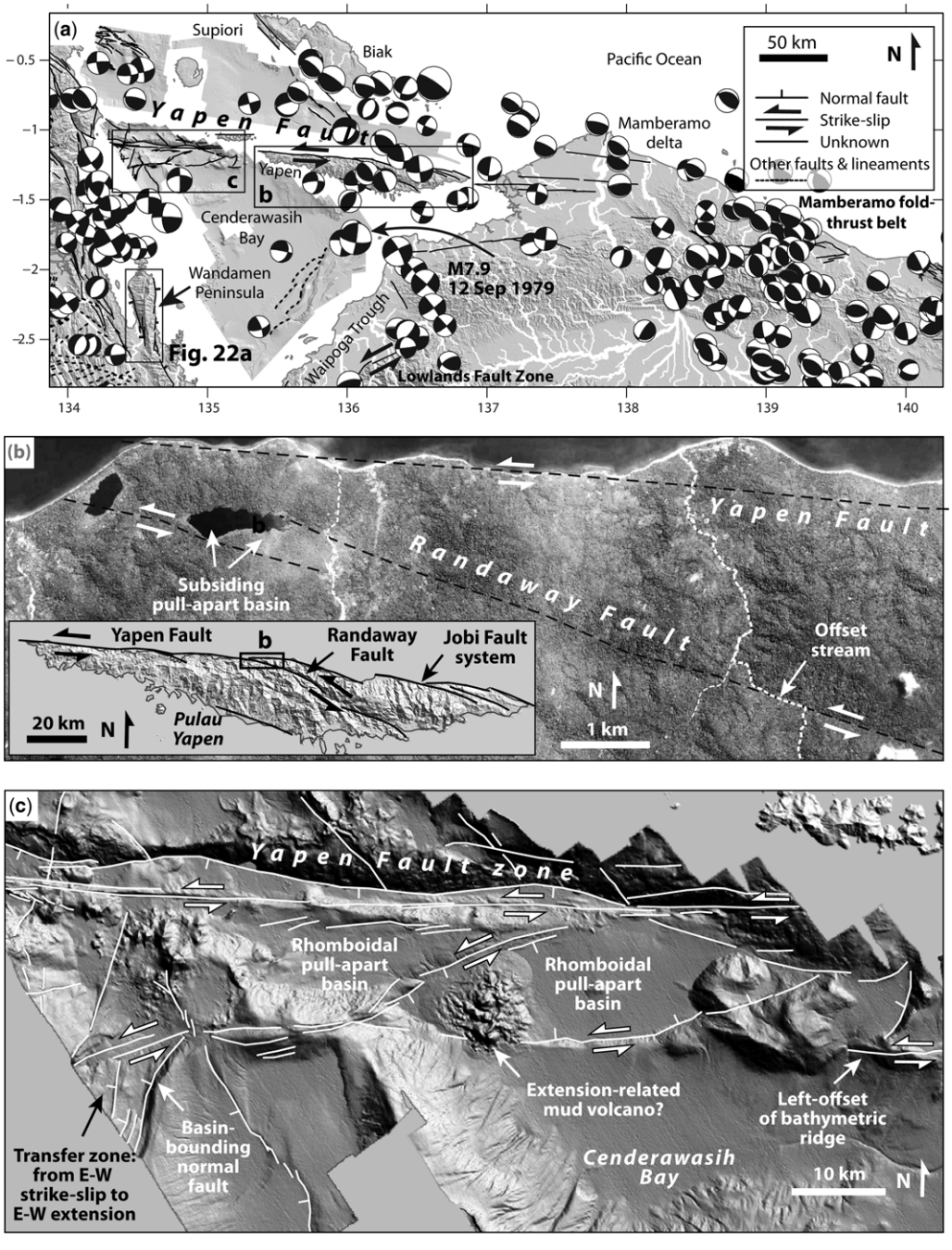

Fig. 21. Northern Papua and Cenderawasih Bay digital elevation model (SRTM), multibeam bathymetry, CMT catalogue earthquakes <35 km depth and structures showing geomorphic evidence of Quaternary tectonic activity. Rivers marked in white. Location shown in Figure 1. (**b**) Expression of the Yapen and Randaway faults along the northern coast of Pulau Yapen, showing evidence for Quaternary sinistral slip along the Randaway Fault. Inset shows the topography and major structures of Yapen. ESRI imagery. (**c**) Multibeam bathymetry detail showing the Yapen Fault to the west of Pulau Yapen; the southern strands appear to transfer to north–south extension via a series of pull-apart basins.

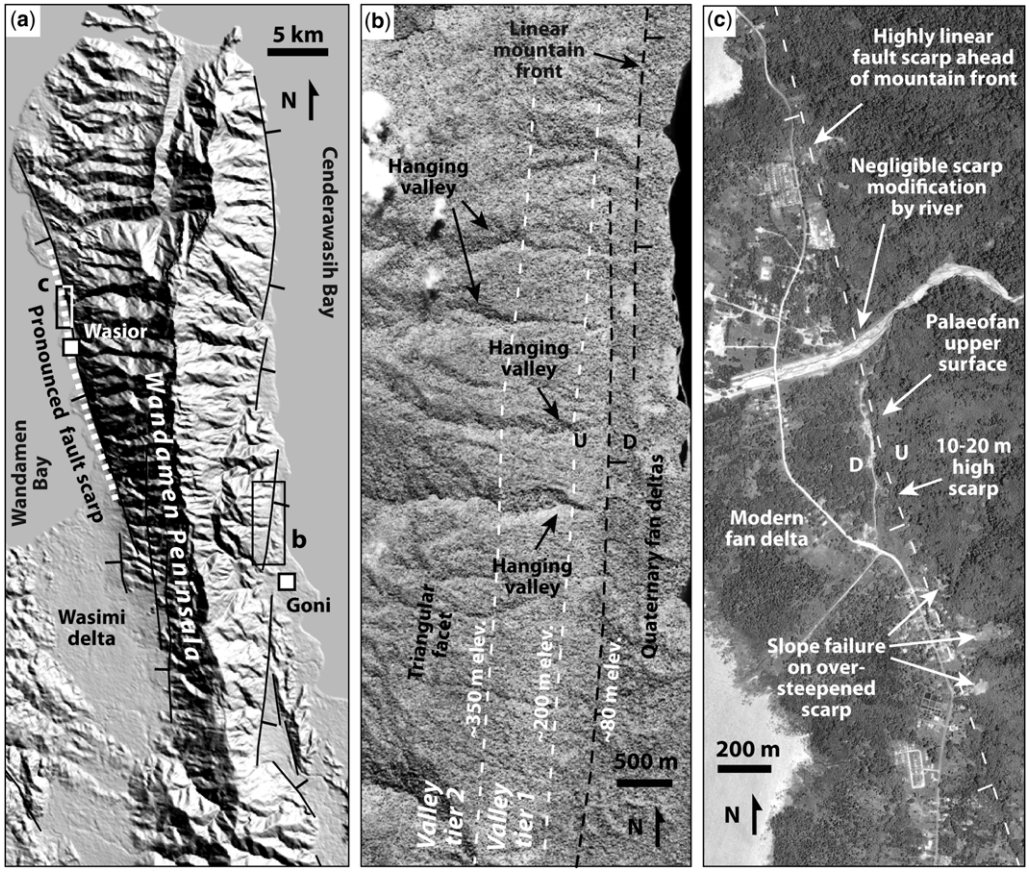

Fig. 22. Evidence of Wandamen Peninsula Quaternary fault activity. (**a**) Overview digital elevation model (SRTM) showing bounding normal faults. Location shown in Figure 21a. (**b**) Pronounced triangular facets and hanging valleys along the eastern bounding fault system. ESRI imagery. (**c**) Inferred Quaternary fault trace across the top of alluvial fans crossing the western fault system. Google Earth imagery. Image © 2016 DigitalGlobe.

Fault via a region of east–west extension, as proposed by Bailly *et al.* (2009).

Mamberamo fold–thrust belt

The Mamberamo fold–thrust belt (Fig. 21a) probably accommodates some Australia–Pacific shortening in eastern Papua and lies north of the Highlands thrust belt of central New Guinea (e.g. Dow & Sukamto 1984). Unlike the complex oblique convergence and strain partitioning further west, the belt contains relatively simple NW-trending active structures oriented normal to convergence (McCaffrey 1996). Despite intense and widespread seismicity, less than 15 mm a^{-1} of shortening occurs across the Mamberamo belt, leaving much of the remaining 45 mm a^{-1} Australia–Pacific convergence and 100 mm a^{-1} of left-lateral motion to offshore structures to the north and the Highlands thrust belt to the south (Puntodewo *et al.* 1994; McCaffrey 1996; Bock *et al.* 2003) (Fig. 1).

Wandamen Peninsula faults

The Wandamen Peninsula projects into Cenderawasih Bay from the eastern edge of the Lengguru fold belt, and is bounded on the east and west sides by north–south-trending faults (Fig. 22). We refer here specifically to these faults, not to the Wandamen Fault Zone of Dow & Sukamto (1984) that connects the Sorong Fault with the Tarera–Aiduna fault system via the Ransiki Fault.

The peninsula is considered to represent the exhumed internal zone of the Lengguru fold belt and is composed of an amphibolite–eclogite grade metamorphic dome rising to >2 km elevation (Robinson *et al.* 1990; Bailly *et al.* 2009; Charlton 2010), which may be a metamorphic core complex

(e.g. Hill *et al.* 2002). Seismicity and GPS vectors either side of Cenderawasih Bay (Stevens *et al.* 2002) suggest active extension accommodated on north–south-trending structures close to the Wandamen Peninsula, which may connect to the western releasing termination array of the Yapen Fault in the north (Fig. 21c).

Normal faults bounding the peninsula are expressed by curvilinear en echelon segments up to 20 km long trending north–south to NNW–SSE. These make up the east and west detachment systems of Bailly *et al.* (2009). Triangular facets, hanging valleys and V-shaped valleys are common and indicate rapid tectonic activity (Fig. 22b). Two tiers of hanging valleys on the eroded scarp of the eastern fault system are defined by changes in valley width or orientation at common elevations along the scarp. They probably record variations in the tectonic rate or climate during exhumation of the fault surface. Mountain front sinuosity values of four segments on the east side are uniform at 1.25, 1.28 and 1.29, with one more eroded segment of 1.72. Fan deltas are well developed at relays between the fault segments, notably at Goni and another smaller delta 21 km further north (Fig. 22a). As well as localizing sediment transport, the relays are likely to be sites of active displacement minima, allowing subaerial delta progradation on the hanging wall.

On the west of the peninsula, S_{mf} values range from 1.05 to 1.43, indicating maximal to rapid tectonic activity. A 21 km long section of the western fault system passing through Wasior shows evidence of recent normal faulting (Fig. 22c). Upper modern fan deltas are abruptly terminated by a linear scarp, above which are narrow truncated palaeofans. Rivers vertically incised into footwall palaeofans show little evidence of lateral erosion and small landslides are localized along the oversteepened scarp. The scarp is marked by a linear change in topography, lines of vegetation and often an abrupt change from meandering rivers upstream to anastomosing rivers downstream of the scarp. A southern continuation of the Wandamen fault system bounds the eastern margin of the Wasimi delta and has an S_{mf} value of 2.33, indicating slow to minimal tectonic activity.

Other circum-Cenderawasih Bay structures

The locus of active Australia–Pacific left-lateral strain partitioning shifts from the Yapen Fault system to the Tarera–Aiduna Fault system across Cenderawasih Bay, defining a 300 km wide shear zone that involves a complex array of Quaternary faults within the two bounding strike-slip zones (e.g. Stevens *et al.* 2002; Bock *et al.* 2003). Along the eastern margin of Cenderawasih Bay, the NE-trending

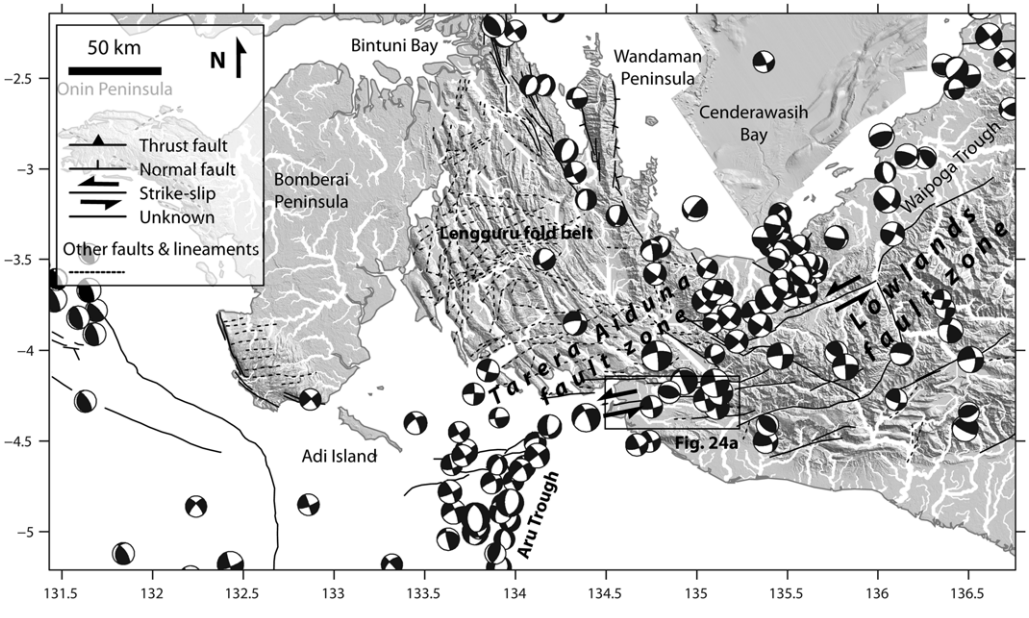

Fig. 23. Southern West Papua and Cenderawasih Bay digital elevation model (SRTM), multibeam bathymetry, CMT catalogue earthquakes <35 km depth and structures showing geomorphic evidence of Quaternary tectonic activity. Rivers marked in white. Location shown in Figure 1. Offshore structures from Teas *et al.* (2009).

Lowlands Fault Zone (bounding the Waipoga Trough of Visser & Hermes 1962) and the Paniai Fault Zone are associated with thrust and left-lateral strike-slip earthquakes (Fig. 23), offset drainage and high fault scarps, indicating modern tectonic activity (Pubellier *et al.* 1999; Stevens *et al.* 2002). The faults have a soft linkage with the Tarera–Aiduna Fault system in the south and splays curve into parallelism with the Yapen Fault and Mamberamo fold–thrust belt in the north.

The Lengguru fold belt (Visser & Hermes 1962) lies SW of Cenderawasih Bay and the Wandamen Peninsula, east of Bintuni Bay and the Bomberai Peninsula, and is bounded by the Tarera–Aiduna fault system in the south (Fig. 23). Compressional deformation terminated during the Pleistocene (Decker *et al.* 2009) and the belt is presently largely inactive, except for a few earthquakes related to gravitational collapse (Bailly *et al.* 2009), often with a left-lateral component related to residual Tarera–Aiduna strain.

Tarera–Aiduna Fault

The Tarera–Aiduna Fault (Visser & Hermes 1962) is an east–west-trending left-lateral shear zone that forms the southern boundary of the Lengguru fold belt and passes offshore to the west, north of the Aru Trough (Fig. 23). The Tarera–Aiduna Fault *sensu stricto* is part of a wide system of faults that pass, via a diffuse zone of sinistral transpression, into the Seram fold–thrust belt in the west (Teas *et al.* 2009). The fault system is at least 130 km long onshore (Fig. 24) and is expressed by straight lineaments clearly visible on satellite imagery (Hamilton 1979) and a set of en echelon folds (Katili 1986). Including possible soft linkage to Seram via sinistral transpression within the Seram fold–thrust belt, imaged in multibeam bathymetric data (Teas *et al.* 2009), the whole fault system may be >700 km long. Geodetic measurements show high relative motion between the Bird's Head north of the Tarera–Aiduna Fault and GPS stations south of the fault, such as Aru and Timika (Bock *et al.* 2003). Earthquake focal mechanisms showing sinistral slip along east–west-trending vertical planes (e.g. Seno & Kaplan 1988) suggest that the motion onshore is seismic and occurs along a broad zone (Fig. 23). Seismicity is largely absent west of the Bomberai peninsula, suggesting either a wide zone of aseismic deformation linking the Tarera–Aiduna Fault with the Seram sinistral transpression (Teas *et al.* 2009), a region of seismic deformation with recurrence times longer than the instrumental record, or no structural connection between the two regions.

The onshore Tarera–Aiduna Fault has a geomorphic expression typical of a major strike-slip fault zone (Fig. 24a). In the west it passes across a low-lying mangrove plain with minimal topographic relief. It is possible to trace several fault strands from linear features revealed by abandoned river channels and coastline segments (Fig. 24b). Its central section is expressed by a series of linear ridges of moderate relief bounding a wide rhomboidal basin (Fig. 24c), across which the captured Aru River passes into the Uruma River in the south. The river is abruptly deflected as it crosses two prominent fault strands, with 65–75 m left-lateral displacement, which may reflect recent Tarera–Aiduna Fault slip (Fig. 24d, e), although this offset is rather speculative.

An asymmetrical graben developed at the eastern termination of the Tarera–Aiduna Fault is bounded by NE–SW-trending normal faults (Fig. 24f). Rivers pressed hard against the NW-dipping bounding faults and a SE-dipping set of antithetic faults indicate active subsidence. The easternmost Tarera–Aiduna Fault itself has a significant dip-slip component, forming the northern margin of an 800 m high ridge. The Tarera–Aiduna Fault and the eastern bounding normal fault have S_{mf} values of 1.08 and 1.21, respectively, indicating that they are both active. Bounding faults along the northern margin of the rhomboidal basin, including segments corresponding to the Aria River Fault of Hamilton (1979), have S_{mf} values of 1.63, 1.91 and >4.00, pointing to slow to inactive tectonics.

Discussion

Challenges

The identification of Quaternary/modern fault activity in eastern Indonesia has historically proved difficult (e.g. Hamilton 1979; Dow & Sukamto 1984; Puntodewo *et al.* 1994; Socquet *et al.* 2006; Bailly *et al.* 2009; Teas *et al.* 2009). In part, this is because eastern Indonesia cannot be well described in terms of rigid plate tectonics, involving instead diffuse boundaries and boundary linkages, lithospheric strength heterogeneity and lower crustal flow (Hall 2011). All the fault zones in the region that are relatively well-constrained by geodetic data display strain gradients that can be explained in terms of multiple fault strands, distributed deformation or elastic strain surrounding a locked fault (e.g. Walpersdorf *et al.* 1998; Rangin *et al.* 1999; Stevens *et al.* 2002; Bock *et al.* 2003; Socquet *et al.* 2006). Poor historical earthquake records and few palaeoseismic data mean that it is difficult to distinguish between these options and so attention is naturally focused on geomorphologically prominent faults and lineaments or structures with instrumentally recorded seismicity. Faults or segments of fault systems with recurrence intervals greater than

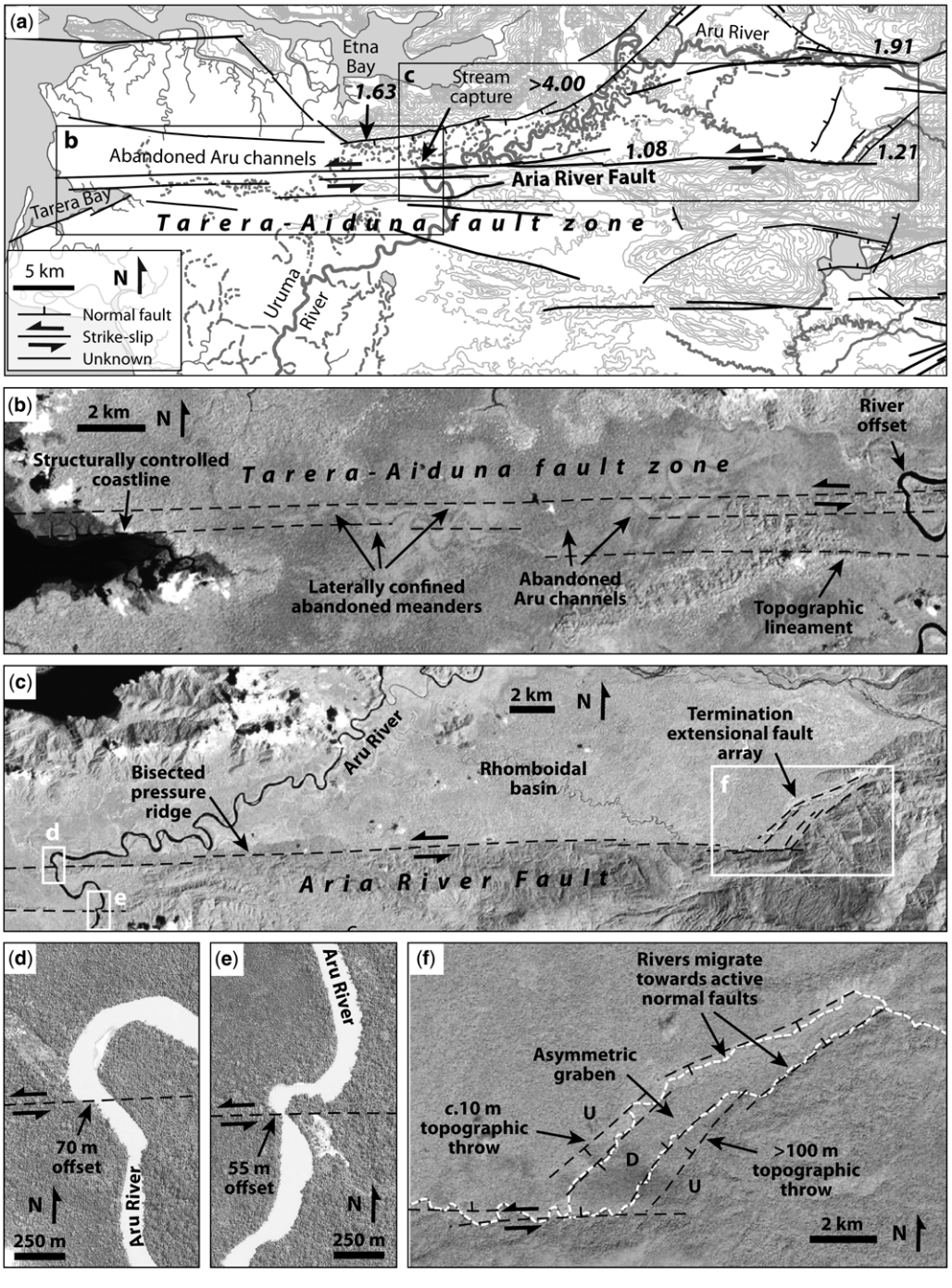

Fig. 24. (**a**) Map of the onshore Tarera–Aiduna Fault showing structures with geomorphic evidence of Quaternary tectonic activity. Bold italic numbers are S_{mf} values. Location shown in Figure 23. (**b**) Detail from greyscale Landsat TM 432 image showing linear confinement of abandoned River Aru channels, indicating strike-slip strands across the plain. (**c**) Major strand of the Tarera–Aiduna Fault bounding a steep-sided ridge and rhomboidal basin. (**d**, **e**) Possible river offset across the Tarera–Aiduna Fault. (**f**) Termination extensional fault array developed at the eastern end of the main Tarera–Aiduna Fault strand. (d, e, f) from ESRI imagery.

the short period of instrumental or even historical seismic records inevitably remain undocumented.

Additional challenges to the identification of Quaternary faults include thick forest over most of the islands (e.g. Pubellier *et al.* 1999), the abundance of important structures located entirely offshore and not readily available for study (e.g. Silver *et al.* 1983*b*; Henry & Das 2002; Teas *et al.* 2009; Liu & Harris 2013), the rapid erosion of tectonic landforms in the humid environment, the rapid burial of co-seismic features by a high sediment flux (e.g. Suggate & Hall 2003) and the high density of active and inactive structures within a large region (e.g. Puntodewo *et al.* 1994; Stevens *et al.* 2002).

Of the 27 fault systems described here, none can be confidently described as inactive during the Quaternary. Eleven show evidence of 'maximal' tectonic activity according to the classification summarized in McCalpin (2009) and a further five show evidence of 'rapid' tectonic activity (Table 3). It is important to note that the Quaternary faults discussed here are not exhaustive – there are numerous other active faults in the region, in addition to major offshore seismic sources, such as the Molucca Sea collision complex, the Banda Sea and Molucca Sea subducted slabs, and ongoing subduction of the Celebes Sea (e.g. Cardwell & Isacks 1978; Silver & Moore 1978; Cardwell *et al.* 1980; Silver *et al.* 1983*a*; Engdahl *et al.* 1998), which also need to be taken into account in any hazard analysis.

Quaternary fault geometry and earthquakes

The largest earthquakes in eastern Indonesia have been thrust and mega-thrust events, including those of the Seram Trough (1629, $M > 8.5$), the Banda Sea (1938, $M > 8.0$) and Biak (1996, M_w 8.2) (e.g. Wichmann 1918; Henry & Das 2002; Okal & Reymond 2003; Liu & Harris 2013). However, many major historical earthquakes in the studied region have occurred on strike-slip faults, including the Sorong Fault (1944, M 7.5), the Yapen Fault (1979, M 7.9) the Ransiki Fault (2002, M 7.6) and perhaps the Kawa Fault (1899, M 7.8) (e.g. Okal 1999; Brune *et al.* 2010; NEIC). Sixteen of the studied faults are dominantly strike-slip and an additional five may have a substantial strike-slip component (Table 3). As they are often long, straight, geometrically simple and subvertical, strike-slip faults are capable of generating large, shallow and damaging earthquakes – for example, the 1906 M 7.7 San Francisco earthquake (e.g. Wald *et al.* 1993), the 2001 M_w 7.8 Kunlun Shan earthquake (e.g. Lin *et al.* 2003) and the 2002 M_w 7.9 Denali earthquake (e.g. Haeussler *et al.* 2004).

A crucial barrier to the propagation of lateral ruptures and hence earthquake magnitude, even on straight strike-slip faults, is the presence of discontinuities or step-overs (e.g. Segal & Pollard 1980; Sibson 1985; Barka & Kadinsky-Cade 1988). The majority of historical strike-slip earthquake ruptures were arrested by step-overs wider than 3–5 km (Lettis *et al.* 2002; Wesnousky 2006). For example, the 1999 M_w 7.1 Düzce earthquake ruptured a 40 km segment of the North Anatolian Fault (Aydın & Kalafat 2002) and terminated in the >4 km wide Efteh releasing bend in the west and the 4–5 km wide Bakacak releasing step-over in the east (Duman *et al.* 2005). Straight, continuous faults are therefore capable of generating larger earthquakes than curved or segmented faults, of generating ruptures that penetrate below the seismogenic layer (King & Wesnousky 2007) and of sustained supershear rupture propagation, causing enhanced ground motion (Robinson *et al.* 2010). Eastern Indonesia's major strike-slip faults show a variety of levels of segmentation, which may be viewed as an indication of their structural maturity, with high cumulative displacements empirically known to remove fault zone complexities (e.g. Wesnousky 1988; Stirling *et al.* 1996; King & Wesnousky 2007). Other properties such as block rotation and pre-existing weaknesses may complicate this simple relationship.

The Matano Fault is an example of a structurally immature fault zone. Its onshore length of 195 km is punctuated by three major basins, each one 4–6 km wide, and two major restraining bends. The resultant maximum potential rupture length is 90 km (Table 3). Empirical rupture length–magnitude relationships (Wells & Coppersmith 1994) suggest a potential M 7.4 earthquake for such a rupture length. Uncertainties in this estimate include the unknown ability of a rupture to bypass the relatively gentle restraining bend east of the Mahalona Basin, the possibility of a through-going strike-slip fault at seismogenic depths below Lake Matano, the effect on fault strength of widespread serpentinite smears along the fault zone and the unknown length to which the fault continues offshore to the east.

The Sorong Fault in West Papua, part of the fault system at the southern end of the Philippine Sea plate, is a much more established fault zone with a long history of slip (e.g. Ali & Hall 1995), reflected in an apparent absence of step-overs >1 km and a continuous, straight onshore length of 420 km equating to a potential $M > 8.0$ earthquake if the entire linked system failed. The M_w 7.9 Yapen earthquake of 1979 ruptured an unknown length of the potentially 420 km long quasi-continuous Yapen Fault (Okal 1999), showing that such a scenario is possible. Despite evidence that most left-lateral strain is focused south of the Sorong Fault in West Papua, a conservative slip rate estimate of 2 mm a^{-1} could accumulate 2 m of elastic

Table 3. *Summary of observations made from Quaternary faults in eastern Indonesia, with hypothetical earthquake magnitudes, styles and tsunami risk*

Fault	Typical segment length (km)	Maximum observed total length (km)	Step-over/ relay width (km)	Potential rupture length (km)*	Attributable seismicity	Notable historical events	S_{mf} range	V_f range	Tectonic activity class†	Potential earthquake magnitude‡	Potential earthquake style	Associated tsunami?
Malino boundary	25–75	130	1.2	130	Y		1.05–1.66	0.22–1.01	Maximal to slow	7.6	Normal	Y
Gorontalo	30	95	7	35	N		1.83–2.36	0.88–1.69	Slow to minimal	6.9	Strike-slip	Y
Palu–Koro	10–35	220	<1	135	Y	M_w7.7, 1996	1.08–2.30	0.24–0.89	Maximal to slow	7.6	Strike-slip	Y
Parigi boundary	10–45	95	3	80	Y		1.32–3.25	0.50–1.45	Minimal	7.3	Normal	Y
Sapu valley	5–20	75	? <2	75	N		1.08–1.45	0.40	Maximal to moderate	7.3	Strike-slip	N
Balantak	54	250	10 (offshore)	54	Y		1.04–1.22	0.25–0.47	Maximal to moderate	7.1	Strike-slip	Y
Matano	10–60	195	6	90	Y	M_w 6.1, 2011	1.02–1.9	0.23–0.78	Maximal to slow	7.4	Strike-slip	Y (lake)
Lawanopo and Kendari	10–45	200	7	70	?	M_w 7.5, 2001?	1.21–1.75	0.55–0.83	Moderate to slow	7.2	Strike-slip	N
Towuti bounding	25–55	55	<1	55	N		1.03–2.04	0.41–1.22	Maximal to slow	7.1	Normal	Y (lake)
Kolaka	5–45	175	10	50	Y		1.05–1.64	0.23–1.68	Maximal to slow	7.0	Strike-slip	Y
Mangole	20	135	2	135	Y		1.12–1.57	0.49–0.55	Rapid to slow	7.6	Normal/ strike-slip	Y
Sanana	5–20	60	?	60	Y		1.27	0.44	Rapid	7.2	Normal/strike-slip	Y
Rana	10	65	3–4	>40	N	S_{fc} rupture?	1.01–1.96	0.23–1.53	Maximal to slow	>6.9	?Strike-slip	N
East Buru	10	48	<1	48	Y					7.0	Strike-slip	Y
Southern Seram	5–15	60	2	60	Y	?M 7.6, 1950	1.84–2.08	1.36–1.88	Slow	7.2	Normal	Y

Kawa	15–40	120	2	120	Y		1.10–1.33	0.26–0.28	Rapid to moderate	7.5	Strike-slip	Y
Bobol	10–15	100	2.5	100	N		1.26–1.99	1.04–2.60	Moderate to minimal	7.4	Strike-slip	Y
Combined Kawa–Bobol	10–40	240	2.5	240	Y	?M 7.8, 1899	1.10–1.99	0.26–2.66	Rapid to minimal	7.8	Strike-slip	Y
Seram FTB	5–15	135	>2	?135	Y					7.6	Thrust	Y
Sorong (West Papua)	45–75	420	<1	420	Y	M 7.4, 1944	1.14–2.85	0.27–8.68	Rapid to minimal	>8.0	Strike-slip	Y
Koor	15–35	100	6	75	Y					7.3	Strike-slip	Y
Ransiki	20–50	100	<1	100	Y	M 7.6, 2002	1.06–2.64		Maximal to minimal	7.4	Strike-slip	Y
Yapen	30–50	420	2–3	420	Y	M 7.9, 1979				>8.0	Strike-slip	Y
Mamberamo	10–20	180	<2	?180	Y	Numerous				7.7	Thrust	Y
Wandamen boundary	6–20	55	2	55	Y	S_{fc} rupture?	1.05–2.33		Maximal to slow	7.1	Normal	Y
Lowlands	30–70	220	?	?	Y					?	Normal/strike-slip	N
Paniai	?	150	?	?	Y					?	Normal/strike-slip	N
Tarera–Aiduna	30–60	130	7	90	Y		1.08–4.58		Maximal to minimal	7.4	Strike-slip	Y

*Maximum length of segment(s) separated by step-overs <3 km wide.
†Using scheme modified after McCalpin (2009).
‡Based on potential rupture length estimate and empirical length–magnitude relationships from Wells & Coppersmith (1994).

displacement across the northern Bird's Head (similar to the 1979 Yapen earthquake release; Okal 1999) in 1000 years. Even if all of this occurred west of the 1937 and 1944 earthquakes, and assuming complete stress release during those events, the remaining *c.* 200 km western portion of the fault could still generate a $M > 7.7$ earthquake.

The apparently very young and highly segmented Tarera–Aiduna fault zone and structures in the near-offshore Seram fold–thrust belt (Teas *et al.* 2009) and onshore Seram (Kawa and Bobol faults) could be part of a single soft-linked fault system and seem to partition much of the present day left-lateral motion between Australia and the Bird's Head. This fault system may thus be taking over the Pre-Pleistocene role of the Sorong Fault. Although there is not yet a through-going fault on the scale of the Sorong Fault, the individual components of the Tarera–Aiduna Fault and left-lateral faults in Seram are each capable of generating $M > 7$ earthquakes. Geomorphic observations suggest that they have all been active during the Quaternary, even if some segments (e.g. the Bobol Fault) lack instrumental seismicity records. A major uncertainty in assessing the Tarera–Aiduna fault system is the type and degree of linkage along its segments. The longest segment onshore with geomorphic evidence for rapid activity is 60 km long and may be traced, via an abrupt releasing bend 3 km wide, another 30 km to the east. Assuming rupture is not terminated by the bend, an M 7.4 earthquake is possible on this 90 km long segment. It is reasonable to assume that the fault passes some distance offshore before the next terminating step-over, so the maximum magnitude is likely to be larger.

In a similar manner, the maximum potential magnitudes for observed quasi-continuous segments of the Kawa and Bobol faults of southern Seram are 7.5 and 7.4, respectively, but a continuous rupture linking across Taluti Bay could achieve a length of 240 km and an earthquake magnitude of 7.8. The 1899 M 7.8 event, which caused slope failure north of Tehoru and a tsunami around Taluti Bay, could have originated from such a rupture.

The Palu valley has previously been considered to represent a pull-apart basin between two strands of the Palu–Koro Fault (Bellier *et al.* 2001, 2006; Beaudouin *et al.* 2003; Socquet *et al.* 2006). The width between the two strands would be about 6 km, ample to terminate earthquake rupture, limiting the maximum length and magnitude of Palu–Koro Fault earthquakes to the segments north and south of Palu valley. However, the possibility of a continuous, buried cross-basin fault system within the Palu valley as proposed here has significant implications for seismic hazard assessment in the densely populated valley. A continuous cross-basin fault within the Palu valley, as seen in analogue models (e.g. Wu *et al.* 2009) and natural strike-slip basins (e.g. the Clonard Basin, Haiti; Mann *et al.* 1995), means that the Palu–Koro Fault may be straighter and more continuous than previously suggested and palaeoseismic trenches across the border faults may not record major historical strike-slip earthquakes. The postulated buried and locked section alone is 50 km long and is thus capable of generating an M 7.0 earthquake. The total onshore length of the Palu–Koro Fault between Leboni valley and Palu city, lacking step-overs wider than 1 km and bends greater than 5°, is 135 km. As such, the Palu–Koro Fault must qualify as a 'fault superhighway', potentially capable of sustained super-shear rupture speeds (Robinson *et al.* 2010) and earthquakes up to M 7.6.

Other smaller structures that are geologically less significant because they are either not associated with instrumental seismicity (e.g. the Sapu valley fault system), have very low geomorphic tectonic activity indices (e.g. the Gorontalo Fault) or are composed of short and discontinuous fault segments (e.g. the Namlea fault system) are of particular importance from a hazard analysis perspective because of their proximity to large population centres with little to no earthquake resistance. Similarly, structures such as the Kolaka Fault, which has its most geomorphologically youthful segment bounding steep uplifted topography immediately adjacent to Kolaka town, may also be associated with secondary seismic hazards such as landslides. Large earthquakes along many of the faults, particularly the Palu–Koro, Matano and Balantak faults and the Molino, Towuti and Wandamen Peninsula boundary faults, may also trigger local tsunami, as has been already demonstrated in Palu and Taluti bays (e.g. Prasetya *et al.* 2001; Brune *et al.* 2010).

Conclusions

Neotectonic deformation in eastern Indonesia is rarely focused on discrete shear zones bounding rigid blocks, although this is often how it is interpreted. The pattern of seismicity and the broad distribution of Quaternary faults suggests that the region is more closely approximated by continuum mechanics than by rigid microplates (e.g. Thatcher 1995). All of the studied faults show geomorphic evidence of Quaternary tectonic activity, even in areas where high strain rates are not inferred from geodetic measurements (e.g. Buru, south Seram and northern West Papua).

The zone of left-lateral deformation that includes the Yapen Fault, the Tarera–Aiduna Fault and strike-slip associated with the Seram fold–thrust belt is perhaps the most active onshore/nearshore fault system of eastern Indonesia as recorded by

instrumental seismicity and geodetics. However, in terms of seismic risk, the Palu–Koro Fault is considered to be the most significant structure due to its proximity to Palu city, the possibility of a cross-basin fault system close to the city, the fault's unpredictability as a result of its poorly known seismic history, and the fault's potential to cause large, shallow focus, super-shear earthquakes. Additional factors increasing the risk of the Palu–Koro Fault include the possibility of liquefaction in the deep Quaternary sedimentary basin on which Palu city is built and the low-lying city's vulnerability to tsunami travelling down the narrow Palu Bay.

The Sorong Fault in West Papua should be viewed as the wildcard of eastern Indonesian active tectonics. Although GPS measurements appear to show little sinistral strike-slip motion, or even a degree of dextral slip, station locations in Sorong and Biak cannot resolve the complexity of the Sorong–Yapen–Ransiki Fault and may omit shear to the north. Convincing left-lateral stream offsets and low mountain front sinuosity values show that the fault has been active during the Quaternary. A dearth of seismicity, rather than indicating that the fault is benign, may instead indicate that it is locked and accumulating elastic strain. Magnitude 6.9, 7.2 and 7.4 earthquakes in 1937 and 1944, located on the fault west of Manokwari, prove that the fault is capable of generating large earthquakes. The Sorong Fault's contribution to the seismic hazard of West Papua should not be underestimated, particularly given its proximity to large towns such as Sorong and Manokwari.

There is great potential for the palaeoseismic study of some of the faults discussed in this paper to confirm Quaternary activity and to provide more detailed answers to questions about seismic hazards, particularly characteristic earthquake sizes and recurrence intervals. It is recommended that trenching work is carried out across possible surface ruptures identified along the Matano, Balantak, Rana, Ransiki and Wandamen Peninsula faults. Geophysical studies to image shallow fault strands in the Quaternary sedimentary-fill of several strike-slip basins, including the Palu, Sapu and Mahalona valleys, would help to confirm the existence of cross-basin strike-slip fault systems that may pose a previously unrecognized seismic hazard.

We are grateful to TGS (http://www.tgs.com), who provided the multibeam data, to John Decker, Phil Teas and the crew of the Shakti dive boat for support and valuable discussions during Banda Sea fieldwork. Alfend Rudyawan, Dave Gold, Ferry Yulian, Ega Abang Surya Nugraha, Jonathan Pownall and Benjamin Sapiie are thanked for their assistance and contributions to the ideas discussed here. Two anonymous reviewers are thanked for detailed and constructive reviews, which considerably improved the final paper. Recent fieldwork was funded by the SE Asia Research Group, Royal Holloway University of London.

Correction notice: In the revised paper, the meaning was changed in the opening sentence.

References

Abers, G. & McCaffrey, R. 1988. Active deformation in the New Guinea Fold-and-Thrust Belt: seismological evidence for strike-slip faulting and basement-involved thrusting. *Journal of Geophysical Research*, **93**, 13332–13354.

Ahmad, W. 1978. Geology along the Matano Fault Zone, East Sulawesi, Indonesia. *In*: Wiryosujono, S. & Sudradjat, A. (eds) *Proceedings: Regional Conference on the Geology and Mineral Resources of South East Asia*, Jakarta, Indonesia, 4–7 August 1975. Indonesian Association of Geologists, 143–150.

Ali, J.R. & Hall, R. 1995. Evolution of the boundary between the Philippine Sea Plate and Australia: palaeomagnetic evidence from eastern Indonesia. *Tectonophysics*, **251**, 251–275.

Audley-Charles, M.G. 1986. Timor-Tanimbar Trough: the foreland basin to the evolving Banda orogen. *In*: Allen, P.A. & Homewood, P. (eds) *Foreland Basins*. International Association of Sedimentologists, Special Publications, **8**, 91–102.

Audley-Charles, M.G., Carter, D.J. & Milsom, J. 1972. Tectonic development of Eastern Indonesia in relation to Gondwanaland dispersal. *Nature*, **239**, 35–39.

Aydin, A. & Kalafat, D. 2002. Surface ruptures of the 17 August and 12 November 1999 Izmit and Duzce earthquakes in northwestern Anatolia, Turkey: their tectonic and kinematic significance and the associated damage. *Bulletin of the Seismological Society of America*, **92**, 95–106.

Bailly, V., Pubellier, M., Ringenbach, J.-C., de Sigoyer, J. & Sapin, F. 2009. Deformation zone 'jumps' in a young convergent setting; the Lengguru fold-and-thrust belt, New Guinea Island. *Lithos*, **113**, 306–317.

Barka, A. & Kadinsky-Cade, K. 1988. Strike-slip fault geometry in Turkey and its influence on earthquake activity. *Tectonics*, **7**, 663–684.

Bath, M. & Duda, S.J. 1979. *Some Aspects of Global Seismicity*. Seismological Institute, Uppsala, 1–79.

Beanland, S. & Clark, M. 1994. *The Owens Valley Fault Zone, Eastern California, and Surface Faulting Associated with the 1872 Earthquake*. US Geological Survey Bulletin, **1982**. US Government Printing Office, Washington DC.

Beaudouin, T. 1998. *Tectonique active et sismotectonique du système de failles décrochantes de Sulawesi Central*. Thèse de Doctorat, Universitá Paris-Sud.

Beaudouin, T., Bellier, O. & Sebrier, M. 2003. Present-day stress and deformation fields within the Sulawesi Island area (Indonesia): geodynamic implications. *Bulletin de la Société géologique de France*, **174**, 305–317.

Bellier, O., Beaudouin, T. *et al.* 1998. Active faulting in central Sulawesi (eastern Indonesia). *In*: Wilson, P.

& Michel, G.W. (eds) *The Geodynamics of S, SE Asia (GEODYSSEA Project)*. GeoForshingsZentrum, Potsdam, 276–312.

Bellier, O., Sebrier, M. *et al*. 2001. High slip rate for a low seismicity along the Palu-Koro active fault in central Sulawesi (Indonesia). *Terra Nova*, **13**, 463–470.

Bellier, O., Sébrier, M., Seward, D., Beaudouin, T., Villeneuve, M. & Putranto, E. 2006. Fission track and fault kinematics analyses for new insight into the Late Cenozoic tectonic regime changes in West-Central Sulawesi (Indonesia). *Tectonophysics*, **413**, 201–220.

Bock, Y., Prawirodirdjo, L. *et al*. 2003. Crustal motion in Indonesia from global positioning system measurements. *Journal of Geophysical Research*, **108**, 2367.

Brune, S., Babeyko, A.Y., Ladage, S. & Sobolev, S.V. 2010. Landslide tsunami hazards in the Indonesian Sunda Arc. *Natural Hazards Earth Systems Science*, **10**, 589–604.

Bull, W.B. 1978. *Geomorphic Tectonic Activity Classes of the South Front of the San Gabriel Mountains, California*. Final Report, US Geological Survey, Contract No. 14-08-0001-G-394.

Bull, W.B. 2007. *Tectonic Geomorphology of Mountains: a New Approach to Paleoseismology*. Blackwell Publishing, Malden, MA.

Bull, W.B. & McFadden, L.D. 1977. Tectonic geomorphology north and south of the Garlock fault, California. *In*: Doehering, D.O. (ed.) *Geomorphology in Arid Regions. Proceedings at the Eighth Annual Geomorphology Symposium*. State University of New York, Binghamton, NY, 115–138.

Burchfiel, B.C., Royden, L.H. *et al*. 2008. A geological and geophysical context for the Wenchuan earthquake of 12 May 2008, Sichuan, People's Republic of China. *Geological Society of America Today*, **18**, 4–11.

Camplin, D.J. & Hall, R. 2014. Neogene history of None Gulf, Sulawesi, Indonesia. *Marine and Petroleum Geology*, **57**, 88–108.

Cardwell, R.K. & Isacks, B.L. 1978. Geometry of the subducted lithosphere beneath the Banda Sea in eastern Indonesia from seismicity and fault plane solutions. *Journal of Geophysical Research*, **83**, 2825–2838.

Cardwell, R.K., Isacks, B.L. & Karig, D.E. 1980. The spatial distribution of earthquakes, focal mechanism solutions, and subducted lithosphere in the Philippine and northeastern Indonesian islands. *In*: Hayes, D.E. (ed.) *The Tectonic, Geologic Evolution of Southeast Asian Seas, Islands*. American Geophysical Union, Geophysical Monograph, **23**, 1–35.

Charlton, T.R. 2010. The Pliocene–Recent anticlockwise rotation of the Bird's Head, the opening of the Aru Trough–Cenderawasih Bay sphenochasm, and the closure of the Banda double arc. *In*: *Proceedings, Indonesian Petroleum Association, 34th Annual Convention and Exhibition*. IPA10-G-008.

Chen, W.-P. & Hsu, L. 2013. Historic seismicity near the source zone of the great 2008 Wenchuan earthquake: implications for seismic hazards. *Tectonophysics*, **584**, 114–118.

Cottam, M.A., Hall, R., Forster, M.A. & Boudagher-Fadel, M.K. 2011. Basement character and basin formation in Gorontalo Bay, Sulawesi, Indonesia: new observations from the Togian Islands. *In*: Hall, R., Cottam, M.A. & Wilson, M.E.J. (eds) *The SE Asian Gateway: History, Tectonics of the Australia–Asia Collision*. Geological Society, London, Special Publications, **355**, 177–202, https://doi.org/10.1144/SP355.9

Decker, J., Bergman, S.C., Teas, P.A., Baillie, P. & Orange, D.L. 2009. Constraints on the tectonic evolution of the Bird's Head, West Papua. *In*: *Proceedings, Indonesian Petroleum Association, 33rd Annual Convention and Exhibition*, IPA09-G-139.

Dehbozorgi, M., Pourkermani, M., Arian, M., Matkan, A.A., Motamedi, H. & Hosseiniasl, A. 2010. Quantitative analysis of relative tectonic activity in the Sarvestan area, central Zagros, Iran. *Geomorphology*, **121**, 329–341.

DeMets, C., Gordon, R., Argus, D. & Stein, S. 1994. Effects of recent revisions to the geomagnetic reversal time scale on estimates of current plate motions. *Geophysical Research Letters*, **21**, 2191–2194.

Dow, D.B. & Hartono, U. 1982. The nature of the crust underlying Cenderawasih (Geelvink) Bay, Irian Jaya. *Proceedings of the Indonesian Petroleum Association*, **11**, 203–210.

Dow, D.B. & Sukamto, R. 1984. Western Irian Jaya: the end-product of oblique plate convergence in the Late Tertiary. *Tectonophysics*, **106**, 109–139.

Duman, T.Y., Emre, O., Dogan, A. & Ozalp, S. 2005. Step-over and bend structures along the 1999 Duzce Earthquake surface rupture, North Anatolian Fault, Turkey. *Bulletin of the Seismological Society of America*, **95**, 1250–1262, https://doi.org/10.1785/0120040082

Engdahl, E.R., van der Hilst, R. & Buland, R. 1998. Global teleseismic earthquake relocation with improved travel times and procedures for depth determination. *Bulletin of the Seismological Society of America*, **88**, 722–743.

Eshghi, S. & Zare, M. 2003. Bam (SE Iran) Earthquake of 26 December 2003, Mw 6.5. A Preliminary Reconnaissance Report, www.iiees.ac.ir/en/wp-content/uploads/2010/12/Bam_report_zare.pdf [last accessed 29 October 2016].

Ferdian, F., Hall, R. & Watkinson, I. 2010. A structural re-evaluation of the north Banggai-Sula area, eastern Indonesia. *In*: *Proceedings, Indonesian Petroleum Association, 34th Annual Convention*, IPA07-G-009, 1–20.

Fu, B., Ninomiya, Y., Lei, X., Toda, S. & Awata, Y. 2004. Mapping active fault associated with the 2003 M_w 6.6 Bam (SE Iran) earthquake with ASTER 3D images. *Remote Sensing of Environment*, **92**, 153–157.

Garrard, R.A., Supandjono, J.B. & Surono, 1988. The geology of the Banggai-Sula microcontinent, eastern Indonesia. *In*: *Proceedings, Indonesian Petroleum Association, 17th Annual Convention*, 23–52.

Germeraad, J.H. 1946. Geology of central Seran. *In*: Rutten, L. & Hotz, W. (eds) *Geological, Petrographical, and Palaeontological Results of Explorations Carried Out September 1917–June 1919, Island of Ceram*. De Bussy, Amsterdam.

Haeussler, P.J., Schwartz, D.P., Dawson, T.E., Stenner, H.D., Lienkaemper, J.J., Sherrod, B. & Personius, S.F. 2004. Surface rupture and slip

distribution of the Denali and Totschunda faults in the 3 November 2002 M 7.9 earthquake, Alaska. *Bulletin of the Seismological Society of America*, **94**, S23–S52.

Haffner, G.D., Hehanussa, P.E. & Hartoto, D. 2001. The biology and physical processes of large lakes of Indonesia: Lakes Matano and Towuti. *In*: Munawar, M. & Hecky, R.E. (eds) *The Great Lakes of the World (GLOW): Food-Web, Health, Integrity, Ecovision*. Ecovision World Monograph Series. Backhuys Publishers, Leiden, 183–192.

Hall, R. 1987. Plate boundary evolution in the Halmahera region, Indonesia. *Tectonophysics*, **144**, 337–352.

Hall, R. 1996. Reconstructing Cenozoic SE Asia. *In*: Hall, R. & Blundell, D.J. (eds) *Tectonic Evolution of SE Asia*. Geological Society, London, Special Publications, **106**, 153–184, https://doi.org/10.1144/GSL.SP.1996.106.01.11

Hall, R. 2002. Cenozoic geological and plate tectonic evolution of SE Asia and the SW Pacific: computer-based reconstructions, model and animations. *Journal of Asian Earth Sciences*, **20**, 353–434.

Hall, R. 2011. Australia–SE Asia collision: plate tectonics and crustal flow. *In*: Hall, R., Cottam, M.A. & Wilson, M.E.J. (eds) *The SE Asian Gateway: History, Tectonics of the Australia–Asia Collision*. Geological Society, London, Special Publications, **355**, 75–109, https://doi.org/10.1144/SP355.5

Hall, R. 2012. Late Jurassic–Cenozoic reconstructions of the Indonesian region and the Indian Ocean. *Tectonophysics*, **570**, 1–41.

Hall, R., Fuller, M., Ali, J.R. & Anderson, C.D. 1995. The Philippine Sea plate: magnetism and reconstructions. *In*: Taylor, B. & Natland, J.H. (eds) *Active Margins, Marginal Basins: a Synthesis of Western Pacific Drilling Results*. American Geophysical Union Monograph, **88**, 371–404.

Hamilton, W. 1979. *Tectonics of the Indonesian Region*. US Geological Survey, Professional Papers, **1078**.

Harris, R.A. 1992. Peri-collisional extension and the formation of Oman type ophiolites in the Banda Arc and Brooks Range. *In*: Parson, L.M., Murton, B.J. & Browning, P. (eds) *Ophiolites, their Modern Oceanic Analogues*. Geological Society, London, Special Publications, **60**, 301–325, https://doi.org/10.1144/GSL.SP.1992.060.01.19

Hennig, J., Advokaat, E., Rudyawan, A. & Hall, R. 2014. Large sediment accumulations and major subsidence offshore; rapid uplift on land: consequences of extension of Gorontalo Bay and Northern Sulawesi. *In*: *Proceedings, Indonesian Petroleum Association, 38th Annual Convention and Exhibition*, IPA14-G-304.

Henry, C. & Das, S. 2002. The M_w 8.2, 17 February 1996 Biak, Indonesia, earthquake: rupture history, aftershocks, and fault plane properties. *Journal of Geophysical Research*, **107**, https://doi.org/10.1029/2001jb000796

Hill, K.C., Hoffman, N., Lunt, P. & Paul, R. 2002. Structure and hydrocarbons in the Sareba block, 'Bird's Neck', West Papua. *In*: *Proceedings, Indonesian Petroleum Association, 28th Annual Convention*, IPA01-G-115, 227–248.

Holzer, L.T. & Savage, J.C. 2013. Global earthquake fatalities and population. *Earthquake Spectra*, **29**, 155–175.

Huang, W. 1993. Morphologic patterns of stream channels on the active Yishi Fault, southern Shandong Province, Eastern China: implications for repeated great earthquakes in the Holocene. *Tectonophysics*, **219**, 283–304.

Hutchison, C.S. 1989. *Geological Evolution of South-East Asia*. Clarendon Press, Oxford.

Jablonski, D., Priyono, P., Westlake, S. & Larsen, O.A. 2007. Geology and exploration potential of the Gorontalo basin, central Indonesia – eastern extension of the North Makassar Basin? *In*: *Proceedings, Indonesian Petroleum Association, 31st Annual Convention and Exhibition*. IPA07-G-083.

Katili, J.A. 1970. Additional evidence of transcurrent faulting in Sumatra and Sulawesi. *Bandung National Institute of Geology and Mining Bulletin*, **3**, 15–28.

Katili, J.A. 1973. On fitting certain geological and geophysical features of the Indonesian island arc to the new global tectonics. *In*: Coleman, P.J. (ed.) *The Western Pacific: Island Arcs, Marginal Seas, Geochemistry*. Western Australia University Press, Perth, 287–305.

Katili, J.A. 1975. Volcanism and plate tectonics in the Indonesian island arcs. *Tectonophysics*, **26**, 165–188.

Katili, J.A. 1986. Geology and hydrocarbon potential of the Arafura Sea. *In*: Halbouty, M.T. (ed.) *Future Petroleum Provinces of the World*. AAPG Memoirs, **40**, 487–501.

Kavalieris, I., van Leeuwen, T.M. & Wilson, M. 1992. Geological setting and styles of mineralization, north arm of Sulawesi, Indonesia. *Journal of Southeast Asian Earth Sciences*, **7**, 113–130.

Keller, E.A. 1986. Investigation of active tectonics: use of surficial Earth processes. *In*: Wallace, R.E. (ed.) *Active Tectonics*, Studies in Geophysics. National Academy Press, Washington, DC, 136–147.

King, G.C.P. & Wesnousky, S.G. 2007. Scaling of fault parameters for continental strike-slip earthquakes. *Bulletin of the Seismological Society of America*, **97**, 1833–1840.

Lacassin, R., Replumaz, A. & Leloup, P.H. 1998. Hairpin river loops and slip-sense inversion on Southeast Asian strike-slip faults. *Geology*, **26**, 703–706.

Lettis, W., Bachhuber, J. *et al.* 2002. Influence of releasing step-overs on surface fault rupture and fault segmentation: examples from the 17 August 1999 Izmit earthquake on the North Anatolian Fault, Turkey. *Bulletin of the Seismological Society of America*, **92**, 19–42.

Lin, A., Kikuchi, M. & Fu, B. 2003. Rupture segmentation and process of the 2001 M_w 7.8 central Kunlun earthquake, China. *Bulletin of Seismological Society of America*, **93**, 2477–2492.

Linthout, K., Helmers, H., Sopaheluwakan, J. & Surya Nila, E. 1989. Metamorphic complexes in Buru and Seram, northern Banda Arc. *Netherlands Journal of Sea Research*, **24**, 345–356.

Linthout, K., Helmers, H. & Andriessenm, P.A.M. 1991. Dextral strike-slip in Central Seram and 3–4.5 Ma Rb/Sr ages in pre-Triassic metamorphics

related to Early Pliocene counterclockwise rotation of the Buru-Seram microplate (E. Indonesia). *Journal of Southeast Asian Earth Sciences*, **6**, 335–342.

Liu, Z.Y.-C. & Harris, R.A. 2013. Discovery of possible mega-thrust earthquake along the Seram Trough from records of 1629 tsunami in eastern Indonesian region. *Natural Hazards*, **72**, 1311–1328.

Mann, P. 2007. Global catalogue, classification and tectonic origins of restraining- and releasing bends on active and ancient strike-slip fault systems. *In*: Cunningham, W.D. & Mann, P. (eds) *Tectonics of Strike-Slip Restraining and Releasing Bends*. Geological Society, London, Special Publications, **290**, 13–142, https://doi.org/10.1144/SP290.2

Mann, P., Taylor, F.W., Lawrence Edwards, R. & Teh-Lung, Ku. 1995. Actively evolving microplate formation by oblique collision and sideways motion along strike-slip faults: an example from the northeastern Caribbean plate margin. *Tectonophysics*, **246**, 1–69.

McCaffrey, R. 1989. Seismological constraints and speculations on Banda arc tectonics. *Netherlands Journal of Sea Research*, **24**, 141–152.

McCaffrey, R. 1996. Slip partitioning at convergent plate boundaries of SE Asia. *In*: Hall, R. & Blundell, D.J. (eds) *Tectonic Evolution of Southeast Asia*. Geological Society, London, Special Publications, **106**, 3–18, https://doi.org/10.1144/GSL.SP.1996.106.01.02

McCaffrey, R. & Sutardjo, R. 1982. Reconnaissance microearthquake survey of Sulawesi, Indonesia. *Geophysical Research Letters*, **9**, 793–796.

McCalpin, J.P. (ed.) 2009. *Palaeoseismology*. 2nd ed. International Geophysics Series, **95**. Academic Press, Burlington, USA.

Michetti, A.M., Audemard, F.A. & Marco, S. 2005. Future trends in palaeoseismology: integrated study of the seismic landscape as a vital tool in seismic hazard analyses. *Tectonophysics*, **408**, 3–21.

Milsom, J., Masson, D., Nichols, G., Sikumbang, N., Dwiyanto, B., Parson, L. & Kallagher, H. 1992. The Manokwari Trough and the western end of the New Guinea Trench. *Tectonics*, **11**, 145–153.

Molnar, P. & Dayem, K.E. 2010. Major intercontinental strike-slip faults and contrasts in lithospheric strength. *Geosphere*, **6**, 444–467.

Natawidjaja, D.H. & Daryono, M.R. 2014. The Lawanopo Fault, Central Sulawesi, East Indonesia. *In*: *Proceedings, 4th International Symposium on Earthquake and Disaster Mitigation 2014 (ISEDM 2014)*. 11–12 November 2014, Bandung, Indonesia, https://doi.org/10.1063/1.4915009

National Earthquake Information Centre (NEIC). http://earthquake.usgs.gov/contactus/golden/neic.php [last accessed 29 October 2016].

National Geophysical Data Center/World Data Service. Global Significant Earthquake Database. National Geophysical Data Center, NOAA, https://doi.org/10.7289/V5TD9V7K [last accessed 29 October 2016].

Norvick, M.S. 1979. The tectonic history of the Banda arcs, eastern Indonesia: a review. *Journal of the Geological Society, London*, **136**, 519–527, https://doi.org/10.1144/gsjgs.136.5.0519

Okal, E.A. 1999. Historical seismicity and seismotectonic context of the great 1979 Yapen and Biak, Irian Jaya earthquakes. *Pure and Applied Geophysics*, **154**, 633–675.

Okal, E.A. & Reymond, D. 2003. The mechanism of great Banda sea earthquake of 1 February 1938: applying the method of preliminary determination of focal mechanism to a historical event. *Earth and Planetary Science Letters*, **216**, 1–15.

Pairault, A.A., Hall, R. & Elders, C.F. 2003. Tectonic Evolution of the Seram Trough, Indonesia. *In*: *Proceedings, Indonesian Petroleum Association, 29th Annual Convention*, 355–370.

Pavlides, S.B. 1989. Looking for a definition of neotectonics. *Terra Nova*, **1**, 233–235, https://doi.org/10.1111/j.1365-3121.1989.tb00362.x

Pelinovsky, E., Yuliadi, D., Prasetya, G. & Hidayat, R. 1997. The 1996 Sulawesi tsunami. *Natural Hazards*, **16**, 29–38.

Pholbud, P., Hall, R., Advokaat, E., Burgess, P. & Rudyawan, A. 2012. A new interpretation of Gorontalo Bay, Sulawesi. *In*: *Proceedings, Indonesian Petroleum Association, 36th Annual Convention*, IPA12-G-029, 197–224.

Piety, L., Sullivan, J.T. & Anders, M.H. 1992. Segmentation and paleoseismicity of the Grand Valley Fault, southeastern Idaho and western Wyoming. *In*: Link, P.K., Kuntz, M.A. & Platt, L.B. (eds) *Regional Geology of Eastern Idaho and Western Wyoming*. Geological Society of America, Memoirs, **179**, 155–182.

Pigram, C.J. & Panggabean, H. 1984. Rifting of the eastern margin of the Australian continent and the origin of some microcontinents in Indonesia. *Tectonophysics*, **107**, 331–353.

Pigram, C.J. Surono & Supandjono, J.B. 1985. Origin of the Sula Platform, eastern Indonesia. *Geology*, **13**, 246–248.

Pownall, J.M., Hall, R. & Watkinson, I.M. 2013. Extreme extension across Seram and Ambon, eastern Indonesia: evidence for Banda slab rollback. *Solid Earth*, **4**, 277–314.

Pownall, J.M., Hall, R., Armstrong, R.A. & Forster, M.A. 2014. Earth's youngest known ultrahigh-temperature granulites discovered on Seram, eastern Indonesia. *Geology*, **42**, 279–282.

Prasetya, G.S., de Lange, W.P. & Healy, T.R. 2001. The Makassar Strait Tsunamigenic Region, Indonesia. *Natural Hazards*, **24**, 295–307.

Pubellier, M., Desfontaines, B., Chorowicz, J., Rudant, J.-P. & Permana, H. 1999. Active denudation morphostructures from SAR ERS-1 images (SW Irian Jaya). *International Journal of Remote Sensing*, **20**, 789–800.

Puntodewo, S.S.O., McCaffrey, R. *et al.* 1994. GPS measurements of crustal deformation within the Pacific–Australia plate boundary zone in Irian Jaya, Indonesia. *Tectonophysics*, **237**, 141–153.

Quigley, M., van Dissen, R. *et al.* 2012. Surface rupture during the 2010 M_w 7.1 Darfield (Canterbury) earthquake: implications for fault rupture dynamics and seismic-hazard analysis. *Geology*, **40**, 55–58.

Ramírez-Herrera, M.T. 1998. Geomorphic assessment of active tectonics in the Acambay Graben, Mexican Volcanic Belt. *Earth Surface Processes and Landforms*, **23**, 317–332.

RANGIN, C., LE PICHON, X. *ET AL.* 1999. Plate convergence measured by GPS across the Sundaland/Philippine Sea plate deformed boundary: the Philippines and eastern Indonesia. *Geophysical Journal International*, **139**, 296–316.

ROBINSON, D.P., DAS, S. & SEARLE, M.P. 2010. Earthquake fault superhighways. *Tectonophysics*, **493**, 236–243.

ROBINSON, G.P. & RATMAN, N. 1978. The stratigraphic and tectonic development of the Manokwarai area, Irian Jaya. *BMR Journal of Australian Geology & Geophysics*, **3**, 19–24.

ROBINSON, G.P., RYBURN, R.J., HARAHAP, B.H., TOBING, S.L. & ACHDAN, A. 1990. *Geology of the Steenkool Sheet Area, Irian Jaya. 1:250,000 Scale*. Geological Research and Development Centre, Bandung.

ROCKWELL, T.K., KELLER, E.A. & JOHNSON, D.L. 1984. Tectonic geomorphology of alluvial fans and mountain fronts near Ventura, California. *In*: MORISAWA, M. (ed.) *Tectonic Geomorphology. Proceedings of the 15th Annual Geomorphology Symposium*. Allen and Unwin, Boston, MA, 183–207.

ROQUES, D. 1999. *The Metamorphic Core of Buru*. Southeast Asia Research Group, London, Report No. 204.

ROYDEN, L.H. 1993. Evolution of retreating subduction boundaries formed during continental collision. *Tectonics*, **12**, 629–638.

RUDYAWAN, A. 2011. *Tectonostratigraphy and structural style of the South Banggai–Sula Block and NW Banda Basin, Indonesia*. MSc thesis, University of London.

SEGAL, P. & POLLARD, D.D. 1980. Mechanics of discontinuous faults. *Journal of Geophysical Research*, **85**, 4337–4350.

SENO, T. & KAPLAN, D.E. 1988. Seismotectonics of western New Guinea. *Journal of Physics of the Earth*, **36**, 107–124.

SIBSON, R.H. 1985. Stopping of earthquake ruptures at dilational fault jogs. *Nature*, **316**, 248–251.

SIEH, K.E. & JAHNS, R.H. 1984. Holocene activity of the San Andreas fault at Wallace Creek, California. *Journal of Geophysical Research*, **95**, 883–896.

SILVA, P.G., GOY, J.L., ZAZO, C. & BARDAJÍ, T. 2003. Fault-generated mountain fronts in southeast Spain: geomorphologic assessment of tectonic and seismic activity. *Geomorphology*, **50**, 203–225.

SILVER, E.A. & MOORE, J.C. 1978. The Molucca Sea collision zone, Indonesia. *Journal of Geophysical Research*, **83**, 1681–1691.

SILVER, E.A., MCCAFFREY, R. & SMITH, R.B. 1983*a*. Collision, rotation and the initiation of subduction in the evolution of Sulawesi, Indonesia. *Journal of Geophysical Research*, **88**, 9407–9418.

SILVER, E.A., MCCAFFREY, R., JOYODIWIRYO, Y. & STEVENS, S. 1983*b*. Ophiolite emplacement by collision between the Sula Platform and the Sulawesi Island Arc, Indonesia. *Journal of Geophysical Research*, **88**, 9419–9435.

SIMANDJUNTAK, T.O. 1986. *Sedimentology and tectonics of the collision complex in the East Arm of Sulawesi, Indonesia*. PhD thesis, University of London.

SIMANDJUNTAK, T.O., SURONO & SUKIDO. 1984. *Geological Report of the Kolaka Quadrangle, 394 Sulawesi, Scale 1:250,000*. Open File Report. Indonesian Geological Research and Development 395 Centre, Bandung.

SIMANDJUNTAK, T.O., SURONO & SUKIDO. 1994. *Geological Map of the Kolaka Quadrangle, Sulawesi, 1:250,000 scale*. Geological Research and Development Centre, Bandung.

SOCQUET, A., VIGNY, C., CHAMOT-ROOKE, N., SIMONS, W., RANGIN, C. & AMBROSIUS, B. 2006. India and Sunda plates motion and deformation along their boundary in Myanmar determined by GPS. *Journal of Geophysical Research*, **111**, https://doi.org/10.1029/2005JB003877

SOHONI, P.S., MALIK, J.N., MERH, S.S. & KARANTH, R.V. 1999. Active tectonics astride Katrol Hill Zone, Kachchh, Western India. *Journal of the Geological Society of India*, **53**, 579–586.

SPAKMAN, W. & HALL, R. 2010. Surface deformation and slab–mantle interaction during Banda Arc subduction rollback. *Nature Geoscience*, **3**, 562–566.

SPENCER, J.E. 2010. Structural analysis of three extensional detachment faults with data from the 2000 Space-Shuttle Radar Topography Mission. *Geological Society of America Today*, **20**, 4–10.

SPENCER, J.E. 2011. Gently dipping normal faults identified with Space Shuttle radar topography data in central Sulawesi, Indonesia, and some implications for fault mechanics. *Earth and Planetary Science Letters*, **308**, 267–276.

STEIN, S., GELLER, R.J. & LIU, M. 2012. Why earthquake hazard maps often fail and what to do about it. *Tectonophysics*, **562–563**, 1–25.

STEVENS, C.W., MCCAFFREY, R. *ET AL.* 1999. GPS evidence for rapid rotations about a vertical axis in a collisional setting: the Palu fault of Sulawesi, Indonesia. *Geophysical Research Letters*, **26**, 2677–2680.

STEVENS, C.W., MCCAFFREY, R., BOCK, Y., GENRICH, J.F., PUBELLIER, M. & SUBARYA, C. 2002. Evidence for block rotations and basal shear in the world's fastest slipping continental shear zone in NW New Guinea. *In*: STEIN, S. & FREYMUELLER, J. (eds) *Plate Boundary Zones*. American Geophysical Union, Geodynamics Series, **30**, 87–99.

STIRLING, M.W., WESNOUSKY, S.G. & SHIMAZAKI, K. 1996. Fault trace complexity, cumulative slip, and the shape of the magnitude-frequency distribution for strike-slip faults: a global survey. *Geophysical Journal International*, **124**, 833–868.

SUGGATE, S. & HALL, R. 2003. Predicting sediment yields from SE Asia: a GIS approach. *In*: *Proceedings, Indonesian Petroleum Association, 29th Annual Convention*, IPA03-G-015, 289–304.

SUKAMTO, R. & SIMANDJUNTAK, T.O. 1983. Tectonic relationship between geologic provinces of western Sulawesi, eastern Sulawesi and Banggai-Sula in the light of sedimentological aspects. *Bulletin Geological Research and Development Centre, Bandung*, **7**, 1–12.

SURONO 1994. Stratigraphy of the southeast Sulawesi continental terrane, Eastern Indonesia. *Journal of Geology and Mineral Resources*, **4**, 4–11.

TEAS, P.A., DECKER, J., ORANGE, D. & BAILLIE, P. 2009. New insight into structure and tectonics of the Seram Trough from SEASEEPTM high resolution

bathymetry. *In*: *Proceedings, Indonesian Petroleum Association, 33rd Annual Convention and Exhibition*, IPA09-G-091.

THATCHER, W. 1995. Microplate v. continuum descriptions of active tectonic deformation. *Journal of Geophysical Research*, **100**, 3885–3894.

TJOKROSAPOETRO, S., BUDHITRISNA, T. & RUSMANA, D. 1981. *Geological Map of the Buru Island Quadrangle, Maluku, 1:250,000 Scale*. Geological Research and Development Centre, Bandung.

TJOKROSAPOETRO, S., ACHDAN, A., SUWITODIRDJO, K., RUSMANA, E. & ABIDIN, H.Z. 1993. *Geological Map of the Masohi Quadrangle, 2200 Maluku, 1:250000*. Geological Research and Development Centre, Bandung.

USGS EARTHQUAKE HAZARDS PROGRAM. Significant Earthquakes, http://earthquake.usgs.gov/earthquakes/browse/significant.php [last accessed 29 October 2016].

VAN LEEUWEN, T.M. & MUHARDJO, 2005. Stratigraphy and tectonic setting of the Cretaceous and Paleogene volcanic-sedimentary successions in northwest Sulawesi, Indonesia implications for the Cenozoic evolution of Western and Northern Sulawesi. *Journal of Asian Earth Sciences*, **25**, 481–511.

VAN LEEUWEN, T., ALLEN, C.M., KADARUSMAN, A., ELBURG, M., PALIN, J.M., MUHARDJO & SUWIJANTO 2007. Petrologic, isotopic, and radiometric age constraints on the origin and tectonic history of the Malino Metamorphic Complex, NW Sulawesi, Indonesia. *Journal of Asian Earth Sciences*, **29**, 751–777.

VECCHIOTTI, F. 2008. Calculating geomorphic indices in SE Asia using a SRTM derived DEM: a worked example from West Sulawesi, Indonesia. *In*: MICHEL, U., CIVCO, D.L., EHLERS, M. & KAUFMAN, H.J. (eds) *Remote Sensing for Environmental Monitoring*. GIS Applications and Geology VIII, SPIE Proceedings, **7110**, https://doi.org/10.1117/12.800240

VISSER, W.A. & HERMES, J.J. 1962. *Geological Results of the Exploration for Oil in Netherlands New Guinea*. Verhandelingen Koninklijk Nederlands Geologisch en Mijnbouwkundig Genootschap, Geologische Serie 20. Staatsdrukkerij-en Uitgeverijbedrijf, The Hague.

WALD, D.J., KANAMORI, H., HELMBERGER, D.V. & HEATON, T.H. 1993. Source study of the 1906 San Francisco earthquake. *Bulletin of the Seismological Society of America*, **83**, 981–1019.

WALKER, F. & ALLEN, M.B. 2012. Offset rivers, drainage spacing and the record of strike-slip faulting: the Kuh Banan Fault, Iran. *Tectonophysics*, **530–531**, 251–263.

WALLACE, R.E. 1968. Notes on stream channels offset by the San Andreas fault, southern Coast Ranges, California. *In*: DICKINSON, W. & GRANTZ, A. (eds) *Conference on Geologic Problems of San Andreas Fault System. Proceedings*. Stanford University Publications in the Geological Sciences, **11**, 6–21.

WALLACE, R.E. 1986. *Active Tectonics: Impacts on Society*. Studies in Geophysics. National Academy Press, Washington, DC.

WALLACE, R.E. (ed.) 1990. *The San Andreas Fault System, California*. US Geological Survey, Professional Papers, **1515**.

WALPERSDORF, A., VIGNY, C., SUBARYA, C. & MANURUNG, P. 1998. Monitoring of the Palu-Koro Fault (Sulawesi) by GPS. *Geophysical Research Letters*, **25**, 2313–2316.

WANG, Y., SIEH, K., SOE THURA TUN, LAI, K.-Y. & THAN MYINT, 2014. Active tectonics and earthquake potential of the Myanmar region. *Journal of Geophysical Research: Solid Earth*, **119**, 3767–3822, https://doi.org/10.1002/2013JB010762

WATKINSON, I.M. 2011. Ductile flow in the metamorphic rocks of central Sulawesi. *In*: HALL, R., COTTAM, M.A. & WILSON, M.E.J. (eds) *The SE Asian Gateway: History and Tectonics of the Australia–Asia Collision*. Geological Society, London, Special Publications, **355**, 157–176, https://doi.org/10.1144/SP355.8

WATKINSON, I.M., HALL, R. & FERDIAN, F. 2011. Tectonic re-interpretation of the Banggai-Sula–Molucca Sea margin, Indonesia. *In*: HALL, R., COTTAM, M.A. & WILSON, M.E.J. (eds) *The SE Asian Gateway: History and Tectonics of the Australia–Asia Collision*. Geological Society, London, Special Publications, **355**, 203–224, https://doi.org/10.1144/SP355.10

WELLS, D.L. & COPPERSMITH, K.J. 1994. New empirical relationships among magnitude, rupture length, rupture width, rupture area, and surface displacement. *Bulletin of the Seismological Society of America*, **84**, 974–1002.

WELLS, S.G., BULLARD, T.F. *ET AL*. 1988. Regional variations in tectonic geomorphology along a segmented convergent plate boundary, Pacific Coast of Costa Rica. *Geomorphology*, **1**, 239–265.

WESNOUSKY, S.G. 1988. Seismological and structural evolution of strike-slip faults. *Nature*, **335**, 340–342.

WESNOUSKY, S.G. 2006. Predicting the endpoints of earthquake ruptures. *Nature*, **444**, 358–360.

WHITE, L.T., HALL, R. & ARMSTRONG, R.A. 2014. The age of undeformed dacite intrusions within the Kolaka fault zone, SE Sulawesi, Indonesia. *Journal of Asian Earth Sciences*, **94**, 105–112.

WICHMANN, A. 1918. Die Erdbeben des Indischen Archipels Bis Zum Jahre 1857. *Verhandelingen der Koninklijke Akademie van Wetenschappen te Amsterdam*, **20**, 193 [in Dutch].

WU, J.E., MCCLAY, K., WHITEHOUSE, P. & DOOLEY, T. 2009. 4D analogue modelling of transtensional pull-apart basins. *Marine and Petroleum Geology*, **26**, 1608–1623.

WYSS, M. 2005. Human losses expected in Himalayan earthquakes. *Natural Hazards*, **34**, 305–314.

XU, X., YEATS, R.S. & YU, G. 2010. Five short historical earthquake surface ruptures near the silk road, Gansu Province, China. *Bulletin of the Seismological Society of America*, **100**, 541–561.

YEATS, R. 2010. *Active Faults of the World*. Cambridge University Press, Cambridge.

YILDIRIM, C. 2014. Relative tectonic activity assessment of the Tuz Gölü Fault Zone; Central Anatolia, Turkey. *Tectonophysics*, **630**, 183–192.